Comparison and Results of Sheet Pile Interlock Analysis

by

Ching-Yang Huang

Thesis submitted to the Faculty of the

Virginia Polytechnic Institute and State University

in partial fulfillment of the requirements for the degree of

Master of Science

in

Civil Engineering

APPROVED:

Richard M. Barker

Dr. Richard M. Barker, Chairman

Siegfried Holzer

Dr. Siegfried M. Holzer

Raymond H. Plaut

Dr. Raymond H. Plaut

February, 1988

Blacksburg, Virginia

Comparison and Results of Sheet Pile Interlock Analysis

by

Ching-Yang Huang

Dr. Richard M. Barker, Chairman

Civil Engineering

(ABSTRACT)

A finite element program for analyzing the nonlinear behavior of moving contact problems has been developed and used for the analysis of a single sheet pile interlock (Chan and Barker (1985), Wu and Barker (1986)). In this study, the program is modified to simulate a sheet pile pull-out test with a new finite element mesh. The improved mesh contains a full-length sheet pile with both of its interlocks connected to two half-length sheet piles. The results are presented and compared with the results of the pull-out tests which were conducted by O'Neil and McDonald at WES (1985). The comparison is not completely satisfactory because the initial slack between interlocks is not modeled. Nonetheless, the general behavior of sheet piles under tensile load is correctly predicted by the finite element program.

For easier interpretation of the output from the finite element analysis, the computer graphics software AutoCAD (Autodesk, 1986) is adopted to serve as a postprocessor. Several features of AutoCAD such as overlaying, zooming, and macro instructions are utilized to serve this purpose. Some intermediate programs are also developed for the communication between the finite element program and AutoCAD.

Acknowledgements

I wish to extend to my deepest appreciation to my advisor Dr. Richard Barker for his unending guidance and editorial assistance during the course of this research project.

I also wish to extend my appreciation to Dr. Siegfried Holzer and Dr. Raymond Plaut for their service in the committee.

Table of Contents

List of Illustrations

CHAPTER I

INTRODUCTION

1.1 Purpose and Scope

This study is a continuation of the work by Chan and Barker (1985) and Wu and Barker (1986) on the analysis of steel sheet pile interlocks. In the previous analyses, the finite element program has successfully incorporated the effects of large rotations and displacements, elastic-plastic material response, and moving contact to describe the behavior of sheet pile interlocks.

However, the previous analysis was limited to a single interlock connection. The purpose of this study is to provide an improved finite element idealization which contains both interlocks of a sheet pile and to make a comparison with the pull tests conducted by O'Neil and McDonald (1985) at Waterways Experiment Station (WES). Also,

AutoCAD (Autodesk, Inc) is introduced in this study as a post processor for easier interpretation of the computer program output.

A literature review conducted on sheet pile interlock analysis, nonlinear finite element analysis, and solutions of contact problems is presented in this chapter.

A detailed description of the new finite element idealization is given in Chapter II. Some discussions of the moving contact algorithm and convergence criterion are also presented for a better understanding of the analysis procedure. The last part of this chapter explains how the computer graphics package AutoCAD is used to interpret the results of the finite element analysis.

Chapter III describes the sheet pile pull tests conducted at WES and their results. The results and deformed shapes of the sheet pile interlocks predicted by the finite element program are discussed in this chapter. Some examples of the AutoCAD drawing abilities are also shown. The advantages of using an interactive computer graphics program to interpret lengthy output of an analytical program are made evident in this chapter.

One of the purposes of this study is to compare the behavior of sheet pile interlocks predicted by the finite element program with that found in laboratory tests. This is discussed in Chapter IV and the explanations for the differences are also presented.

Chapter V contains conclusions obtained from the analysis. A few recommendations arising from this study are suggested for future studies.

1.2 Literature Review on Sheet Pile Interlock Analysis

A variety of methods can be found for the design of a cellular cofferdam. These methods include the Terzaghi Method; the Tennessee Vally Authority Method; Corps of Engineers, U.S. Army Method; Cumming's Method; and Hansen's Method. All these methods use a perfect vessel assumption to calculate the interlock tension.

Only a few papers can be found which deal with the analysis of pull-out strength of sheet pile interlocks. Bower (1973) developed the equations for predicting the interlock strength by conducting a number of pull-out tests and using simple statics. The pull-out strength of the sheet pile was obtained when a failure mechanism of two plastic hinges was formed in the thumb and finger portions in either one of the interlocks. It can be found that the finger thickness affects the strength to a great degree.

Kawasaki Steel Company (1981) used the finite element technique to determine the displacement and stress patterns of sheet pile interlocks under tensile loading. In the analysis, the material is assumed to remain in elastic range.

Barker, et al. (1985) conducted six sets of tests for two types of sheet piles. The report suggested the use of 0.3 for the static coefficient of friction to estimate the sheet pile interlock shear strength and the use of the E-ratio concept for calculating interlock tensions.

Chan and Barker (1985) developed a finite element program to predict the interlock behavior. A nonlinear moving contact algorithm with elastic-plastic material response and large displacement and rotation is adopted in the computer program.

In an attempt to more closely study the behavior of sheet pile interlock, Wu and Barker (1986) used the modified Riks-Wempner method instead of the modified Newton-Raphson method to solve nonlinear equilibrium equations. It was found that a modified Riks-Wempner method produced a more satisfactory result when sliding occurred at contact regions.

1.3 Literature Review on Nonlinear Finite Element Analysis

Nonlinear finite element analysis has been intensely studied for decades and a lot of literature has been written on this topic. Depending on the reference state chosen, different schemes can be used to derive the equilibrium equations. If the current state is replaced by the configuration of the body at the end of the previous step, the approach is known as the Mixed Lagrangian-Eulerian or Updated Lagrangian Method. Since it is the method adopted in this study, only the literature related to this approach is reviewed below.

Murray and Wilson (1965) used a displaced local coordinate system to transform the nonlinear strain displacement relationship to a geometric transformation.

Yaghmai and Popov (1971) obtained the incremental equilibrium equation by taking the difference in virtual work done between two consecutive current configurations.

Osias and Swedlow (1974) applied the Galerkin method on the rate form of the equilibrium equations governing the rate of loading upon a deformed solid. They also used the invariant Jaumann stress rate to solve large deformation problems.

Hutchinson (1973) used the variational principle on the incremental form of the virtual work done by a system and discussed the finite strain generalization of plastic flow. The Jaumann stress rate of second Piola-Kirchhoff stress was also used in his work.

According to Bathe (1982), two kinds of formulation are identified for the updated formulation; the Updated Lagrangian with transformation approach and the Updated Lagrangian with Jaumann stress rate approach. The latter is more appropriate for solving elastic-plastic problem with large deformations.

Yamada (1972) and many others based their formulations on the virtual work equation and derived the stiffness equation which contains the initial stiffness matrix and the load correction factor for pertinent geometrically nonlinear behavior. To correct the effect of rotation of the stress field, various definitions of strain and stress rate were introduced. Yamada, et al. (1973) showed in their work that, depending on the type of stress rate chosen, the system stiffness matrix may not be symmetrical. They also concluded that the Jaumann stress rate of the second Piola-Kirchhoff stress will provide a symmetrical matrix and is suitable for elastic-plastic analysis.

An approach was developed by Argyris and Kleiber (1977) and redefined by Argyris, et al. (1978) in which they introduced a distinct updated formulation by choosing an intermediate stress free state as the reference configuration. The nonlinear terms from the incremental strain to the incremental displacement relationship were neglected in their work.

1.4 Literature Review on Solutions of Contact Problems

In recent years, the finite element method has been one of the most popular tools to solve contact problems because of its ability to handle the highly nonlinear nature involved.

Chan and Tuba (1971) developed a method in which the contact force was calculated in each iteration by estimating the amount of overlapping or separation of a point on the side of the contact segment.

Tsuta and Yamaji (1973) used equilibrium and compatibility conditions between contact surfaces to relate the incremental equilibrium equations for the contacting bodies. The system stiffness was modified when there was a change in contact conditions.

Francavilla and Zienkiewicz (1975) used a reduced flexibility matrix to solve the frictionless contact problem. By modifying the contact status of any possible contact point, iteratively, the contact force vector can be obtained after convergence is achieved.

Gaertner (1977) employed an approach in which the nodal unknowns included displacements and their derivatives which were related to strains and stresses. However, in his paper the procedure for including the strains and stresses as unknowns was not clearly explained.

In addition to static contact, Lee and Kamemura (1979,1981) used a part of the flexibility matrix to solve static and dynamic contact problems. During the iterations, the contact status of each point was updated until the assumed contact status agreed with the computed result at each possible point.

Katona (1983) combined the contact constraint condition with a global equation. By incorporating additional contact constraints, the global stiffness matrix, displacement vector, and force vector are extended. The contact constraints were assumed at first and updated by iterating until convergence was obtained.

K. Lee (1985) developed a numerical solution which guarantees the convergence to the corresponding exact solution for a two-dimensional linear elastic frictional contact problem. He used the current gap vector and incremental form of Coulomb's friction law to describe the frictional contact condition.

Bathe and Chaudhary (1985) incorporated a contact constraint equation in the global equation. In their formulation, the total variational function is obtained by summing the usual incremental potential and the incremental potential of the contact forces. This approach was adopted to model the moving contact problem in the previous report by Wu and Barker (1986). It is also followed in this study.

CHAPTER II

METHOD OF ANALYSIS

2.1 Description of Finite Element Program

The purpose of the computer program is to perform two dimensional static analyses using a quadrilateral, isoparametric eight-node element with 16 displacement degrees of freedom. The program is capable of modeling large displacement and rotation effects, elastic-plastic material response, and nonlinearity due to moving contact conditions. The only deviation from the standard finite element displacement formulation is the inclusion of nodal contact forces as unknowns when the moving contact situation is involved in the analysis. Because of these unknowns, the unconstrained global stiffness matrix has zeros in some of the diagonal terms. However, when the boundary conditions are included, the solution of the equations proceeds without numerical difficulty. In addition, the symmetry of the matrix is still preserved.

The nodal displacements are obtained directly from solving the equilibrium equations of the system. These displacements will be used in conjunction with the interpolation functions to calculate the element strains and stresses at the Gauss points. The unknown contact forces are evaluated from the internal load due to element stresses. Coulomb's Law is used when friction is involved in the problem.

The following sections provide a brief review on the theories behind the finite element program used in this study. They are discussed in greater detail in the report by Chan and Barker (1985).

2.1.1 Geometric Nonlinearity

According to Bathe (1982), the Updated Lagrangian approach is the best choice in problems involving both large strain and material nonlinear behavior. To formulate the Updated Lagrangian approach, it is necessary to define three typical configurations of a continuous system deforming under the application of external loads. These are the initial configuration of a system and its deformed configurations at load step n and the subsequent load step n+1 (Fig. 2.1).

It is assumed that all the kinematic and static variables at step n are known. The aim is to establish the incremental finite element equilibrium equations for step n+1 with all variables referred to the configuration at step n. The results of this formulation can be written in matrix form as:

$$\left([{}^{n}K_{l}] + [{}^{n}K_{n}]\right)[\Delta U] = [{}^{n+1}R] - [{}^{n}F] \tag{2.1}$$

where K_l and K_n are the linear and nonlinear stiffness matrices, $\triangle U$ is the incremental nodal displacement vector, R is the sum of the externally applied body and surface forces, and F is the equivalent force vector of the internal stresses. This equation can be solved directly to yield incremental nodal displacements.

2.1.2 Material Nonlinearity

After discretization the finite element equilibrium equations contain both kinematic and constitutive matrices. An elastic-plastic model with isotropic strain hardening is used in this program. Because the total stress depends on the path of deformation, a stress rate is used to update plastic stresses. When large displacements and rotations are involved, the stress rate chosen must be invariant with respect to rigid body motions. The widely used Jaumann stress rate described by Fung (1965) is used herein.

To describe the plastic behavior of the material, the following three criteria are adopted: (1) a Von Mises model which specifies the stress state at which the material yields, (2) a Prandtl-Reuss flow rule which relates the plastic strain increments to the stress increments during the event of plastic flow, and (3) an isotropic hardening rule which allows the yield surface to expand uniformly and without translation or rotation. At step n, the rate of change of the relationship between stress and strain can be stated concisely in matrix form as:

$$[d^n\sigma] = [C^{EP}][d^n\varepsilon^T] \tag{2.2}$$

where C^{EP} is the elastic-plastic incremental constitutive matrix. These matrices are derived by Yamada et al. (1968) and are applicable for small strain conditions. However,

since the deformed configuration of the body is used in the Updated Lagrangian-Jaumann approach, the above results can also be used for large deformations.

2.1.3 Moving Contact Problem

The formulation utilized for the contact forces follows the procedure developed by Bathe and Chaudhary (1985). The general idea is to express the total potential energy of the nodal contact forces in a variational formulation such that the geometric compatibilities are enforced along the contact surfaces. A brief summary is given to provide an overview of the considerations included in the development.

When considering the effect of contact forces, the total potential function Π_1 is obtained by summing the usual incremental potential Π that leads to Eq.(2.1), and the incremental potential of the contact forces which equals the negative of work done W_k, that is:

$$\Pi_1 = \Pi - \sum_k W_k \tag{2.3}$$

However, in the approach adopted the W_k term is obtained after the system is discretized so that reference to a total potential function for the contact surface is not involved.

Since equilibrium iteration is used within each load increment, the value of W_k is written for iteration (i) in load step n+1. At this stage of analysis, the response of the system at step n has been calculated and (i-1) iterations have been performed for the solution at step n+1. After Π_1 is established, a first variation of the potential is carried out and

the corresponding contributions give additional terms to Eq.(2.1). However, the original terms in Eq.(2.1) will remain unaltered.

In evaluating the contribution of W_k, it is necessary to know whether the contact surface is sticking or sliding. A node k of the contact body is said to come into contact with segment AB of the target body when penetration occurs within the target. This is illustrated in Fig. 2.2, where the location of contact on surface AB is not known. If during an iteration a tensile force is found acting on the contact node, debonding occurs and the contact force is set to zero. The motion of the contact bodies is governed by Coulomb's Law of friction with μ_s as the coefficient of static friction and μ_k as the coefficient of kinetic friction. Denoting t_n as the compressive normal traction and t_t as the tangential traction along the contact surface, the motion of the contact point depends on the following equations:

$$\begin{aligned} &\text{sticking} && t_t \leq \mu_s t_n \\ &\text{sliding} && t_t = \mu_k t_n \end{aligned} \tag{2.4}$$

The direction of the tangential traction will always be opposite to the direction of sliding. If t_t drops below the kinetic friction force, sticking is said to take place again.

To construct the finite element equations for contacting systems, the stationarity of the contact potential is invoked. Since there are two variables involved, the change in nodal displacement ΔU and the change in nodal force $\Delta\lambda$, two sets of Euler equations are obtained. These are discretized into finite element equations and can be given as

$$\begin{bmatrix} {}^{n+1}K_T^{(i-1)} & {}^{n+1}K_C^{(i-1)} \\ {}^{n+1}K_C^{(i-1)} & 0 \end{bmatrix} \begin{bmatrix} \Delta U^{(i)} \\ \Delta\lambda^{(i)} \end{bmatrix} = \begin{bmatrix} {}^{n+1}R \\ 0 \end{bmatrix} - \begin{bmatrix} {}^{n+1}F^{(i-1)} \\ 0 \end{bmatrix} + \begin{bmatrix} {}^{n+1}R_C^{(i-1)} \\ {}^{n+1}\Delta_C^{(i-1)} \end{bmatrix} \tag{2.5}$$

where K_T is the sum of the linear and nonlinear stiffness matrices of Eq.(2.1), K_C is the contact stiffness matrix, R_C is the contact force vector, and Δ_C is the overlap vector.

2.1.4 Solution Process and Convergence

Solving Eq.(2.5) requires a combination of incremental and iterative techniques. In the program, a modified Riks-Wempner method is implemented. Convergence tests based on incremental displacement, incremental energy and change in contact forces are used to terminate or advance the iteration procedure.

2.2 Improvement of Finite Element Program

The finite element program used in this study was first developed by Chan and Barker (1985) and later modified by Wu and Barker (1986). It was designed to handle sheet pile interlock analysis. The function of the program was explained and shown in previous reports. However, it was intended to analyze only one interlock. Running a new case with both interlocks of a sheet pile is beyond the capacity of the previous finite element program. It must be updated before the new case can be tested.

The main limitation is the size of array dimensions. After the new test problem is carefully examined, the sizes of array dimensions are enlarged so that the program can handle this new task, and the sizes are bounded by the memory capacity set by the computer operating system.

Also, the default number of contact-target pair was previously set to be 4 and is now changed to 6 to suit the new model. The associated statements are updated too.

2.3 Description of Finite Element Model

Although the interlock geometries in field condition vary from one interlock to another, the previous reports selected the shapes of the interlocks from the Steel Sheet Piling Handbook published by United States Steel (1983) for analysis. In order to compare with the test results provided by WES, the sheet pile geometries identical to those tested at WES must be used. The interlock dimensions provided in the Handbook are no longer appropriate because the specimens used in the test chosen to compare with were not manufactured by United States Steel.

When the pull-out tests were conducted at WES, photographic records were carefully made. With each single pull-out test, a set of photographs was taken and transparencies of the undeformed shapes were also made from the photographs. These transparencies provide the interlock geometries of the sheet piles tested in the laboratory and hence are used to establish the new finite element model.

Two sets of photographs, for PSX32 (US Steel) high strength and PSX31 (Bethlehem Steel) high strength steel sheet piles, were sent to Virginia Tech. From the photographs, large slack was found in the set-up of the PSX32 sheet pile pull-out tests. PSX31 high strength steel sheet pile was selected for the model because it has a better initial contact condition than the PSX32 steel sheet pile.

The transparency of undeformed shape was first copied and then enlarged. This enlarged shape was used for the finite element discretization. Eight-node quadratic isoparametric elements were used and the mesh pattern adopted by Wu and Barker (1986), shown to be suitable for modeling a single sheet pile interlock in their report, was also used. The coordinates of the finite element mesh were scaled from the enlarged drawing of interlocks using the known web dimension provided by WES as reference. The coordinates of the nodes were measured by an electronic digitizer which could give values up to three decimal places. The data were recorded in an IBM personal computer and then transferred to the mainframe. The set-up of the axially loaded tensile pull-out test of sheet piles and the finite element mesh used to simulate the test are shown in Fig. 2.3 and Fig. 2.4, respectively. The finite element mesh contains 185 eight-node isoparametric elements with 790 displacement degrees of freedom.

The material properties of the sheet piles used in this study are basically the same as those reported by Oliver (1985) and subsequently used by Wu and Barker (1986) except for the yield stress. These properties are given below:

Young's modulus = 29500 ksi (203550N/m^2)

Poisson's ratio = 0.3

Yield stress = 60 ksi (414 N/m^2)

Strain hardening modulus = 500 ksi (3450N/m^2)

The coefficients of friction were chosen as 0.3 for both μ_s and μ_k . This value was recommended in the report by Oliver (1985).

The enlarged drawings of the interlocks were carefully studied and six contact regions in the interlocks were chosen. Each of these contact regions included 1 to 3 contact-target

pairs depending on local contact conditions. A contact-target pair included all the possible contact nodes at the contact region (see Fig. 2.5 and Fig. 2.6).

The definition is similar to that given by Wu and Barker (1986). In this analysis, all the contact nodes were assumed to be in sticking contact at the beginning of the solution of the incremental equilibrium equation. In order to simulate the boundary conditions at the grips of the pull-out test, nodes at the ends of the two half-length sheet piles were constrained (Fig. 2.7).

2.4 Role of AutoCAD

AutoCAD is a computer graphics program developed by Autodesk Inc. Several versions have been released so far. In this study, version 2.52 released in 1986 is used.

In recent years, computer graphics systems have been largely adopted as an efficient and useful tool to interpret the output of analytical computer programs. The lengthy output of a finite element program, though sometimes nicely arranged in a tabular format, is usually hard to understand and requires a well-trained engineer to interpret the inside meaning. A well presented drawing provides a better means for easier understanding, especially in the analysis of structural deformation. More and more analytical computer programs now include graphical results along with the numerical results. In this study, AutoCAD is adopted to serve the role as an interpreter of the finite element program for sheet pile interlock analysis.

After the output file of the finite element program is transferred to AutoCAD, the deformed shapes of sheet pile at different load steps are put into the same drawing file so

that they can be moved, overlayed and enlarged on the monitor easily and, if wanted, a plot of any interested portion of a sheet pile can be obtained conveniently.

AutoCAD provides two different ways to create a drawing. A drawing can be created interactively by using input devices like a keyboard or mouse. A data file written outside the of AutoCAD environment can also be loaded to create a new drawing. The latter is used in this study, details of which are discussed below.

2.4.1 Description of DXF file

AutoCAD uses a special format text file, extension DXF file, to communicate with other computer programs. It can convert a drawing to a DXF file or read a DXF file to create a drawing. An example of a DXF file is listed in Fig. 2.8. It draws a circle and a square when it is executed (Fig. 2.9). A DXF file contains all the necessary information required for AutoCAD to create a drawing. The format is complicated but it has a certain pattern. A detailed description can be found in the manual commonly supplied in the software package (Autodesk, 1986).

Since AutoCAD requires this special format, the output file of the finite element program must be rearranged before it can be transferred to AutoCAD to draw the deformed shapes of sheet pile interlocks. Several intermediate programs were developed to perform this task. These programs not only generate the required format but also remove all the unwanted blanks which, in AutoCAD, serve the same function as carriage returns.

Once the DXF files were generated, they were loaded into AutoCAD and were used to create drawings of the deformed shapes of sheet piles. Drawings of deformed sheet pile at different load steps were stored separately at first so that they could be 'inserted' to different 'layers' of one single drawing. Drawings at different layers can be displayed or hidden by turning the corresponding layer on or off. By putting them into different layers, the deformed shape of sheet pile at any load step can be displayed without having to load it every time it needs to be shown. Several layers can be turned on at the same time to have an overlap effect. This is another reason why drawings of sheet piles at different stages were put into different layers.

2.4.2 Description of MENU File

Another feature of AutoCAD called MENU is also used in this study to help users who are not familiar with AutoCAD. A MENU file is a text file containing AutoCAD commands. When it is loaded, it shows a MENU on the right hand side of screen. Each item on the MENU is a macro which is a sequence of AutoCAD commands. When an item is selected, AutoCAD will execute the macro automatically. Following is an example of a macro instruction, which could be used as an item in a MENU file:

```
[ADDRESS]text \.4 0 Civil Engineering;; Virginia Tech;; Blacksburg, Virginia;
```

When [ADDRESS] is executed, it will ask for a start point first and print the text in three lines (Fig. 2.10).

There is no limit on the length of a macro. With this feature, a complex procedure can be easily executed by selecting an item from the MENU.

An item in a MENU can also represent a SUB-MENU. By selecting it, another MENU will show up.

Following is an example:

```
[CIRCLE]$S=CIRCLE_SET

**CIRCLE_SET

[CIRCLE-1]circle 5,5 1;

[CIRCLE-2]circle 5,5 2;

[CIRCLE-3]circle 5,5 3;
```

When the [CIRCLE] is selected, a SUB-MENU shows up on the screen, and any of the three items can be selected to draw a circle at point (5,5) with desired radius. This feature is also adopted in the MENU file developed in this study. The structure of that MENU file is shown in Fig. 2.11.

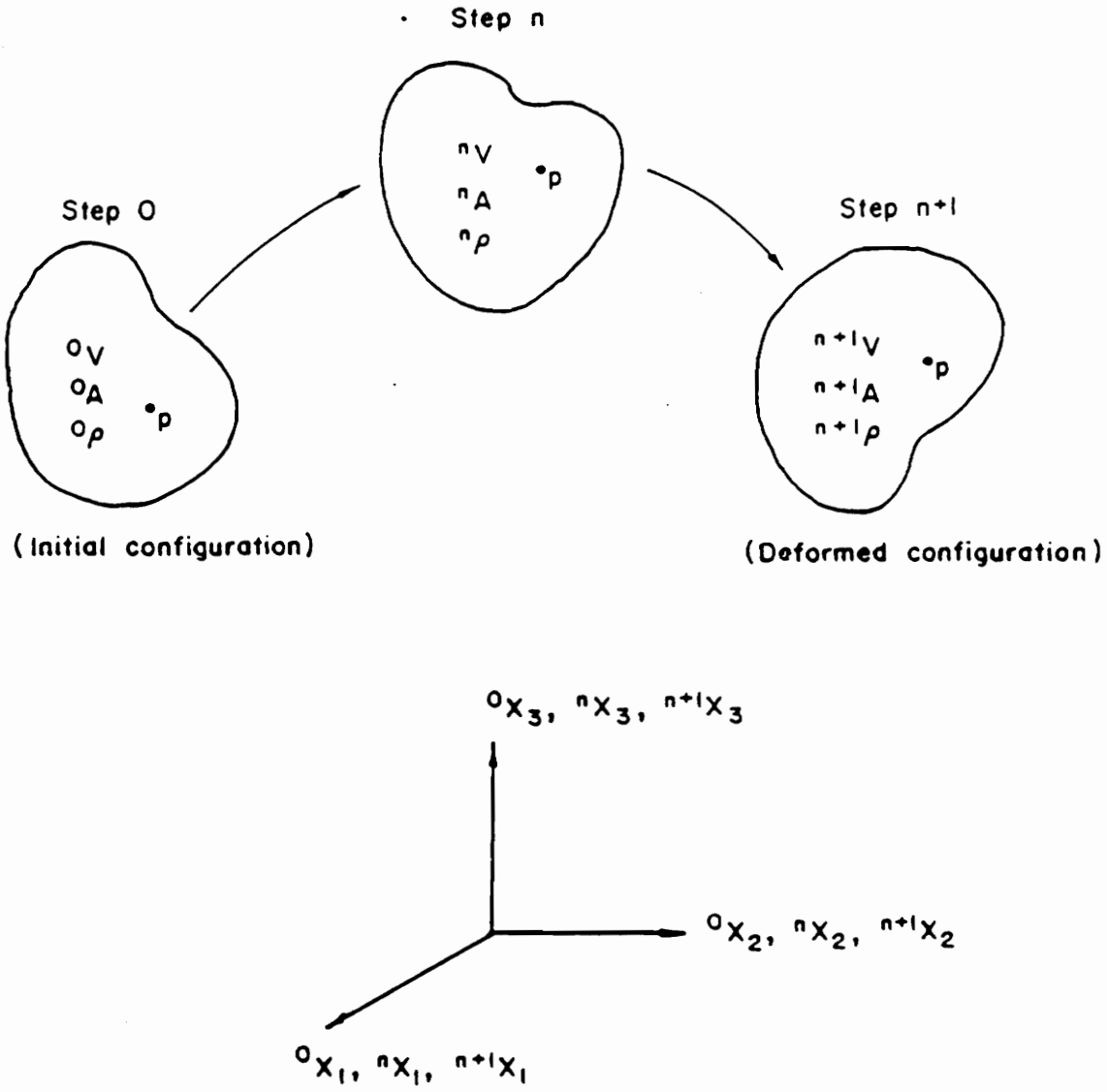

Fig 2.1 Generic Configuration of a System

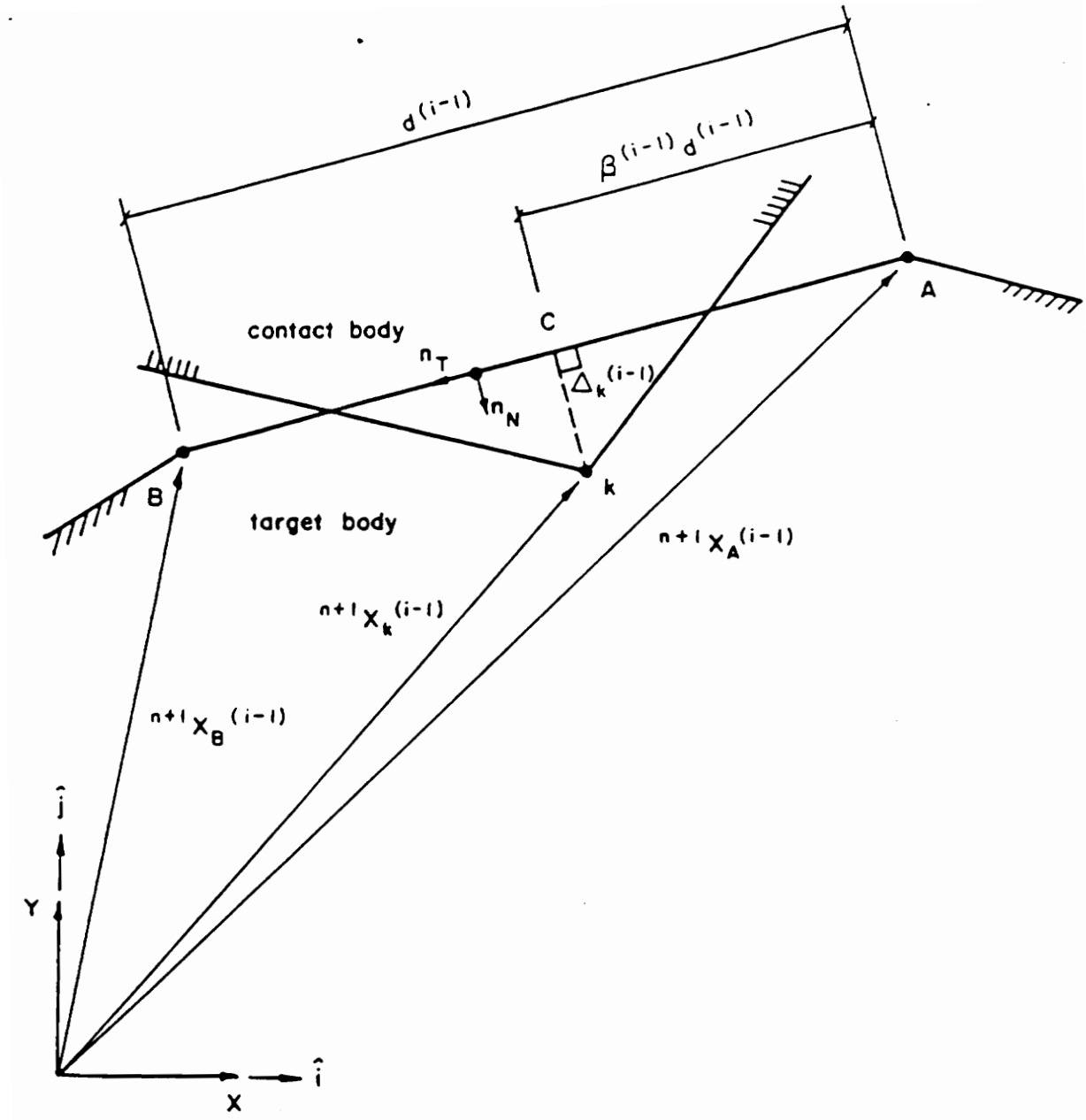

Fig 2.2 Schematic Representation of Contact Condition

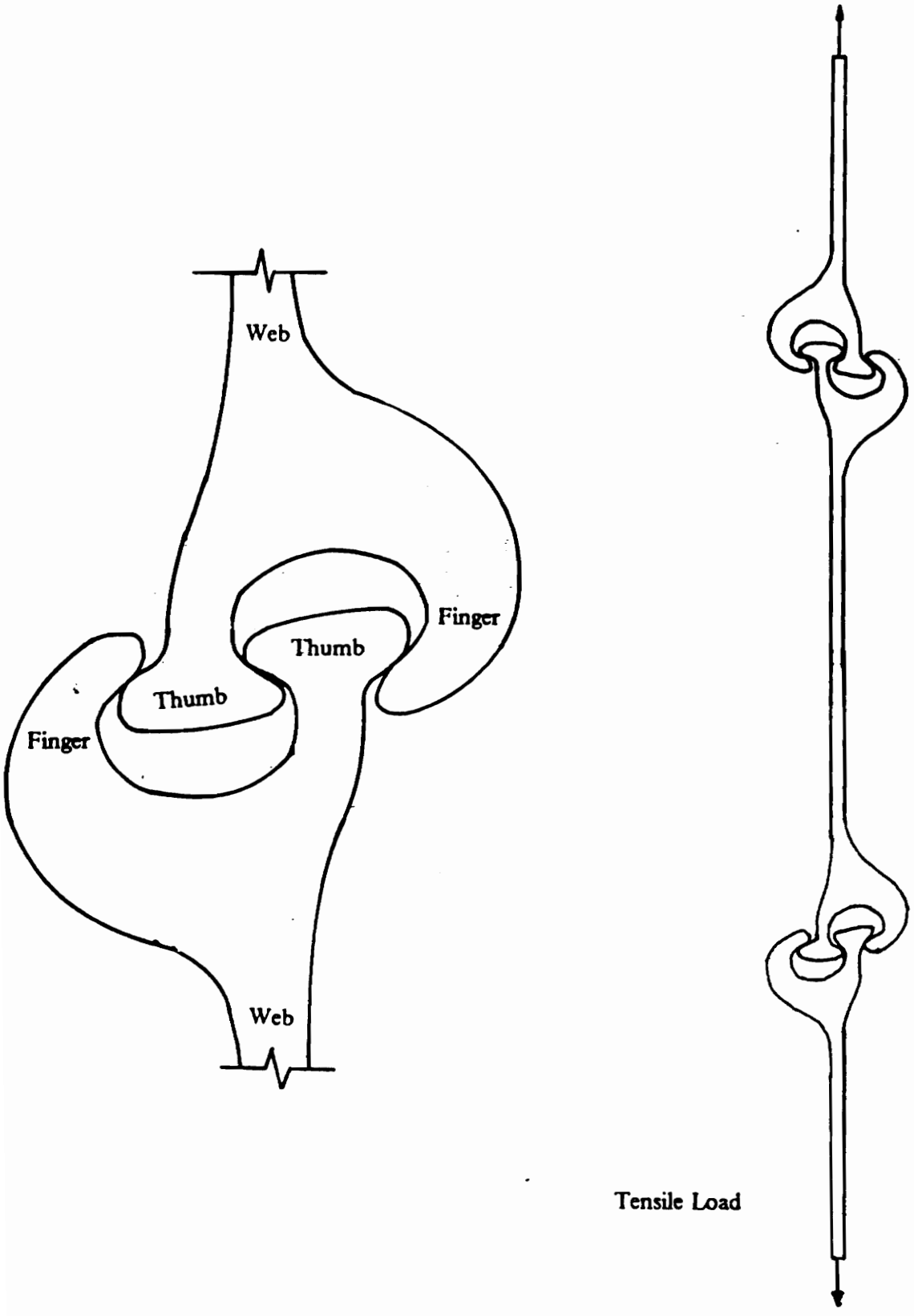

Fig 2.3 Typical Tensile Test of Sheet Pile

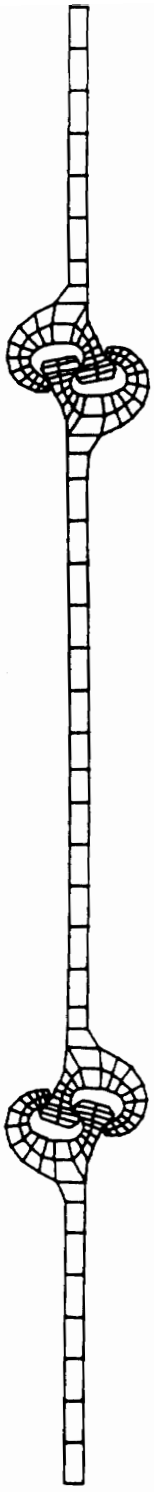

Fig 2.4 Finite Element Mesh for PSX31 High Strength Sheet Pile

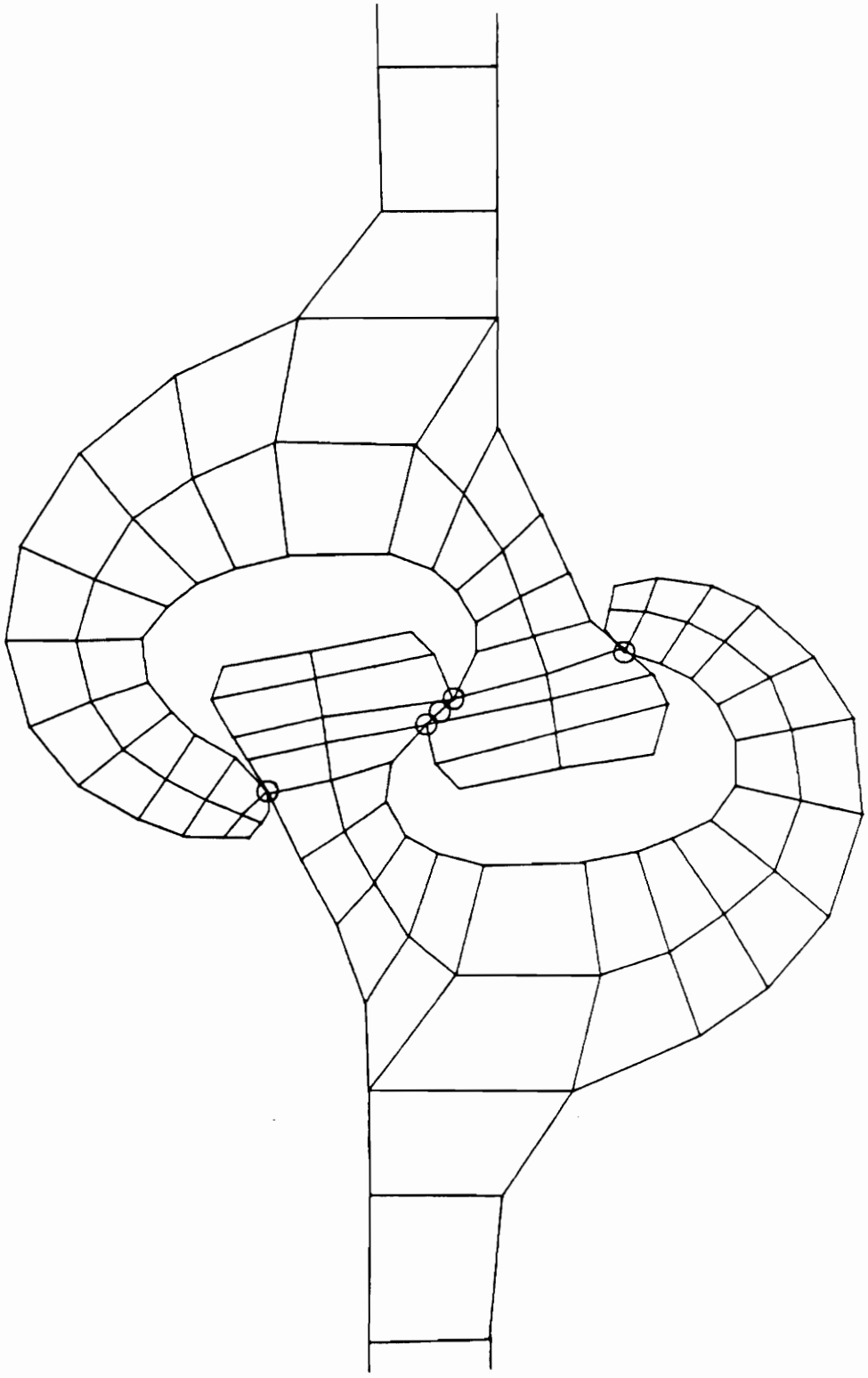

Fig 2.5 Contact Pairs in Top Interlock

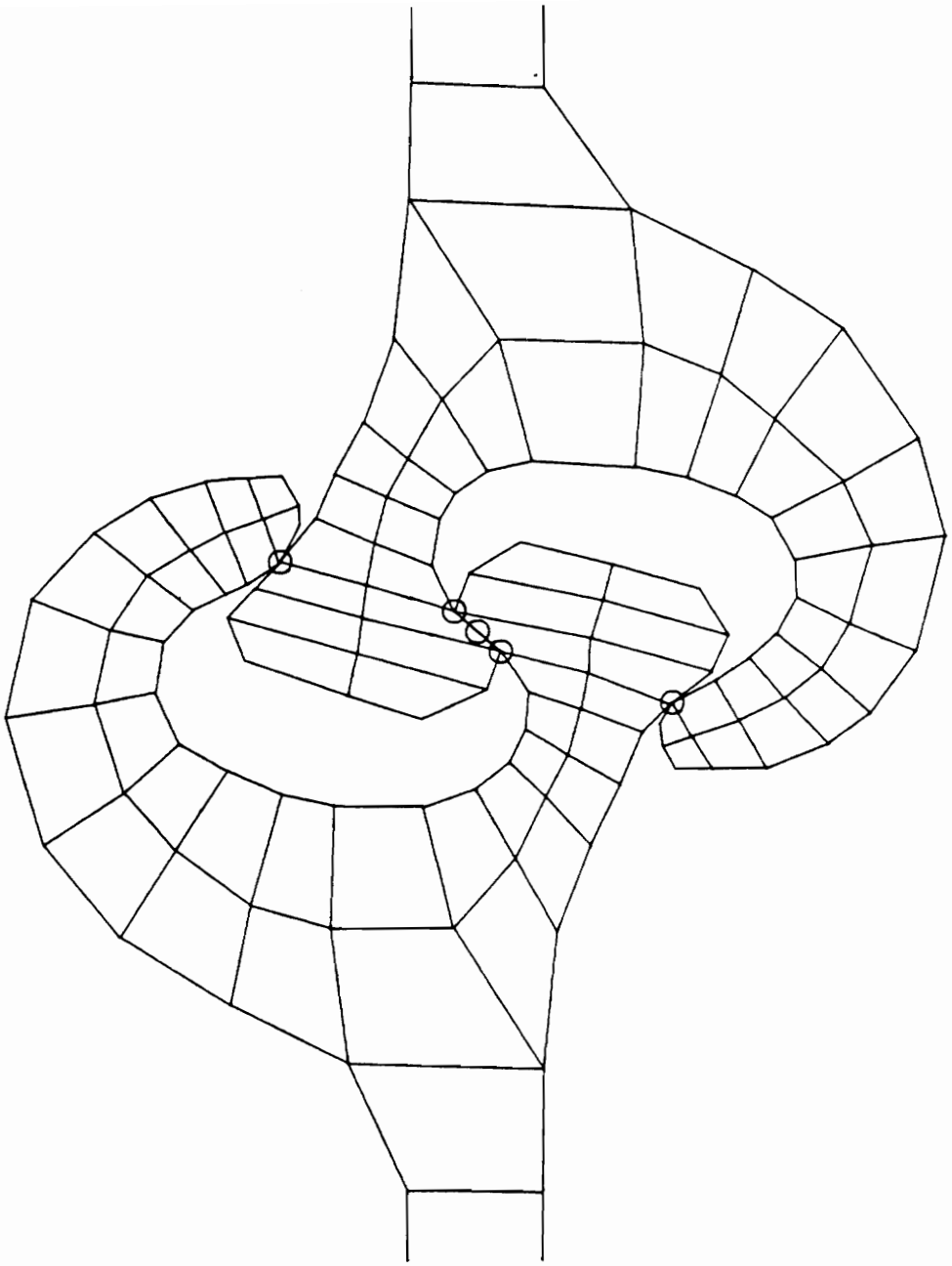

Fig 2.6 Contact Pairs in Bottom Interlock

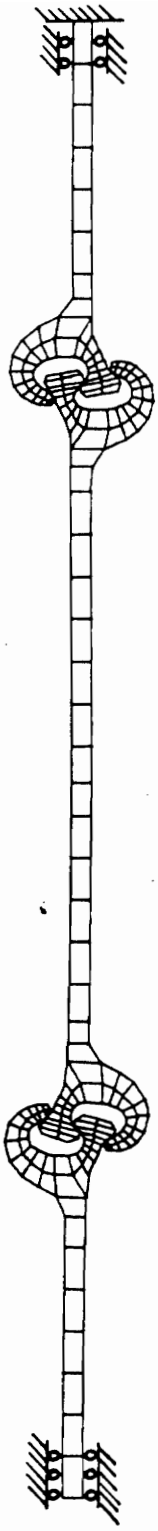

Fig 2.7 Finite Element Model for PSX31 High Strength Sheet Pile

```
  0
SECTION
  2
ENTITIES
  0
CIRCLE
  8
0
 10
7.587137
 20
6.069801
 40
2.277764
  0
LINE
  8
0
 10
5.070445
 20
3.159855
 11
10.885662
 21
3.159855
  0
LINE
  8
0
 10
10.885662
 20
3.159855
 11
10.885662
 21
8.914094
  0
LINE
  8
0
 10
10.885662
 20
8.914094
 11
5.058091
 21
8.914094
  0
LINE
  8
0
 10
5.058091
 20
8.914094
 11
5.070445
 21
3.159855
  0
ENDSEC
  0
EOF
```

Fig 2.8 An Example Of AutoCAD DXF File

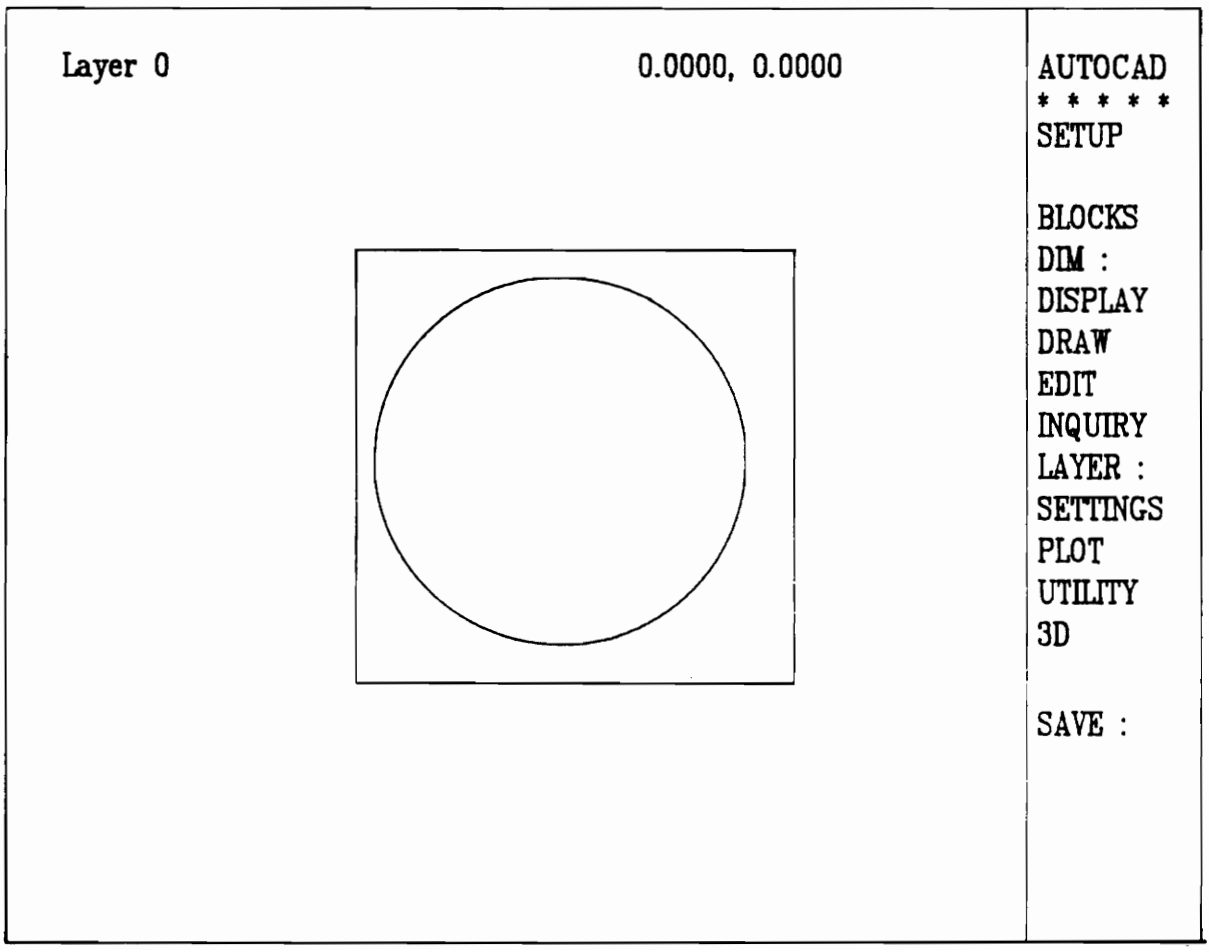

Fig 2.9 Drawing Created by DXF File

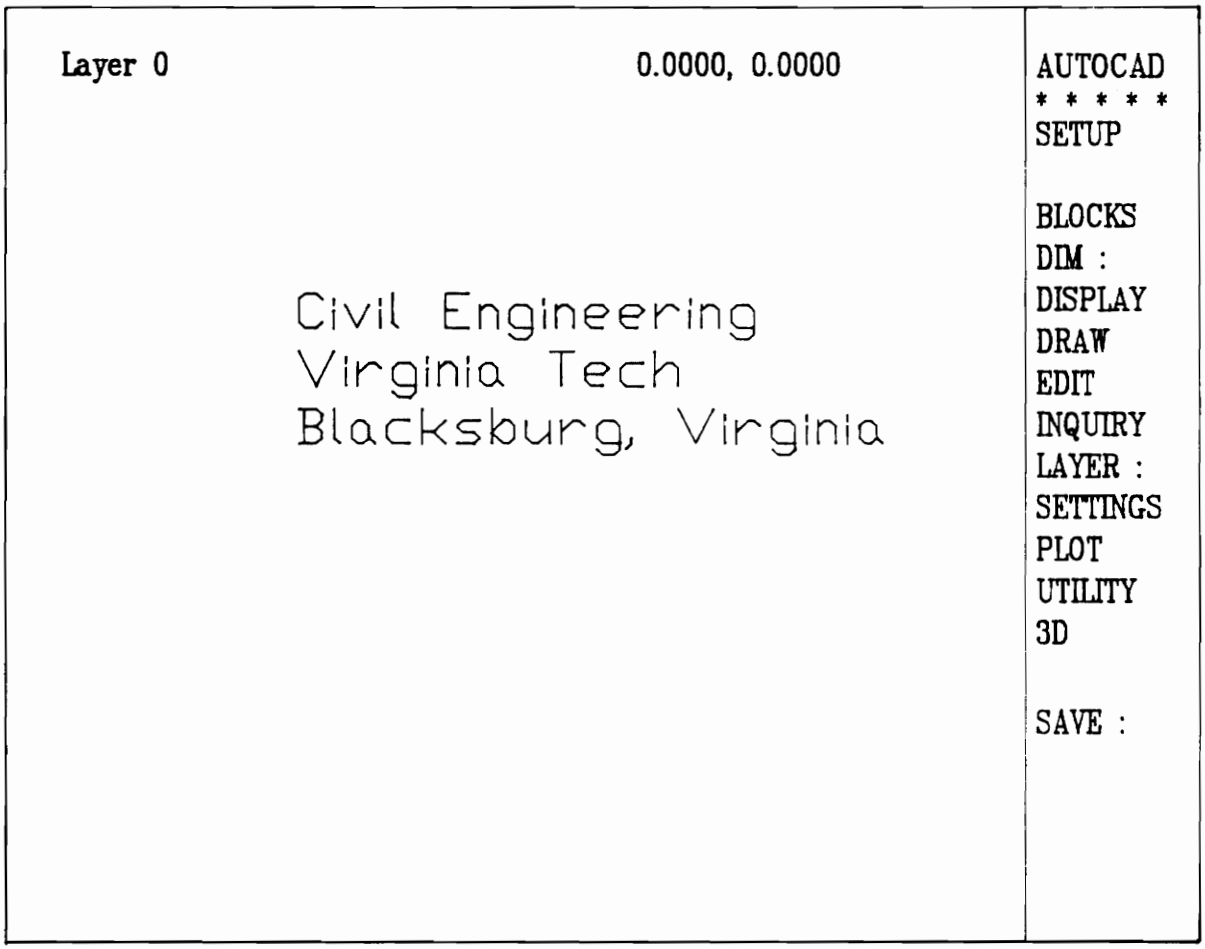

Fig 2.10 Drawing Created by Macro [ADDRESS]

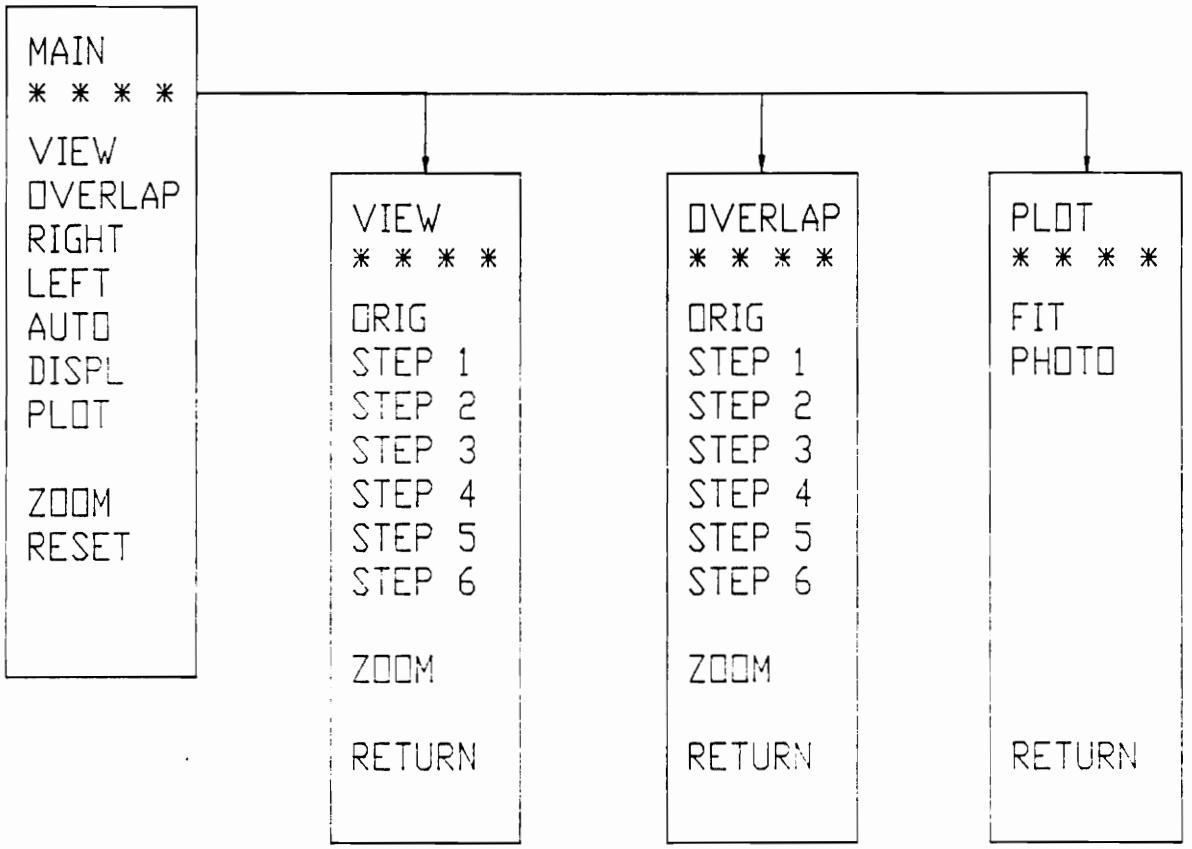

Fig 2.11 Structure of MENU File Used in This Study

CHAPTER III

RESULTS of TESTS and ANALYSES

3.1 Description of the Experimental Work at WES

This experiment was conducted by O'Neil and McDonald (1985) at Waterways Experiment Station, Corps of Engineers. The objective was to develop data that described the load-deformation relationships for regular strength and high strength steel sheet piles, under a given loading configuration. It was conducted to obtain technical data on the deformation of sheet pile systems for the St. Louis District of the Corps of Engineers as part of a cofferdam modeling project. The sheet pile system tested was comprised of three sections of sheet piles coupled together and was loaded in uniaxial tension. In the tests, load, strain and cross head displacement were recorded. Photographs and video pictures over the full loading range were also taken.

3.1.1 Specimen Preparation

A total of ten sheet pile systems was tested, including standard strength and high strength steel sheet piles (Table 3.1). The piles arrived at WES in lengths ranging from 1 ft. long to over 3 ft. long. They were cut perpendicular to the longitudinal axis to produce sections approximately 3 in. wide. Thirty pile sections were produced to be subjected to ten tests. Each test consisted of three pile sections. The two sections that would act as end pieces were cut in the web adjacent to the unused interlock. This allowed the end piece to fit into the grips of the testing machine with one-half of the section available for testing. Each section was then polished at the cut surface and scribed by a laser to make a grid in the surface. The grid was scribed on 0.125 in. centers, longitudinally and laterally, in the area of the interlocks, and 0.125 in. longitudinally, and 0.25 in. laterally on the web of pile (Fig. 3.1). This was done because the results from previous tests conducted by Shannon and Wilson (1983) indicated that a mechanical method of gaging the interlocks could be compromised by the bending of the web. As a result, it was determined that a photographic record would be used in this test to measure interlock deformations. The scribed grid serves as a reference for the deformation measurements.

In order to compare the shape of the three piece sheet pile system before and after testing, the outline of the cross section was also traced. The outline was transferred to a mylar transparency to serve as a reference of the configuration as tested.

3.1.2 Test Procedure

The set-up procedures of the ten tests were the same with only slight changes in a few tests. A top section was mounted first. Approximately 6 in. of the web was inserted into the grips. With the help of a plumb line, the bottom section was put in place and was aligned with the top section. The bottom piece also had about 6 in. in the grips. The two sections were then brought together, by lowering the testing machine crosshead, ensuring that the two sections moved on the same plane. After alignment of top and bottom pieces was insured, the center section was inserted into the interlocks. The center section was aligned with the two end sections by lining up their edges.

Several of the tests used an alternate set-up procedure. The bottom section was mounted before the top section was put in place. This was done to see if the set-up had any effect on the outcome of the tests.

When the center section was inserted into the interlocks, it was noted that the bearing of one interlock section on the other was not always continuous across the entire length of the interlock. This was due to the fabrication quality. To improve the bearing across the width of the test specimen, the pile sections were subjected to two load-unload cycles of 1000 lbs. This was an attempt to eliminate any major misalignment of the bearing points in the interlocks.

The piles were loaded at 5000 lbs. per min., from zero load to failure. The testing machine was a Baldwin 440000-lb Universal Testing Machine. Throughout the tests, photographs were taken at 1500-lb intervals when the load was under 6000 lb. and at 3000-lb

intervals thereafter to failure. All tests were conducted at the same loading rate and photographic records were taken at the same intervals.

After the tests, the outline of the cross section was traced again, so that it could be compared with the sheet pile shape which was taken before the tests.

3.1.3 Instrumentation

Bending and axial strains were recorded by strain gages bonded to the surfaces of the webs of the sheet piles (Fig. 3.1). Six Micro-Measurement type EA-06-500BH-120 gages were bonded to the steel. The gage resistance was $120.0 \pm 0.3\%$ ohms, with a gage factor of $2.04 \pm 0.5\%$. The gages were put on opposite sides of the pile web. Their orientation was along the longitudinal axis of the sheet pile specimen. The gages on the center section were placed at the center of web. The gages on the two end sections were located approximately 3 in. from the interlocks so that they were kept away from the testing machine grips.

Two Hasseblad 2-in. x 2-in. format cameras were used to record the deformation of the steel sheet piles. The two cameras were completely isolated from the testing machine to secure them from experiencing any movement during the tests. They were positioned to cover one interlock each and still have an overlap at the middle section, thus providing a full view of the test assembly (Fig. 3.1). Also, a board with six targets painted on it was placed behind the piles to serve as a reference that did not move with the piles. The six targets were covered by the cameras, too.

3.2 Results of the Experiment

The steel sheet piles used in the tests included four PS31 standard strength, four PSX31 high strength, one PS32 standard strength, and one PSX32 high strength sheet piles. In this report, they are referred to by the description in Table 3.1.

Following is a discussion of the results of the tests.

3.2.1 Failure Mechanism

All the tests failed by separation of the interlocks. The failure locations for all ten tests are listed in Table 3.1. Cracking due to the tensile stress was seen on the inside of the finger of the PSX31 high strength steel sheet pile. Cracking was not seen in other test specimens.

Since the two thumbs fall close to the line of action between the two webs, most of the load was transferred from one thumb to another when the loading began. As the load increased, the thumbs would move sideways due to the slope of the bearing surfaces in the interlocks. The movement was resisted by the pressure exerted from the opposing fingers. The load increased and the thumb kept wedging its way through the opposite thumb and finger. As a result, the finger bent outward, the bearing surface became smaller, and the two thumbs slipped further. At the moment before failure, there was no bearing surface between the thumb and the opposite finger any more. The thumb was prevented from sliding away only by the edge of the opposite finger. Greater tensile load caused the thumb to slide further off the surface of the opposing thumb and finally

out of the confinement of the finger. The interlock was totally separated and the sequence of separation was completed.

It was observed that the three sections deformed into an "S" shape during the test (Fig. 3.2). The top and bottom sections bent in one direction while the center section bent in another direction. The characteristic "S" shape was formed because of the misalignment of the center lines of the three sections. When a test was set up, top and bottom sections were set in alignment by a plumb line. However, the center section always had an offset, due to the geometry of the sheet pile section. As a result, couples were formed at the two interlocks where the center line of the center section deviated from colinearity, when tensile load was applied. The bending moment caused the pile system to bend into a "S" shape. An ideal moment diagram is also shown in Fig. 3.2. Since the ends of the top and bottom sections were fixed in the machine grips and were not allowed to rotate, the couples at the interlocks also caused a moment at the gripped ends.

3.2.2 Load versus Crosshead Movement

In the testing, an LVDT was attached to the movable crosshead of the testing machine (Fig. 3.3). It recorded the movement of the crosshead during the course of the test. Fig. 3.4 and Fig. 3.5 show the load-displacement relationships, recorded by LVDT, of standard-strength and high-strength steel sheet piles, respectively. The last six data points of curve BEBT6 (Fig. 3.4) and the first seven data points of curve USY9 (Fig. 3.5) are wrong due to malfunction of LVDT and should be ignored.

Fig. 3.4 includes both PS31 (Bethlehem Steel) and PS32 (US Steel) standard strength sheet piles. The plot shows a very consistent load-deformation behavior for all piles

except USY9 (PS32). This is reasonable because PS31 and PS32 have different geometries. The curves can be broken into three stages. First, deformation increases nonlinearly as load goes up. It is then followed by an approximately linear segment, which is expected in a typical tensile test. Finally, the deformation increases significantly again while the load only increases slightly.

The nonlinear behavior at the early stage of the plots, which is not normal in a theoretical load-deformation curve, is not unreasonable here. As mentioned in Section 3.1.2, the bearing surfaces are not always continuous over the entire length across the interlocks. When the loading began, the thumbs and fingers of the interlocks would bend in order to seat themselves under the load. Besides, when the grips tried to develop their hold on the specimen, there would be slippage. These movements caused the additional deformations during the early portion of the test history.

Beyond approximately 3 kips/in., the plots begin to have a linear load-deflection relationship. This is a typical elastic behavior for which the strain increases proportionally with stress.

At the final stage of the plot, the rapid increase of deformation implies that the interlocks begin to separate due to yielding in the interlock areas.

The behavior of high-strength steel sheet pile under tensile load is similar to that of standard-strength pile. However, the plots show a longer linear elastic portion and a shorter nonlinear portion before failure occurs. And as would be expected for high-strength steel piles, the ultimate load and deformation are higher than for standard-strength piles.

3.2.3 Load versus Deformation

The LVDT records the movement of the crosshead, including strain in steel, deformation of interlock, and slippage of the machine grips. Since the slippage can not be considered as a normal component of sheet pile deformation under tensile load, another method of measurement was used and is discussed below.

During the testing, photographic records were made as discussed in Section 3.1.3. Deformations can be obtained from the photographs. Two points on the photograph of undeformed shape were chosen and the distance was measured by using a steel rule with graduation to the 1/100th of an inch. The length was used as a reference. The same two points were measured on all the photographs taken at different loadings. The deformation was calculated by subtracting the reference length from the measured length at different loadings.

Figs. 3.6 to 3.15 give the load-deformation curves obtained from the photographic records. In each figure, there are three different curves referring, respectively, to deformation for bottom, top, and total gage length which are shown in Fig. 3.1. These plots give saw-toothed graphs, unlike those obtained by using the LVDT data. It is the result of the measuring method used here. Since the steel rule only had divisions up to 0.01 inch, accuracy beyond that level would not have been possible without better instruments. There is also the possibility of minute variations in the photographic scale from photo to photo due to processing deficiencies. However, the overall trends of data are still valid. It is hard to tell the load-deformation relationship from these saw-toothed plots. A regression analysis can be used to evaluate the nature of the data.

The plots represent the deformation between the extremes of two gage lengths. They give a deformation smaller than that obtained from LVDT data because the slippage of testing machine grips is excluded. Only the strain in steel and deformation of the interlocks are included.

3.2.4 Load versus Bending Strain

Bending strain was recorded by the six gages attached to the pile assembly (Fig. 3.1). The plots of load versus bending strain are shown in Figs. 3.16 to 3.25. The three curves in each figure are plots of the average of readings of top, bottom, and middle gage pairs, respectively. A positive result represents bending in one direction and a negative result represents bending in the opposite direction.

It is observed that the bending strain increased rapidly as the load was applied and then it became approximately linear during most of the rest of the testing. This can be explained by realizing that the pile system would bend under the tensile load because of the couples produced by the offset of the center section. When the bending of the test assembly was sufficient to match the couples, the system would just stay in the same configuration. Near failure, the thumb and finger of an interlock would be free from each other's constraint and the interlocks were able to rotate. The rotation relieved the moment on the connection and thus relieved the strain in the web. This is shown by the rapid drop of the stress-strain curve which represents the strain of the failing end piece.

The characteristic "S" shape, typically observed when the pile system deformed, is also confirmed here. The top and bottom gage pairs always show bending in one direction

while the middle gage pair shows bending in the opposite direction. The reason has been explained in Section 3.2.1.

In the plot of load-bending strain relationship for PSX32 high-strength sheet pile, the strains are inappropriately high when compared with other tests. Although not confirmed, it is suspected that the gages were not set correctly in that test.

3.3 Result of Finite Element Program

To study the behavior of a sheet pile under tensile load, a finite element model of sheet pile was tested using the computer program described in Chapter Two. The new model, as described in the previous chapter, contains a full-length sheet pile with both of its interlocks connected to two half-length sheet piles. The new model was intended to simulate the pull-out tests conducted at WES (1985). The sheet pile geometry was taken directly from the transparency provided by WES so that a comparison between experimental results and analytical results would be possible. Following is the result from the finite element program.

3.3.1 Load versus Deformation

The finite element program gives the updated coordinates of every node at the end of each load step. Displacements of the nodes can be obtained by calculating the difference of the node coordinates at different load steps. In the tests conducted at WES, three reference points, which are the locations of the three gage pairs, were used to find the deformations of the pile assembly. The procedure is discussed in the previous section.

Three nodes, corresponding to the three reference points, are used to find the deformation. A plot of the load-deformation relationship predicted by the computer program is shown in Fig. 3.26. Displacement along the X-axis, i.e., longitudinal direction, is taken as the deformation in the plot. The curves in the plot stop at the point where loading equals 10.36 kips/in., because the finite element program fails to converge after that load step. The plot shows a nonlinear load-deformation relationship which is expected in a nonlinear problem like sheet pile interlock analysis.

3.3.2 Deformed Shapes

The deformed meshes of the interlocks at different load steps are shown in Figs. 3.27 to 3.32. A magnification factor of ten is used for the nodal displacements to show the response of the pile assembly more clearly. However, the magnification factor also causes some overlaps in the interlock area. The overlap would not exist if the plot were presented in the original scale.

The deformed meshes show that the piles deform by bending until sufficient deformation causes the interlocks to separate. Although the loading stops at 10.36 kips/in., before the interlocks separate, the slippage between thumb and finger of the interlock can be observed.

The characteristic "S" shape of the pile system observed during the experiment is also shown in the plots. The cause for this characteristic deformed shape is the offset of the center section with respect to the two end sections. Detailed discussion is presented in Section 3.2.1.

3.4 Results from AutoCAD

As stated before, the purpose of adopting AutoCAD in this study is for easier interpretation of finite element program results. It is intended to display the deformed shapes on a computer screen so that the response of sheet pile under tensile loading can be observed more closely by overlaying or zooming. Several examples are presented in the following sections.

3.4.1 Overlaying

One of the biggest advantage of using AutoCAD is its capability to show two drawings simultaneously. By showing two drawings at the same time, an overlay effect is produced. Differences between two drawings are easier to tell if they are overlaid.

Looking at one single plot of the deformed shape of sheet pile at a certain load step, it might not be easy to see how it differs with the plots of sheet piles at other load steps. However, by overlaying them, the difference is clear and easy to interpret.

As mentioned in Chapter Two, shapes of sheet piles under different loading are stored in different layers of a big drawing file. Turning a layer on or off will show or hide the drawing put into the layer. To see an overlay picture, one just needs to turn on the desired layers and to shut off all other layers. One example is shown in Fig. 3.33. It is an overlay picture of the original shape and the deformed shape at load step 3. It is produced by turning on layer S0 which stores the original shape, and layer S3 which stores the deformed sheet pile shape at load step 3. The bending of the web and move-

ment of the interlock can be observed here, while looking at a plot of load step 3 alone, they might not be detected.

More than two drawings can be displayed at the same time, too. Fig. 3.34 shows the overlay picture of sheet piles at load step 0 (undeformed), at load step 3, and at load step 5. It is generated by turning on layer S0, S3, and S5 while all other layers are shut off.

3.4.2 Zooming

Another feature of AutoCAD is that it can zoom in or zoom out on a drawing to change the magnification factor, i.e., to make a drawing larger or smaller. There are several ways to zoom in on a drawing. The one adopted in this study requires the choosing of a center point and a magnification factor. There is no limit for the magnification factor. To simplify the operation procedure, a relative magnification factor of 3 is set as default. After choosing a center point, the drawing is enlarged three times automatically.

The purpose for using this feature is to study the movement at contact surfaces more closely. When the whole assembly is presented on the terminal screen, it appears at a scale too small to observe the movement in the interlock area, although the response of the pile assembly is clear. An enlarged picture of the interlock will provide a better view for closer study.

A magnified drawing of the top interlock at load step 3 is presented in Fig. 3.35. The drawing shows slippage between the contact faces, which might not be noticed in a plot like Fig. 3.29. This feature can also be used with an overlay picture as shown in Fig.

3.36, which is obtained by enlarging the drawing shown in Fig. 3.35 at the center of the interlock.

With this feature, any interested portion of the sheet pile system can be closely studied in any desired drawing scale.

3.4.3 Miscellaneous

Several options in the MENU developed in the study are designed to provide some convenient functions (Fig. 3.37).

There are two items called [RIGHT] and [LEFT]. When they are selected, AutoCAD will bring the right or left interlock to the center of screen, depending on the item selected. The drawing scale will remain the current one. This function is provided because the interlocks are usually the portions of interest in this study.

[RESET] serves a very simple but important function. It puts the whole pile system back to the center of screen and resets the magnification factor. In another word, it restores everything back to the beginning stage.

[AUTO] brings up a sequence of plots, starting from load step 0 to the last load step. The sequence is driven by hitting the space bar on the keyboard. No other operation is available before the sequence is through. This is intended to give the user an idea of how the piles deform from the beginning to the end.

Although drawings on a computer screen are very helpful, they can only show on a monitor and can not be carried from one place to another place. A plot on paper is al-

ways necessary. The item [PLOT] is written to provide this function. There are two sub-options, [FIT] and [PHOTO], under this [PLOT] option. [FIT] plots everything displayed on the screen and fits them into the paper used on the plotter. [PHOTO] also plots everything shown on the monitor, but it scales down the plot to the same scale as the photographs were made. It is intended that the plot can be used to make a transparency which can be put over a photograph for comparison. However, it should be noticed that this option is applicable solely to the photographs used in this study. The macro instruction must be rewritten if photographs with different scales are to be compared.

[DISPL] has the ability to measure the distance between any two nodes. After [DISPL] is selected, a small "target" box will appear on the screen. By selecting two nodes with this box, the distance will be displayed in the command line on the text screen.

Table 3.1 Location of Interlock Failure (adapted from O'Neil and McDonald (1985))

Test Specimen	Failure Location	Cracking
PS31 SS, BET01	Bottom	no
PS31 SS, BET02	Bottom	no
PS31 SS, BET03	Top	no
PS31 SS, BET04	Bottom	no
PSX31 HS, BETB5	Top	yes
PSX31 HS, BETB6	Top	yes
PSX31 HS, BETB7	Top	yes
PSX31 HS, BETB8	Bottom	yes
PSX32 HS, USY9	Bottom	no
PS32 SS, USR10	Bottom	no

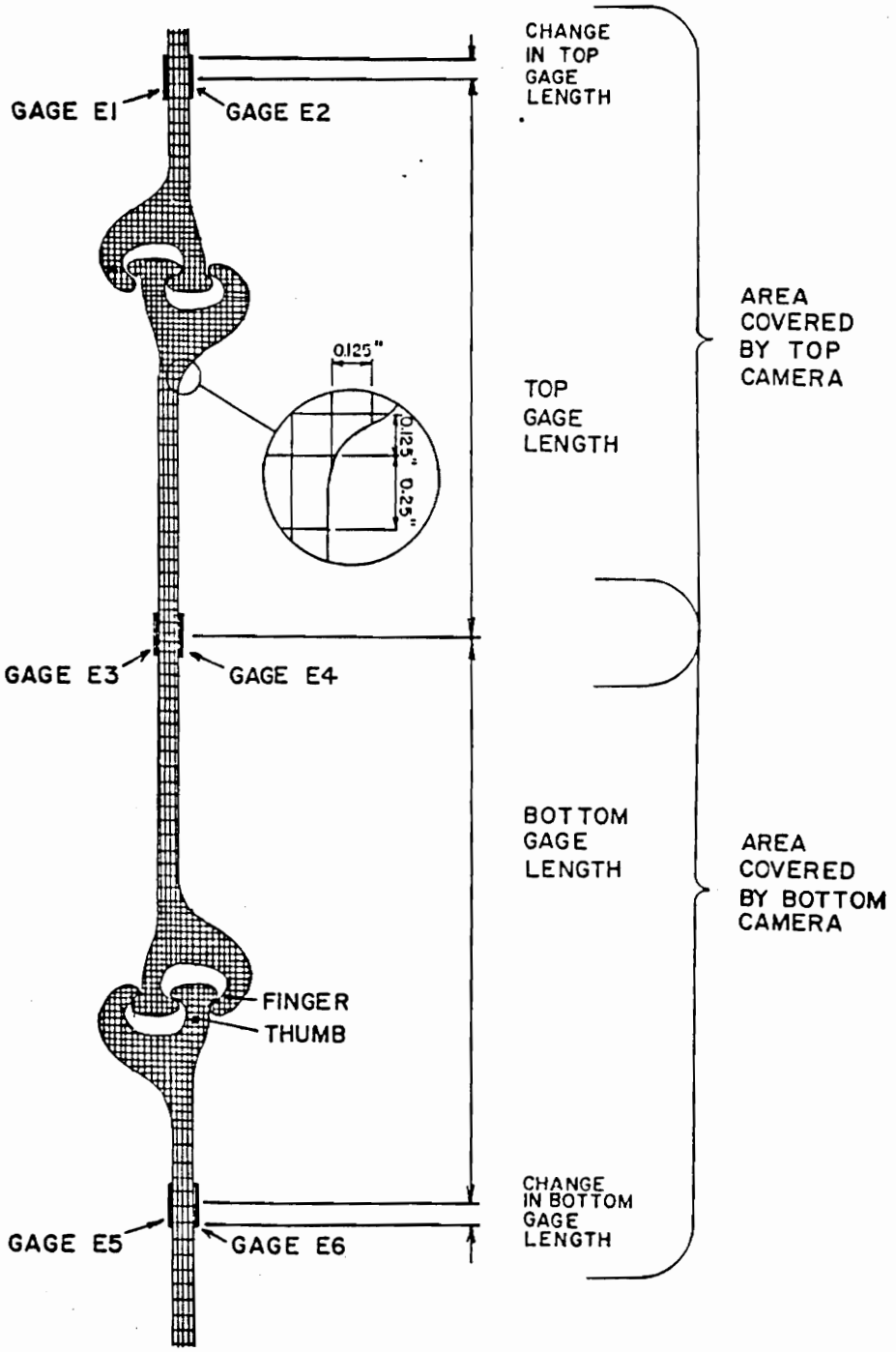

Figure 3.1 Configuration of Test at WES (from O'Neil and McDonald (1985))

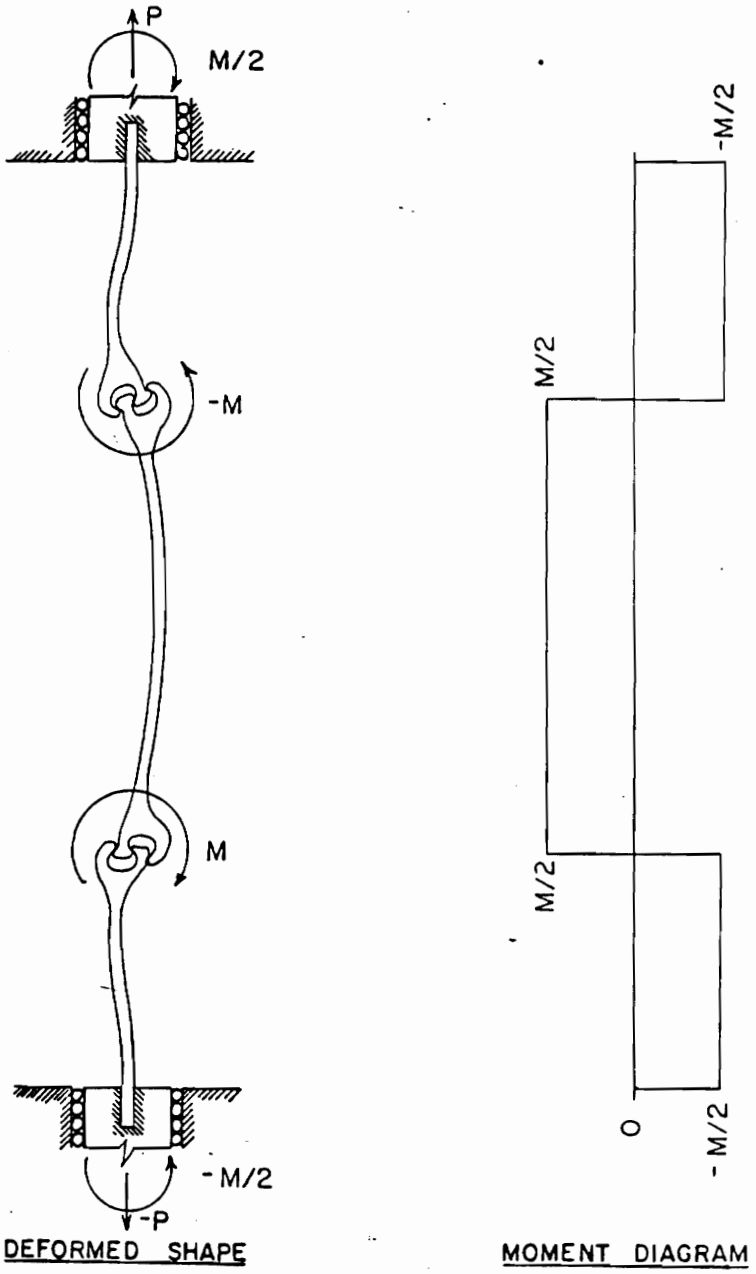

Figure 3.2 Deformed Shape and Moment Diagram (from O'Neil and McDonald (1985))

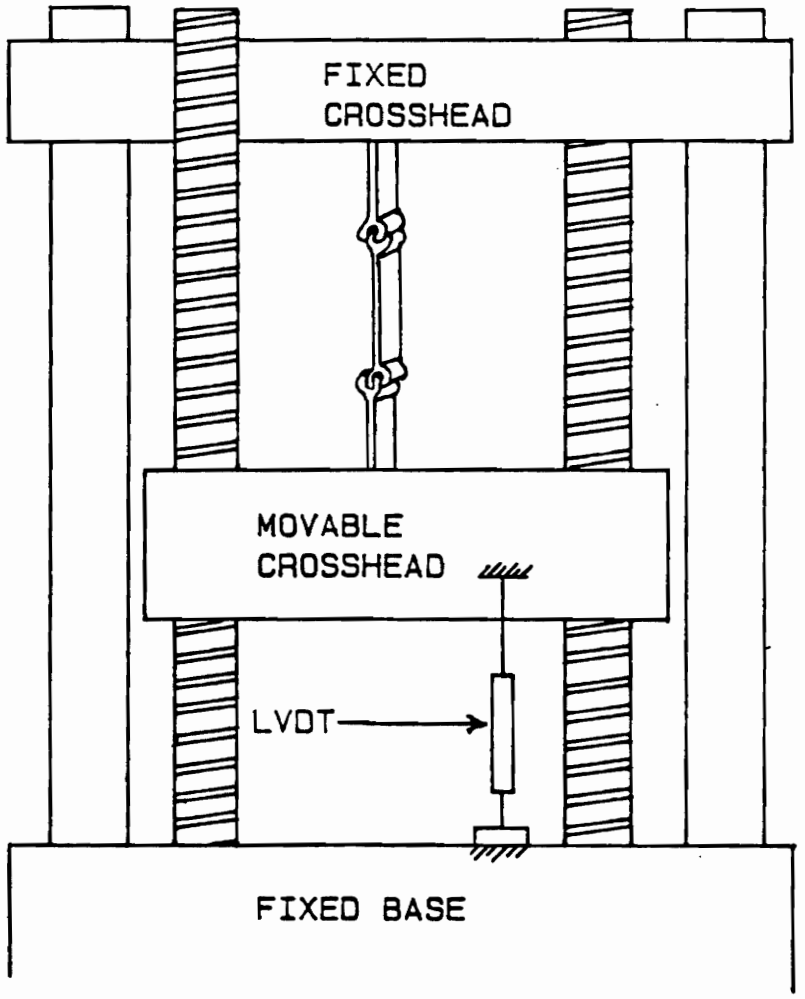

Figure 3.3 Plot of LVDT Orientation (from O'Neil and McDonald (1985))

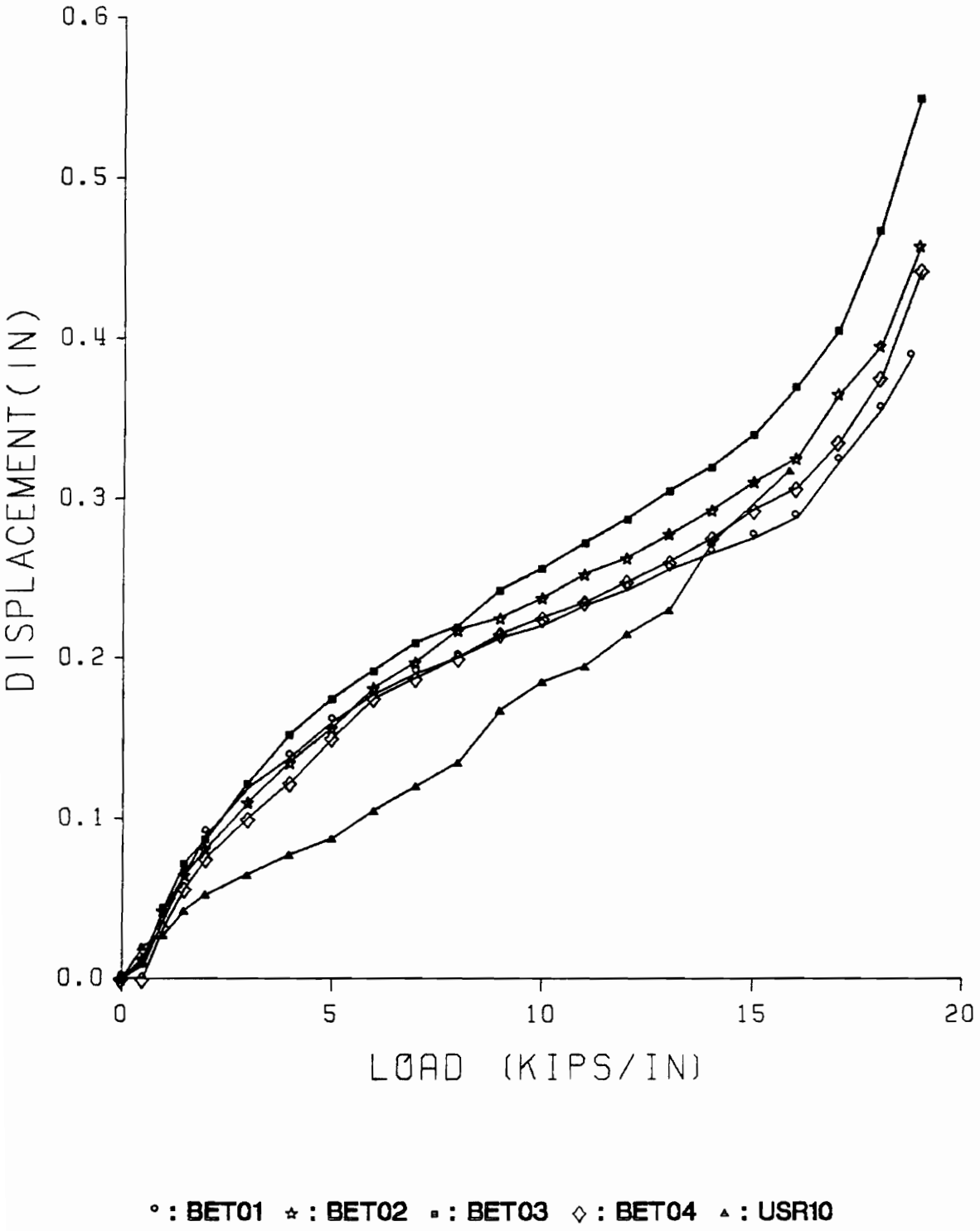

Figure 3.4 Load-LVDT Displacement Relationship for Standard Strength Sheet Pile

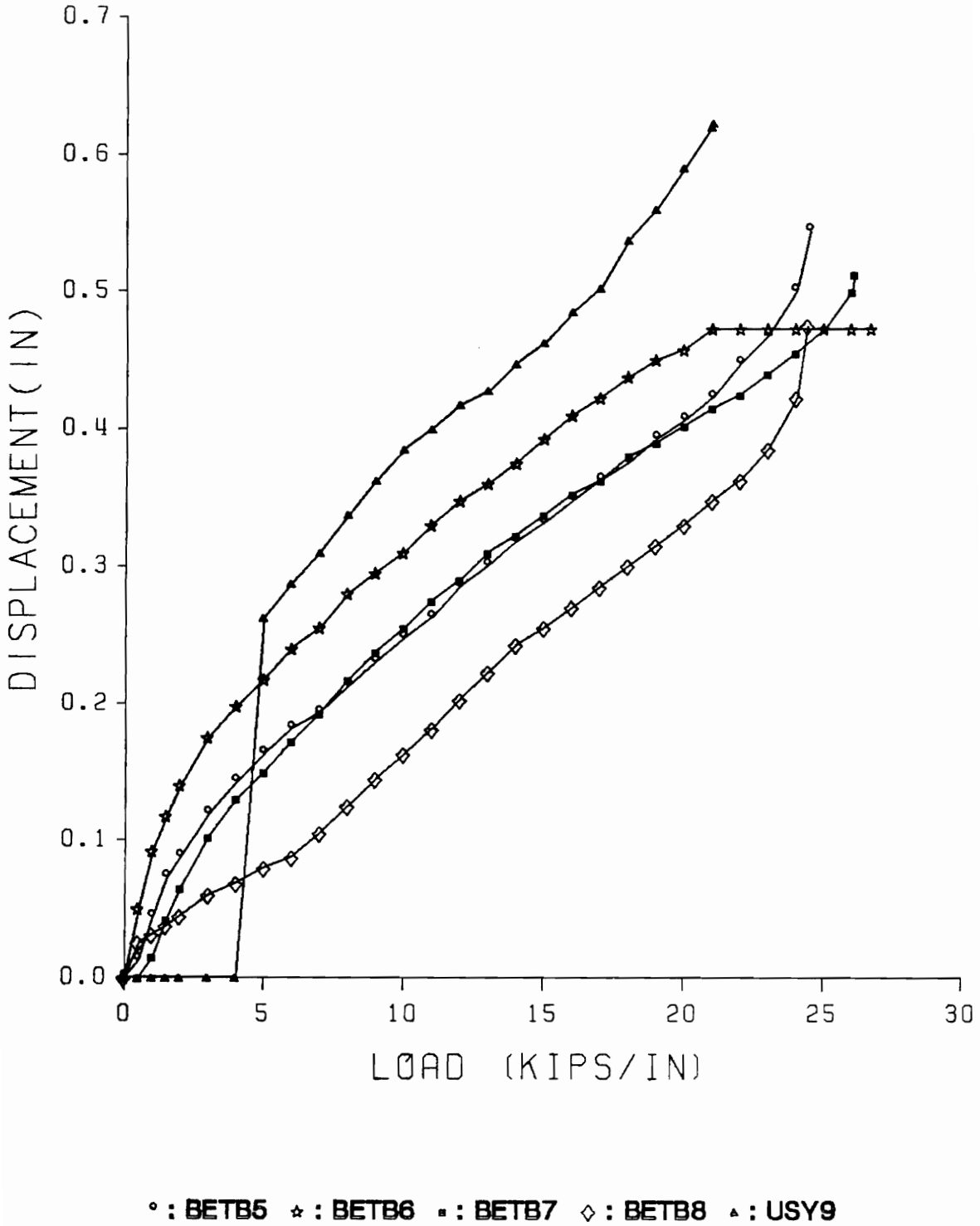

Figure 3.5 Load-LVDT Displacement Relationship for High Strength Sheet Pile

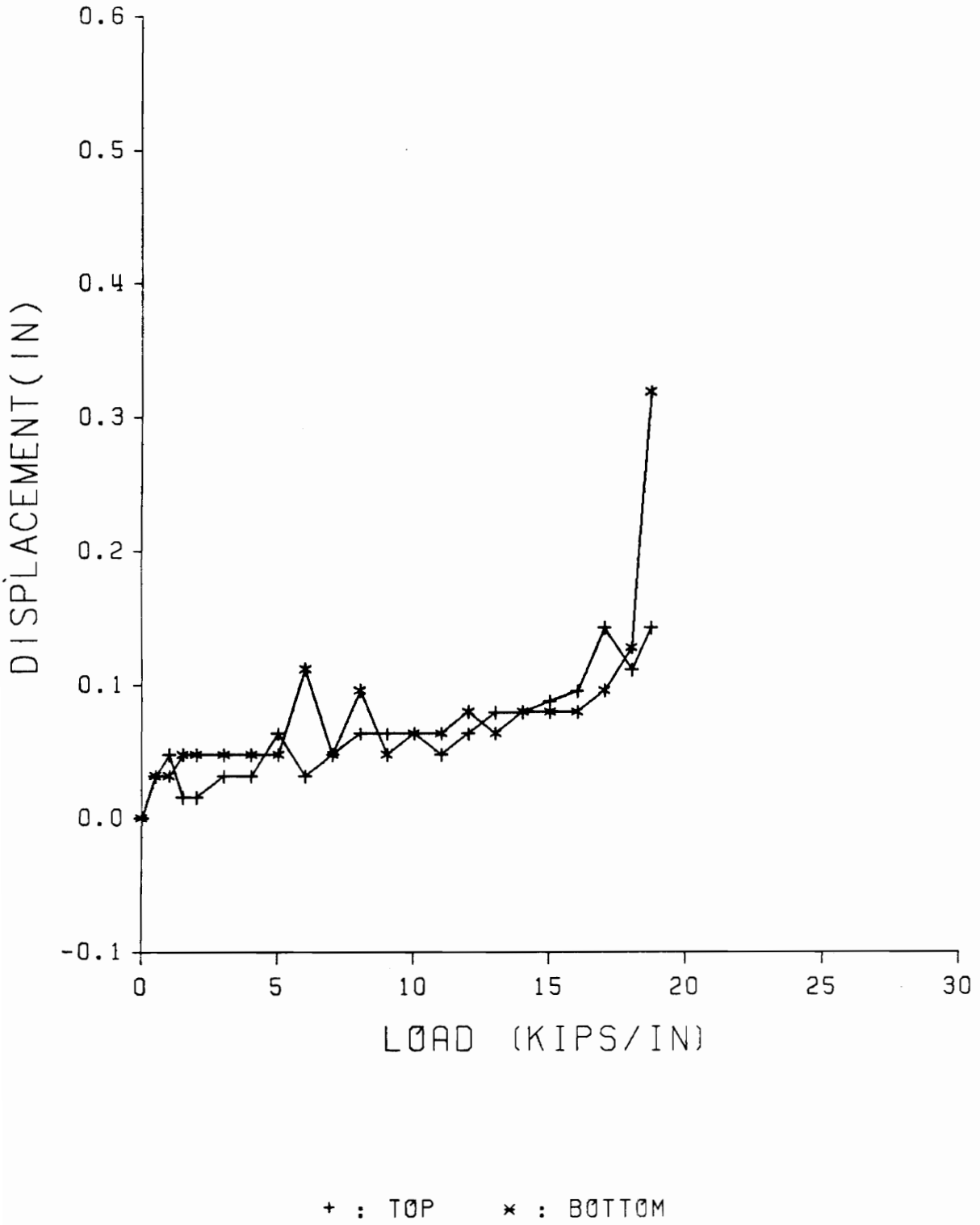

Figure 3.6 Load-Deformation Relationship of BET01 (PS31)

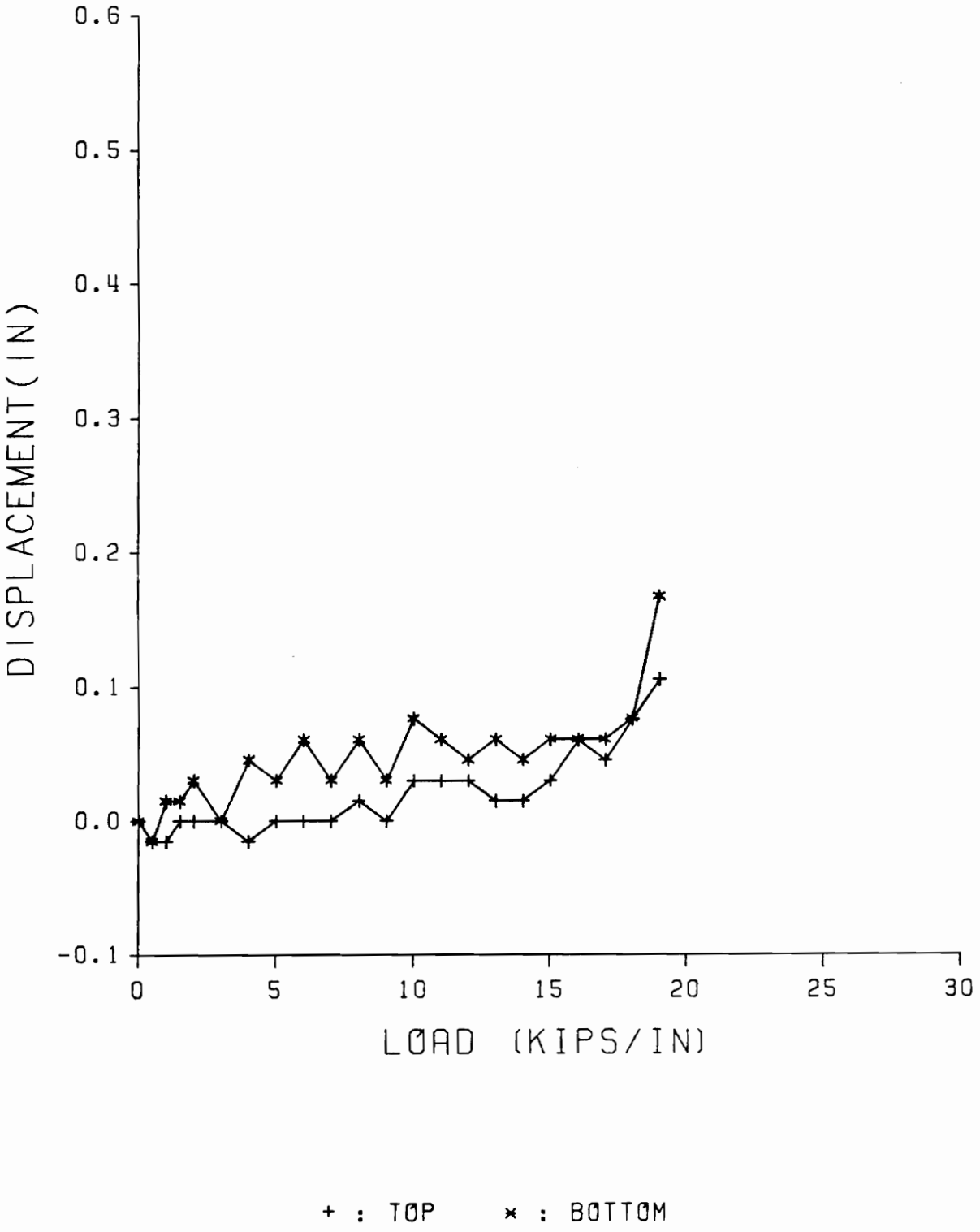

Figure 3.7 Load-Deformation Relationship of BET02 (PS31)

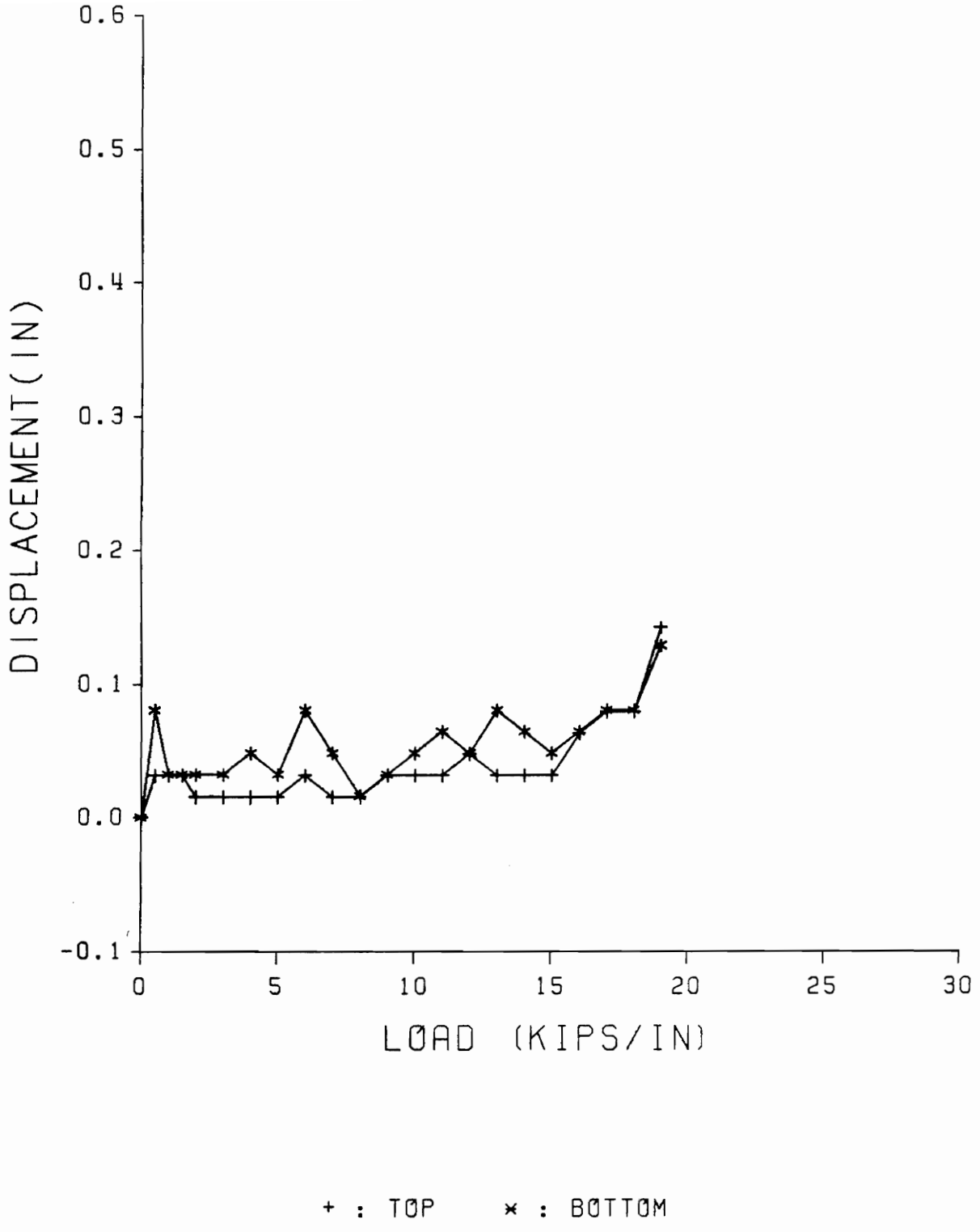

Figure 3.8 Load-Deformation Relationship of BET03 (PS31)

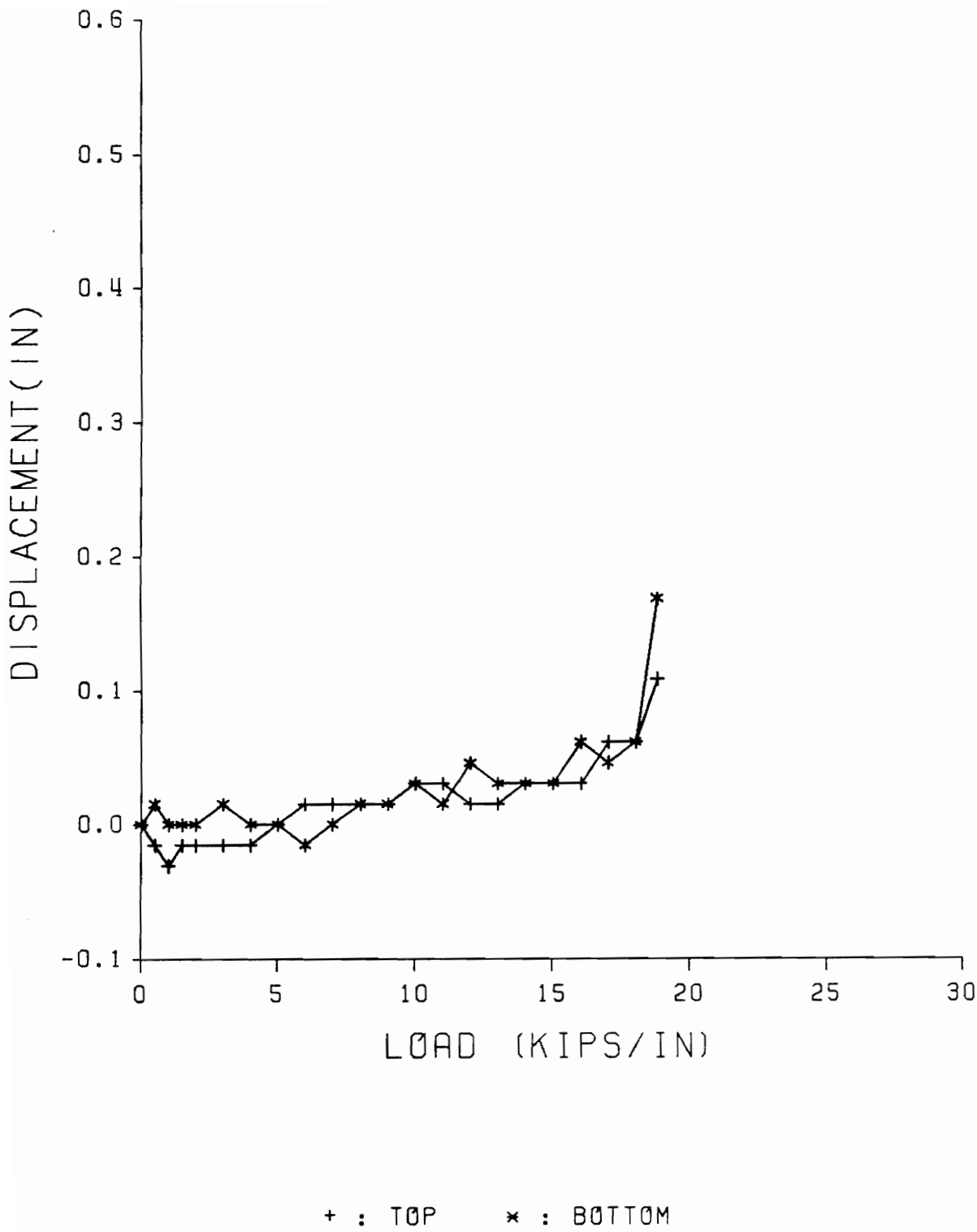

Figure 3.9 Load-Deformation Relationship of BET04 (PS31)

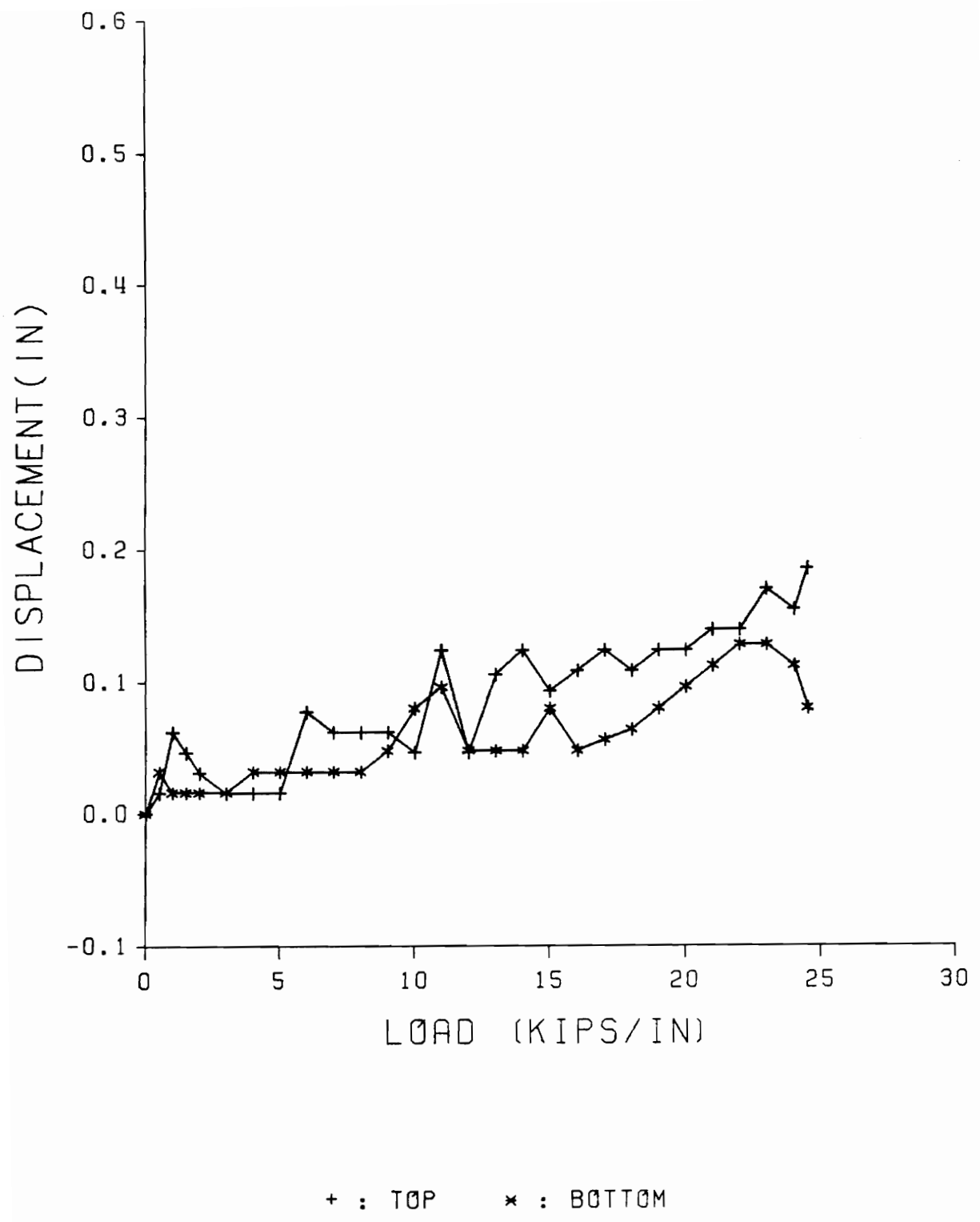

Figure 3.10 Load-Deformation Relationship of BETB5 (PSX31)

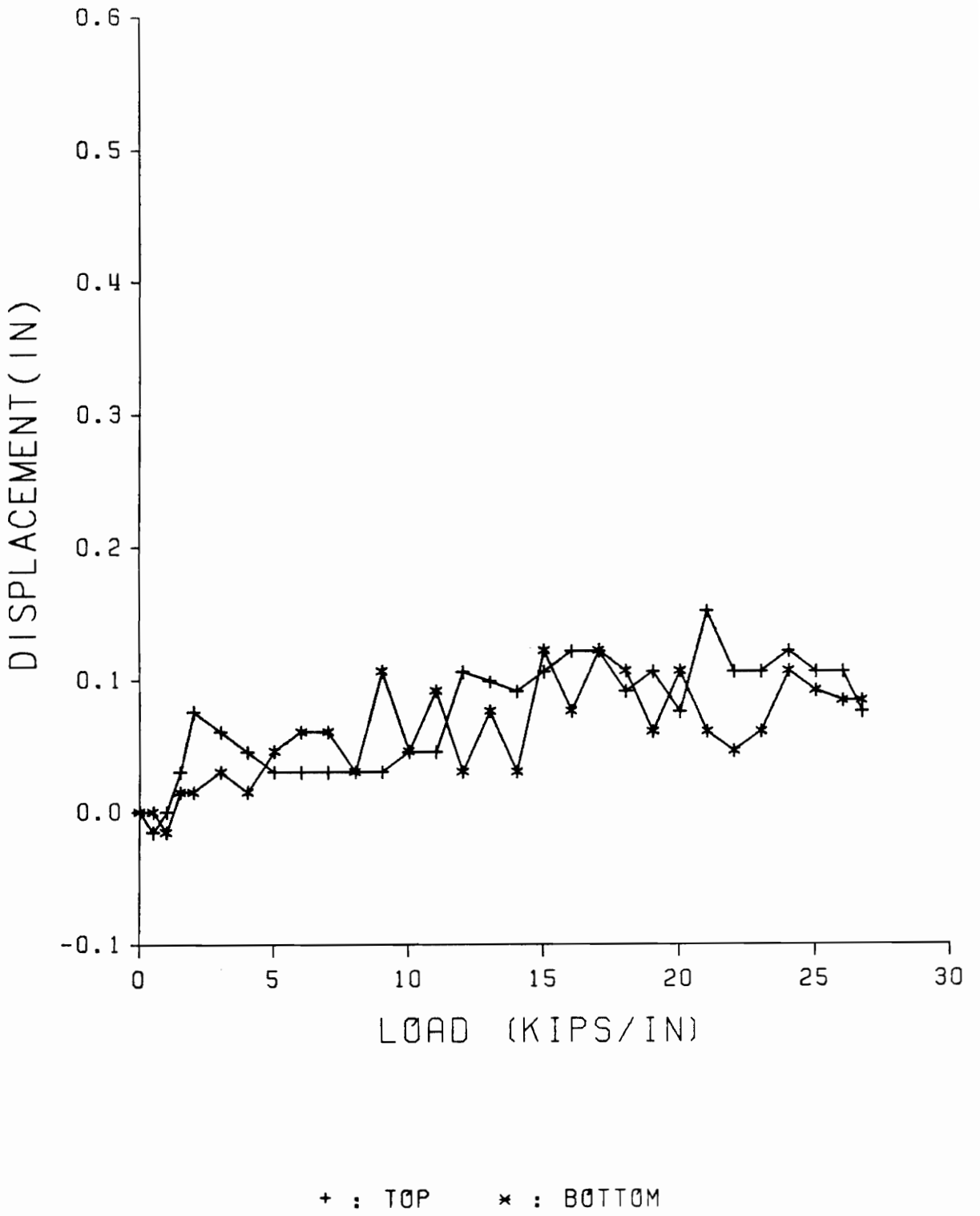

Figure 3.11 Load-Deformation Relationship of BETB6 (PSX31)

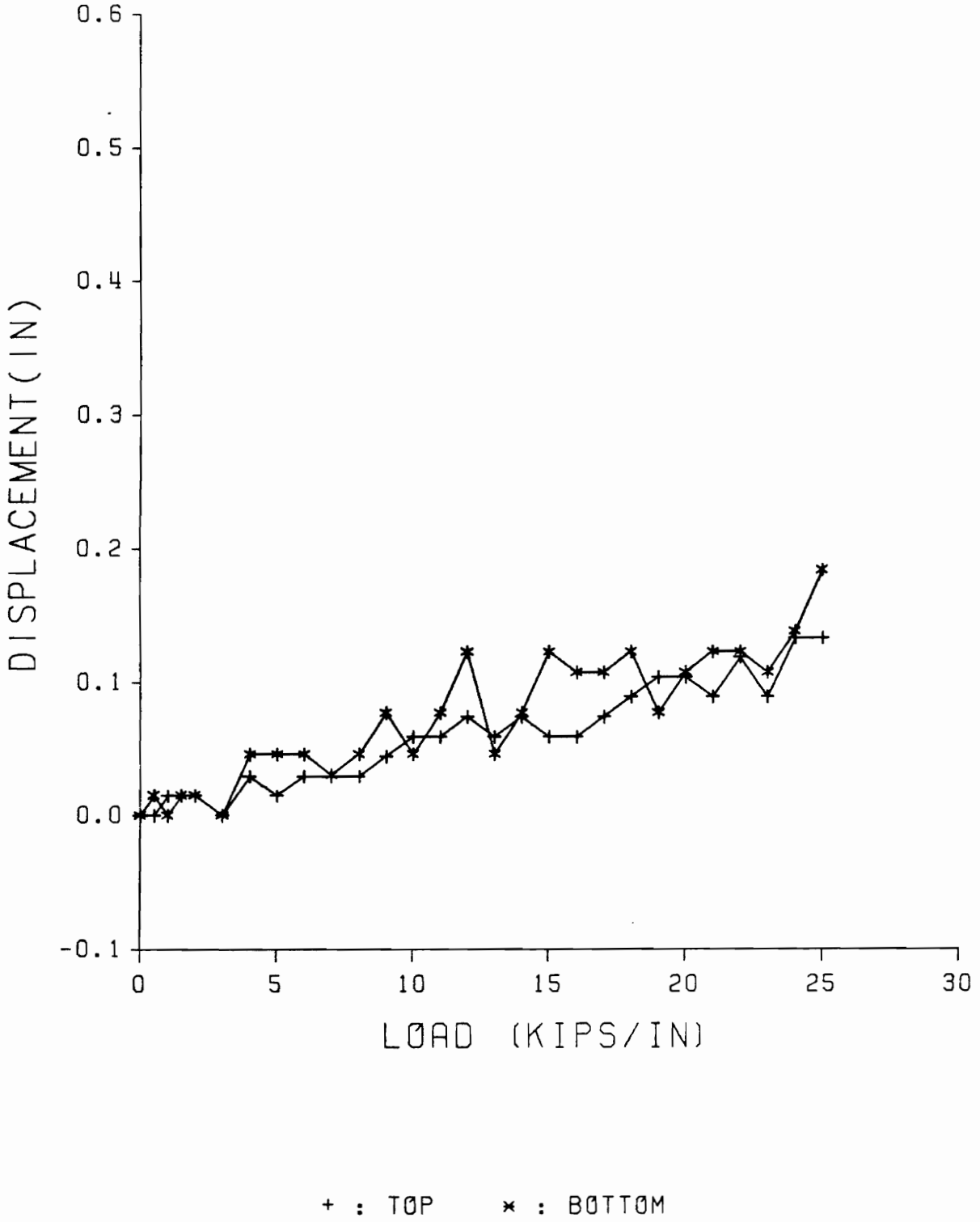

Figure 3.12 Load-Deformation Relationship of BETB7 (PSX31)

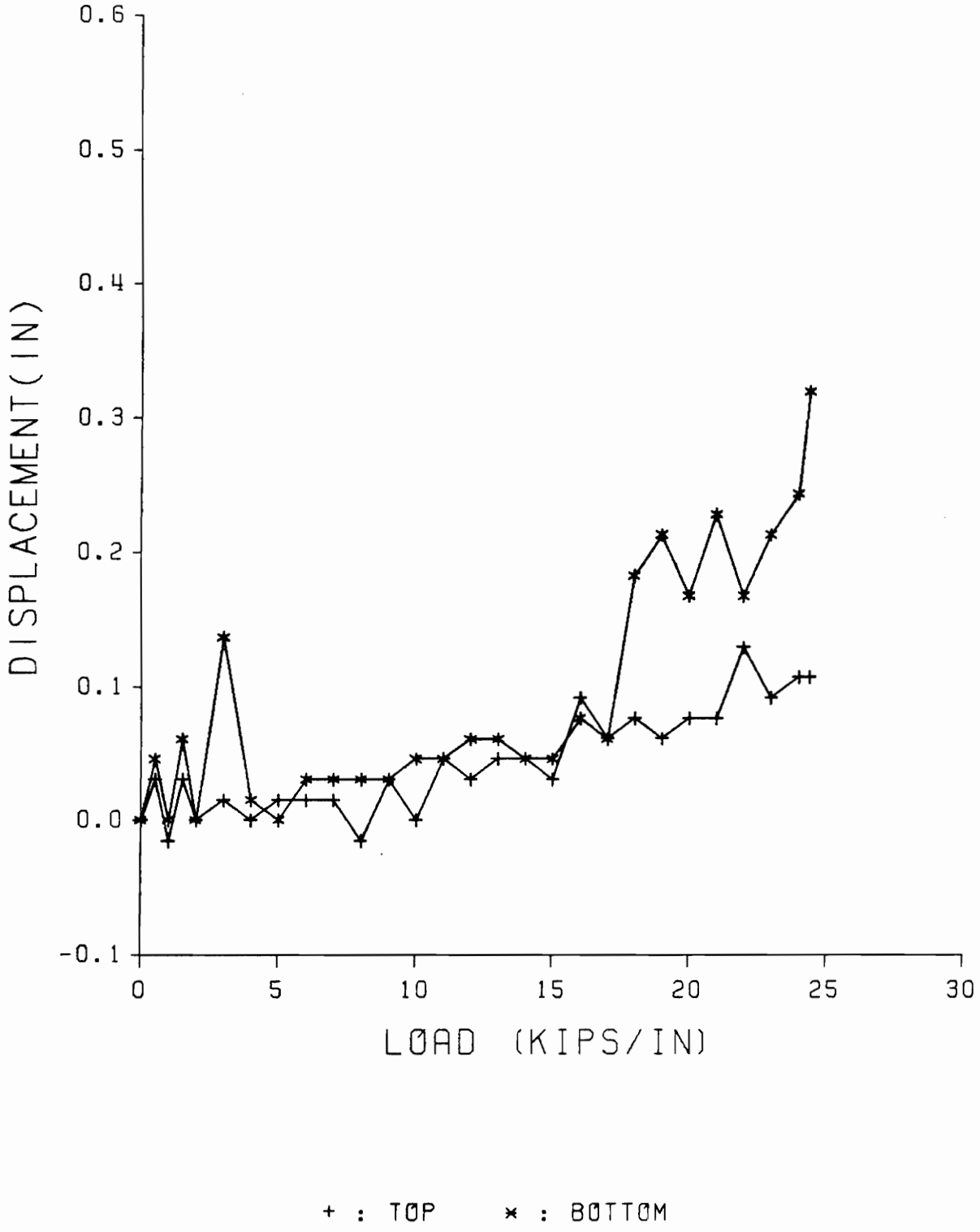

Figure 3.13 Load-Deformation Relationship of BETB8 (PSX31)

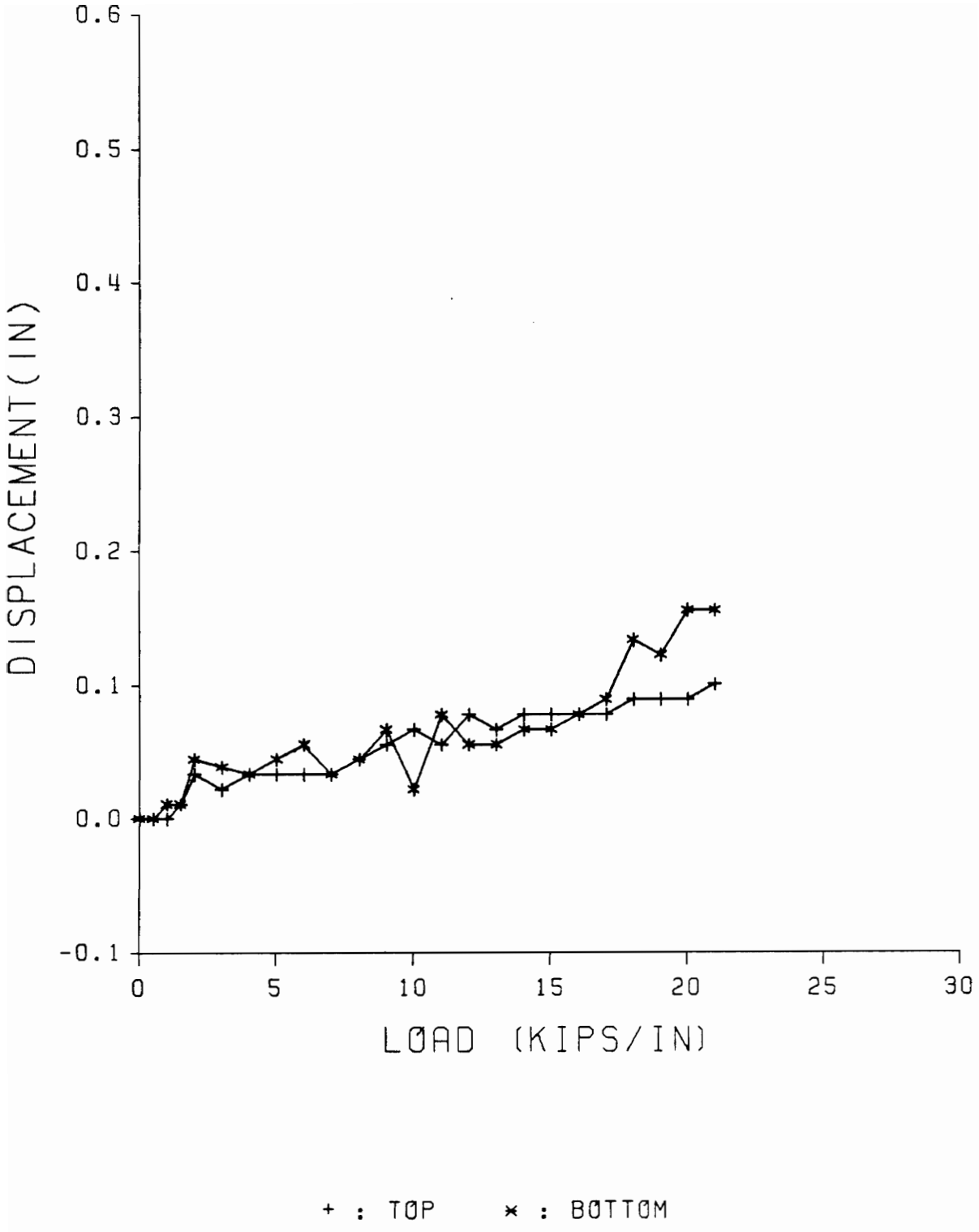

Figure 3.14 Load-Deformation Relationship of USY9 (PSX32)

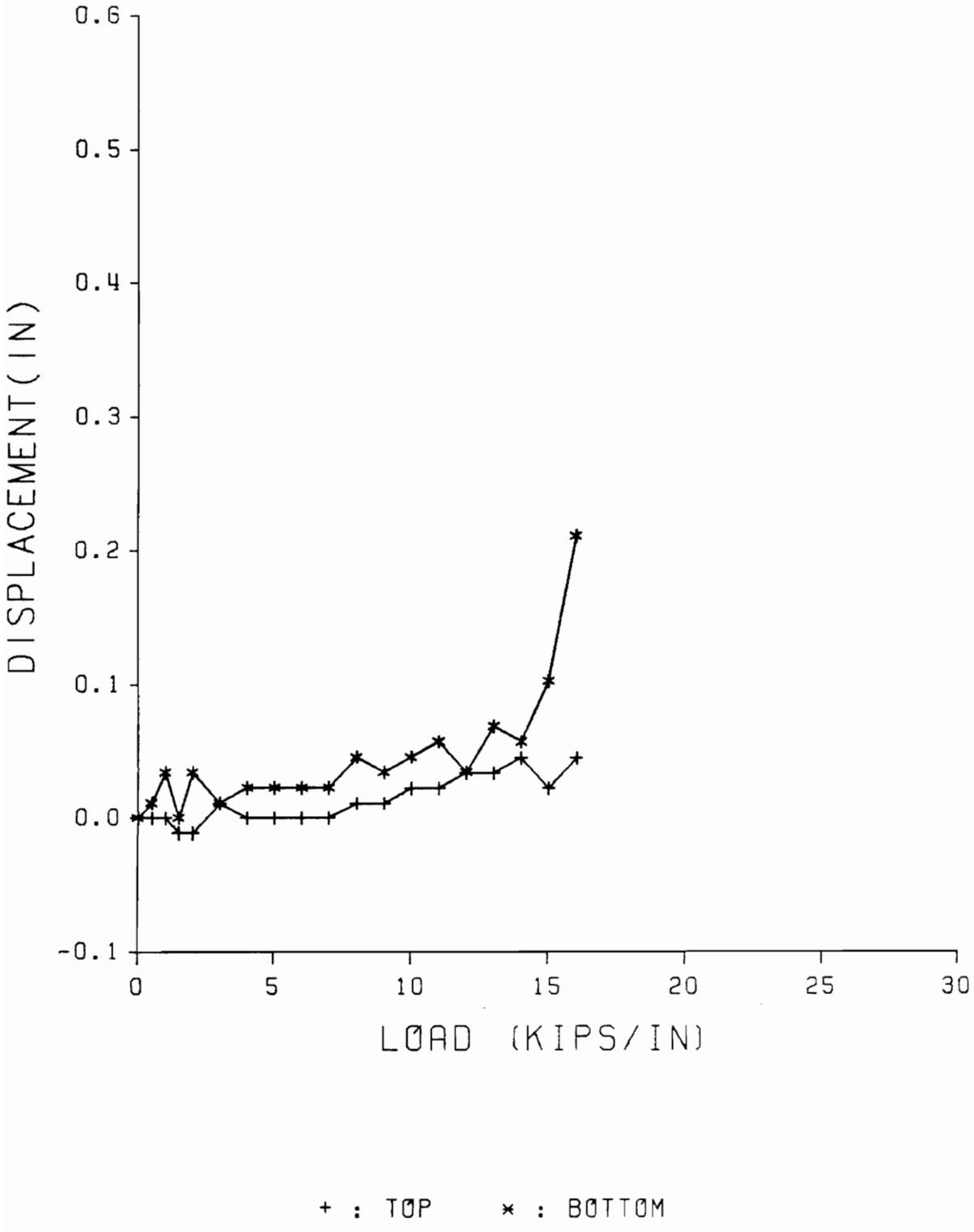

Figure 3.15 Load-Deformation Relationship of USR10 (PS32)

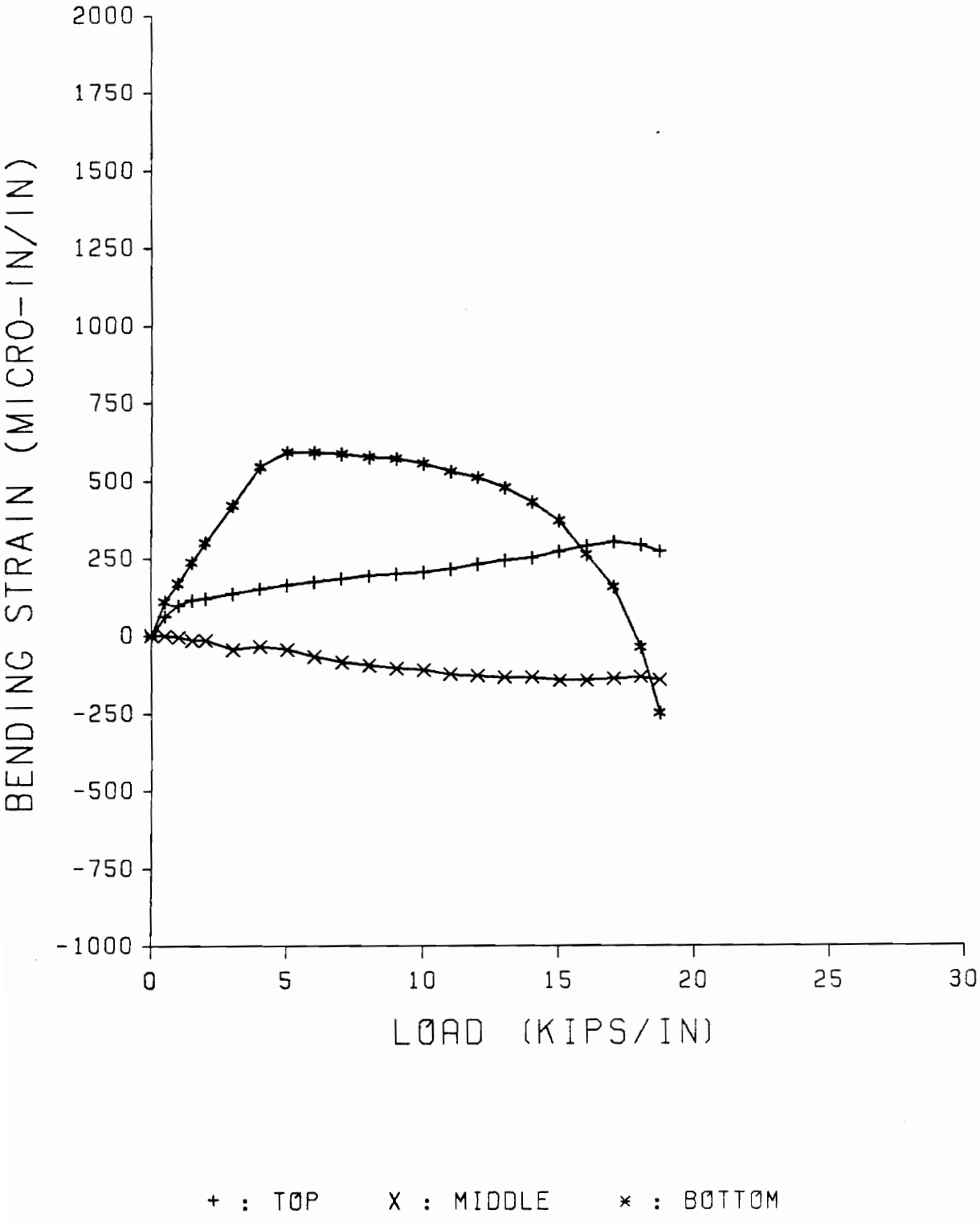

Figure 3.16 Load-Bending Strain Relationship of BET01 (PS31)

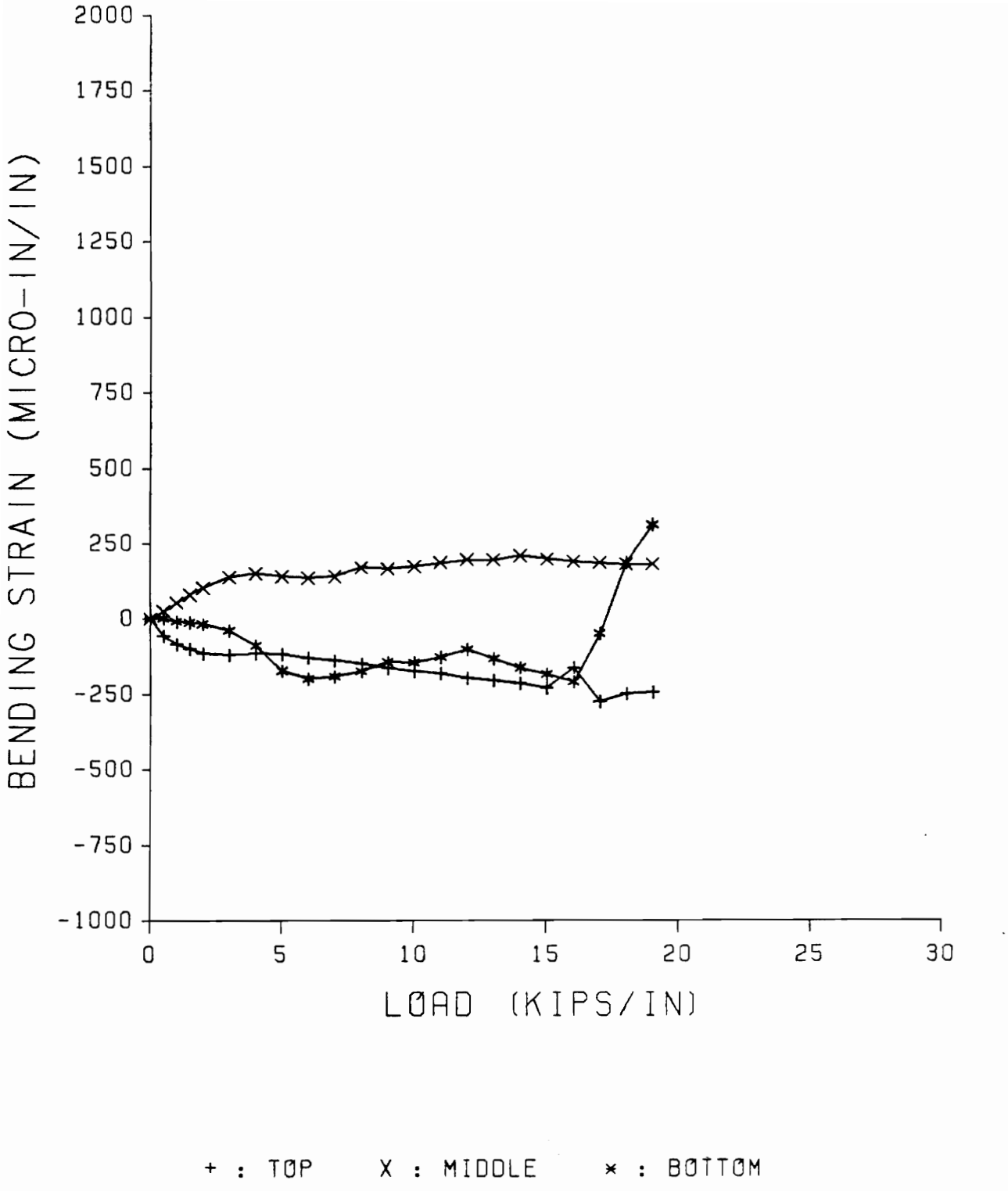

Figure 3.17 Load-Bending Strain Relationship of BET02 (PS31)

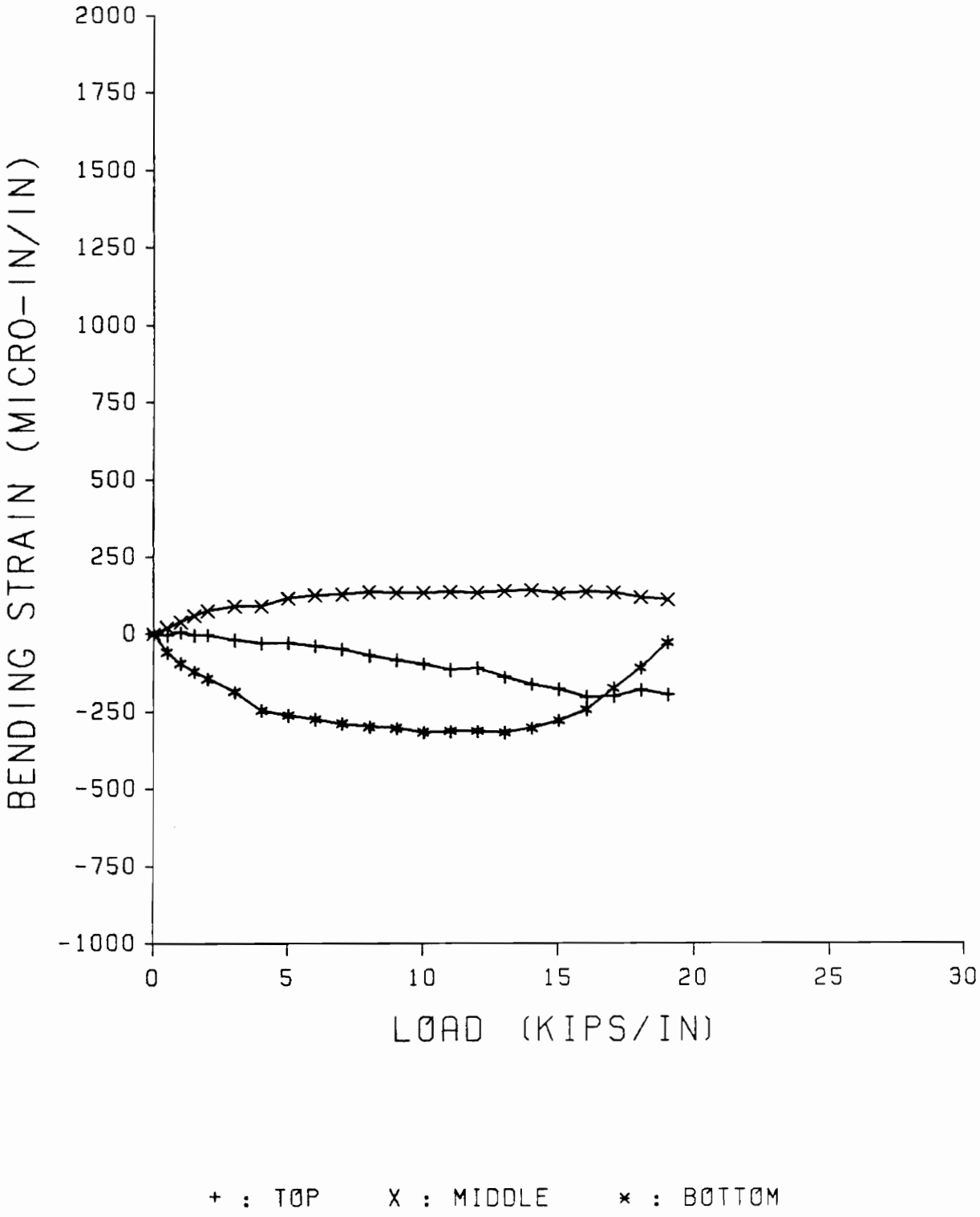

Figure 3.18 Load-Bending Strain Relationship of BET03 (PS31)

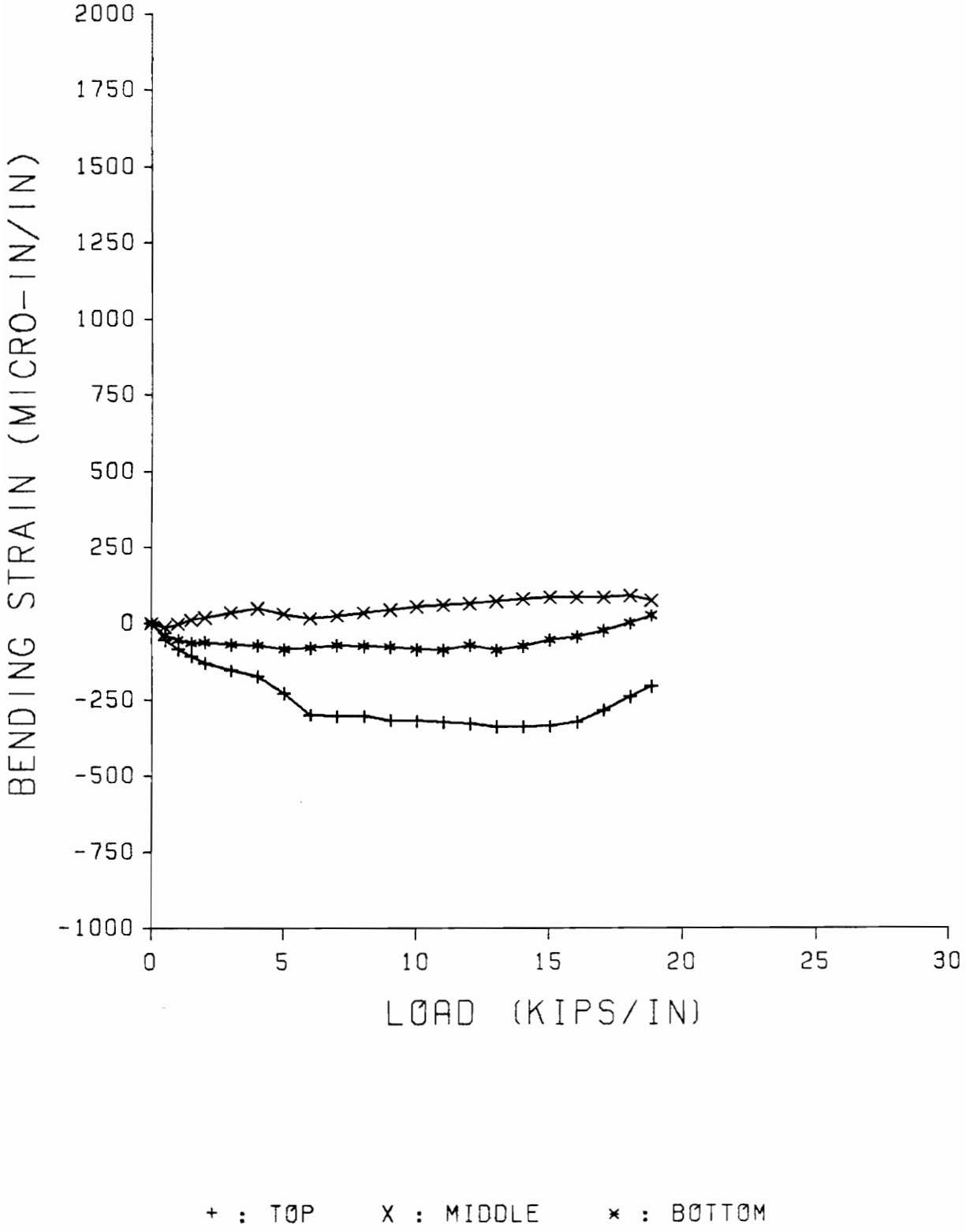

Figure 3.19 Load-Bending Strain Relationship of BET04 (PS31)

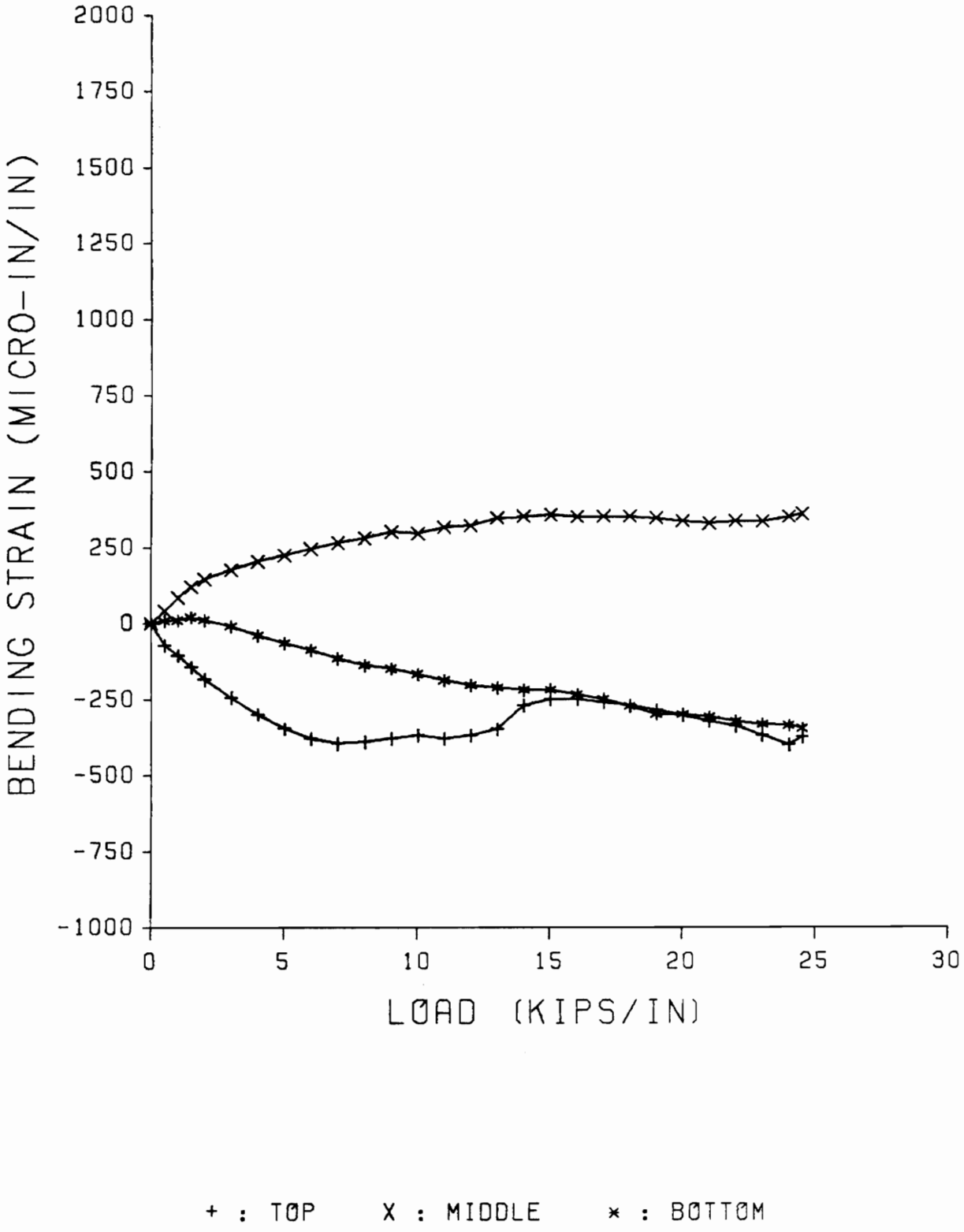

Figure 3.20 Load-Bending Strain Relationship of BETB5 (PSX31)

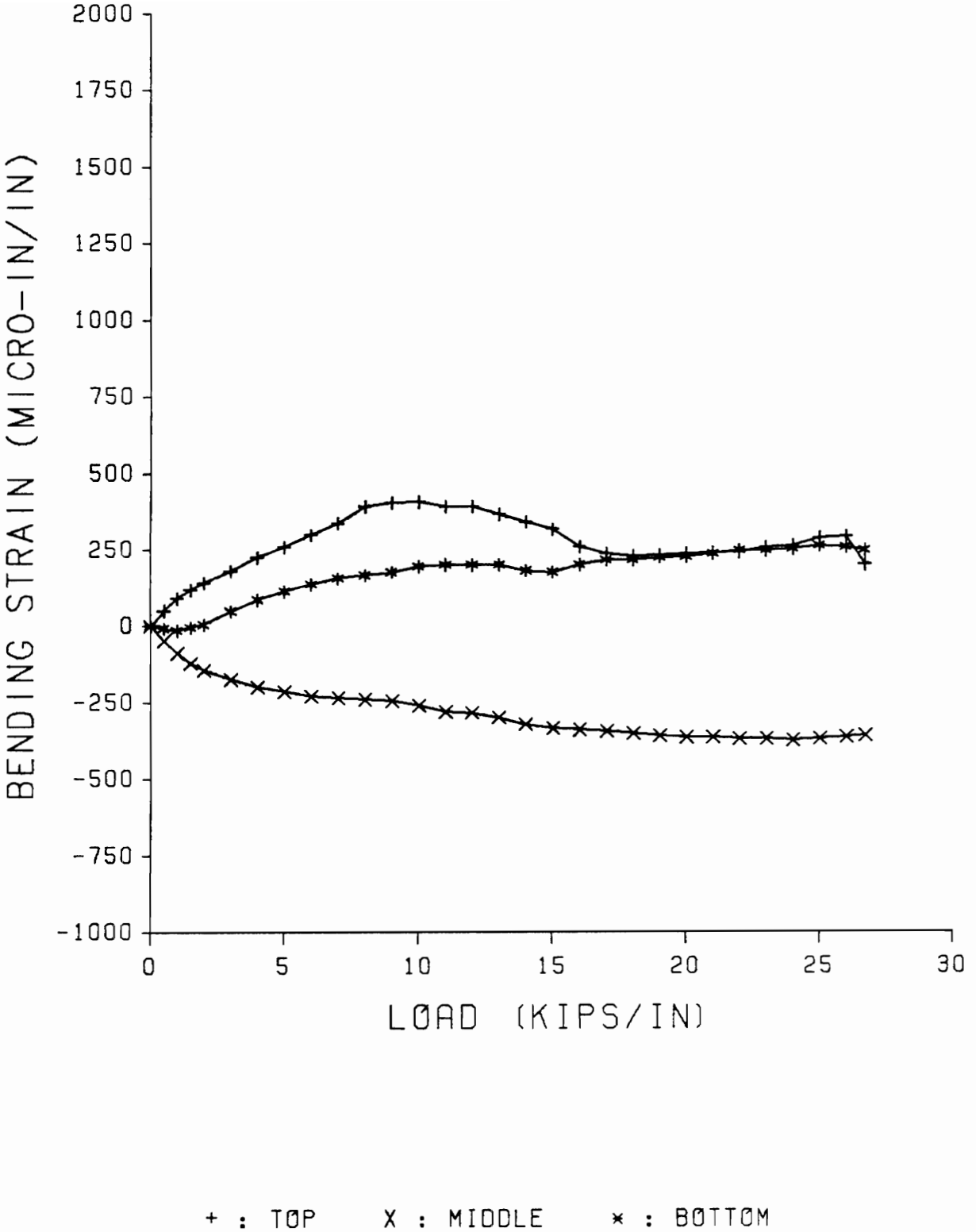

Figure 3.21 Load-Bending Strain Relationship of BETB6 (PSX31)

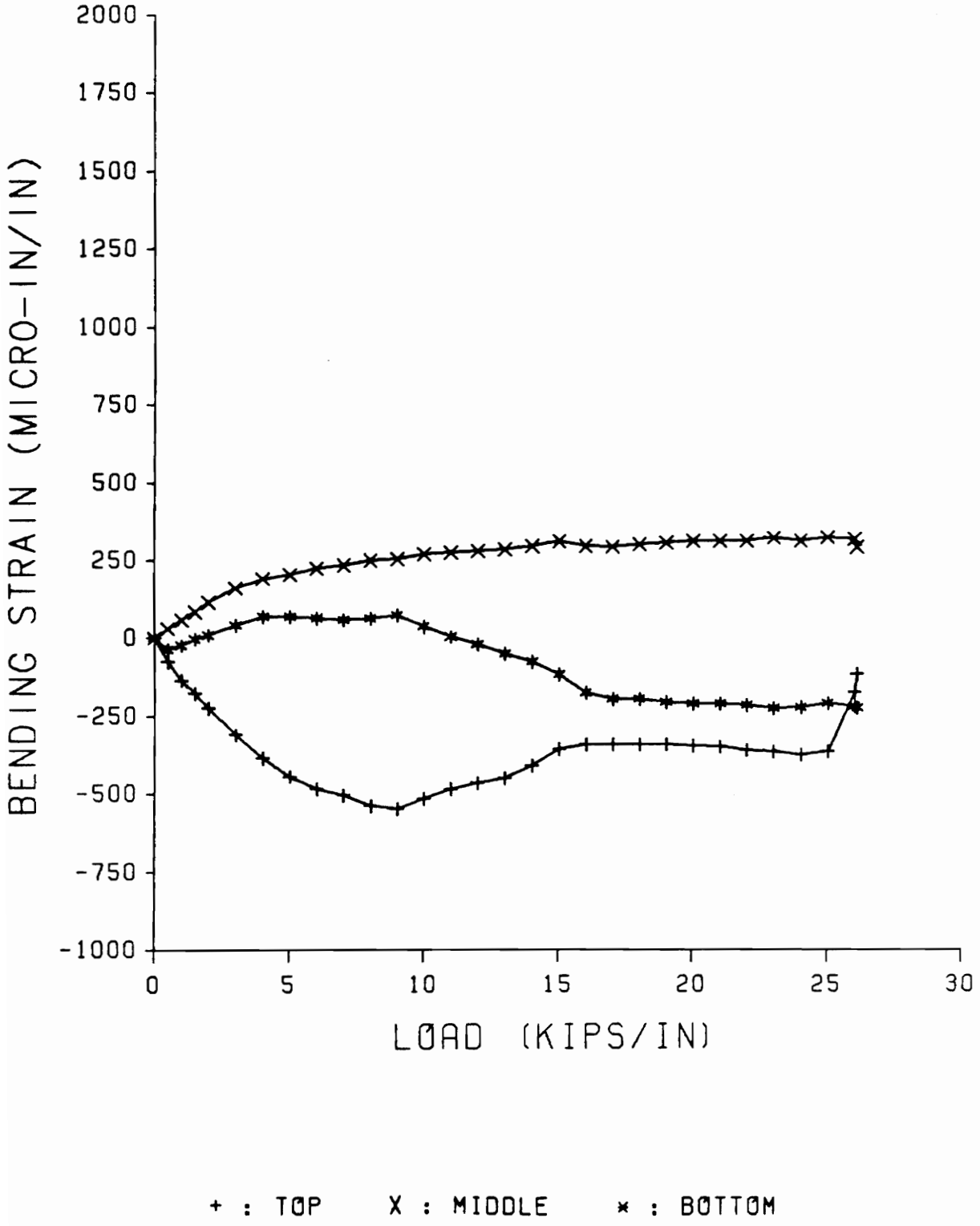

Figure 3.22 Load-Bending Strain Relationship of BETB7 (PSX31)

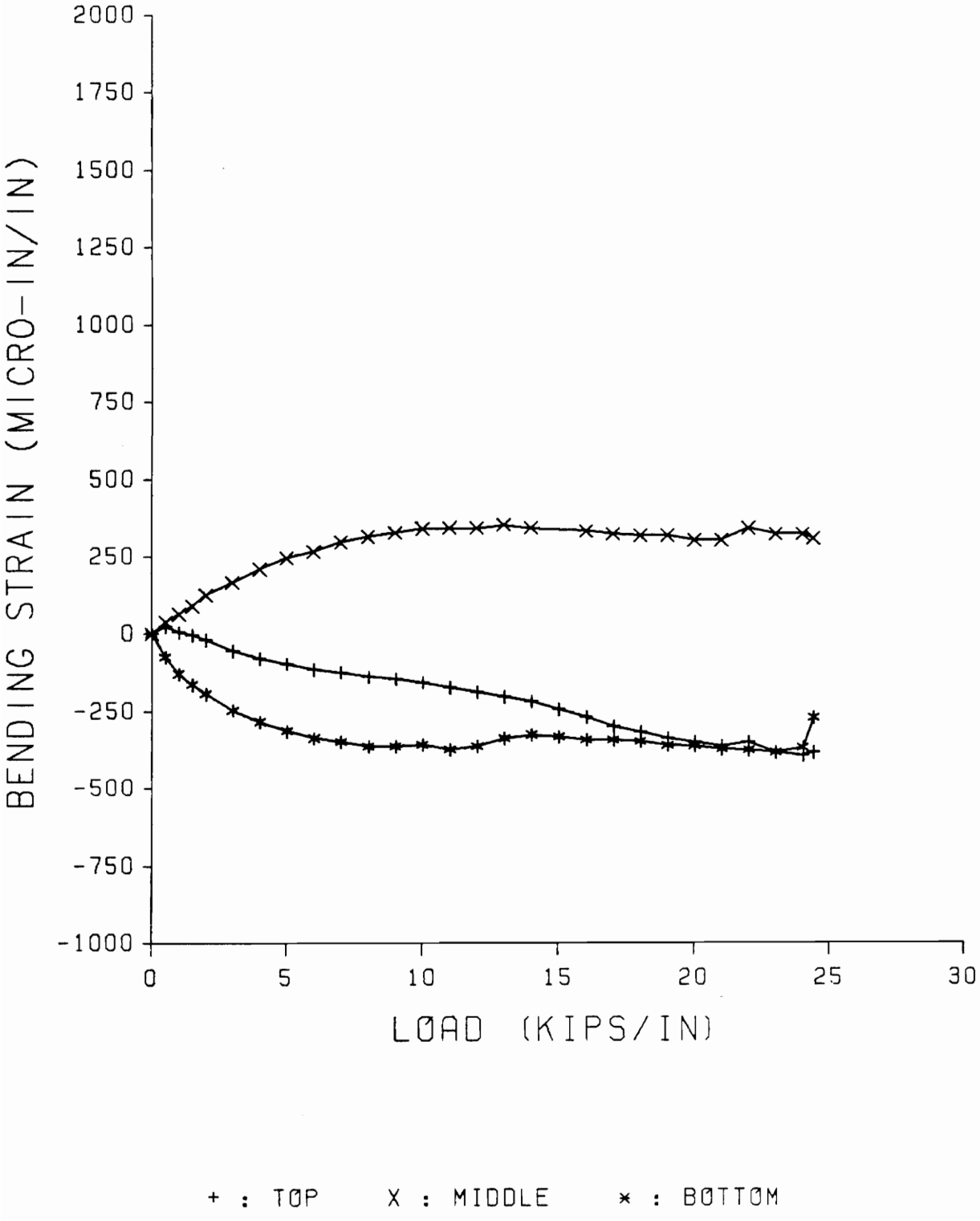

Figure 3.23 Load-Bending Strain Relationship of BETB8 (PSX31)

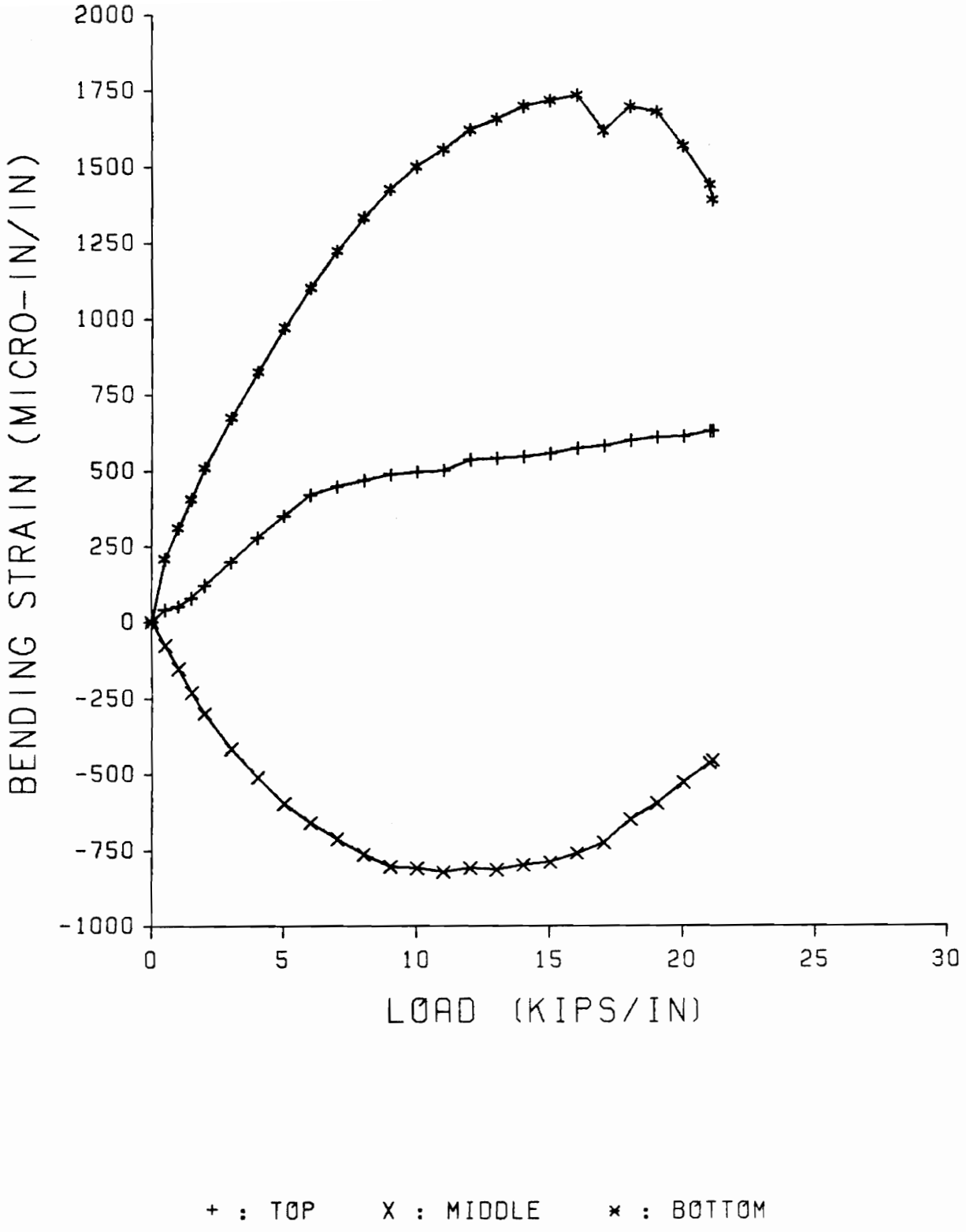

Figure 3.24 Load-Bending Strain Relationship of USY9 (PSX32)

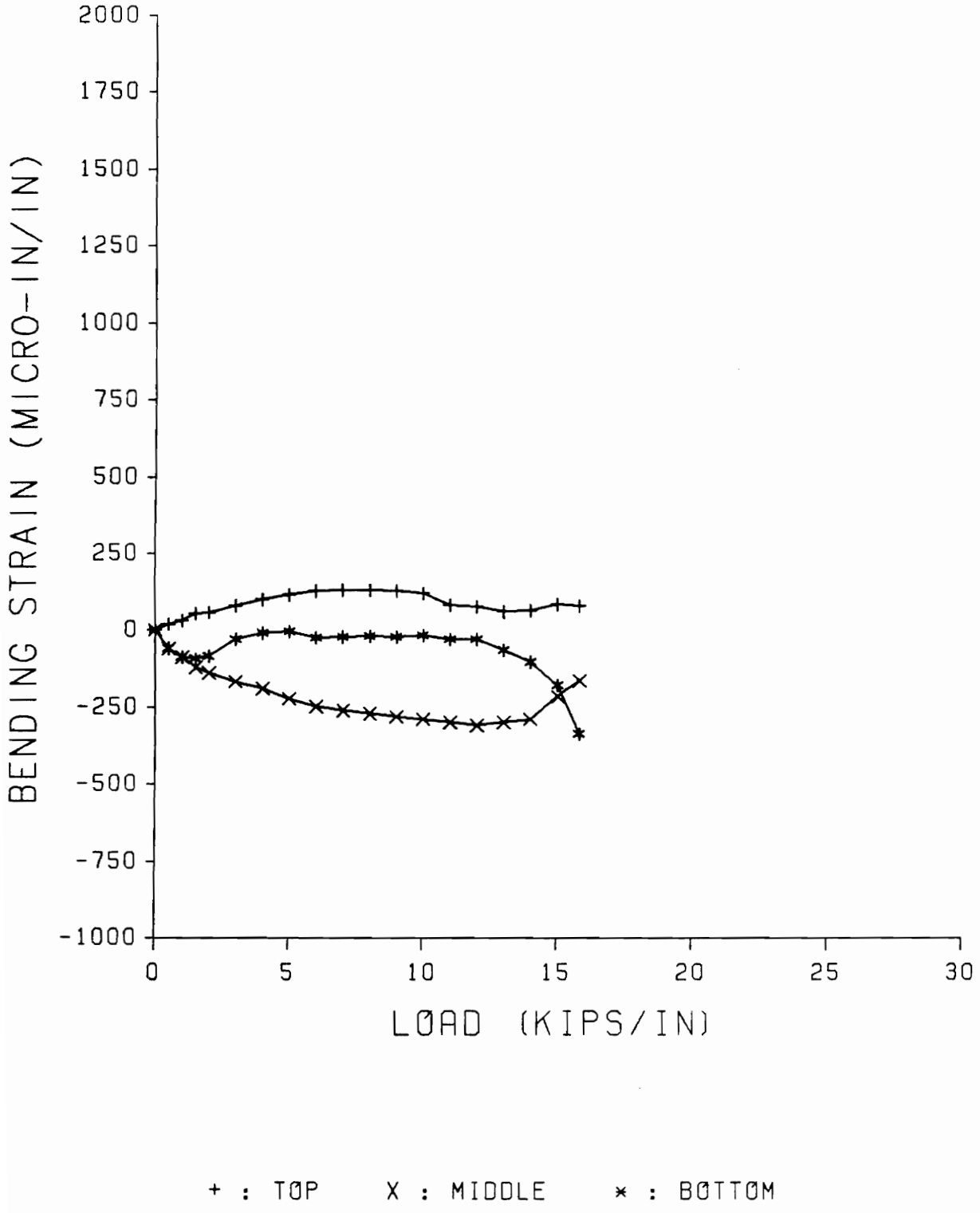

Figure 3.25 Load-Bending Strain Relationship of USR10 (PS32)

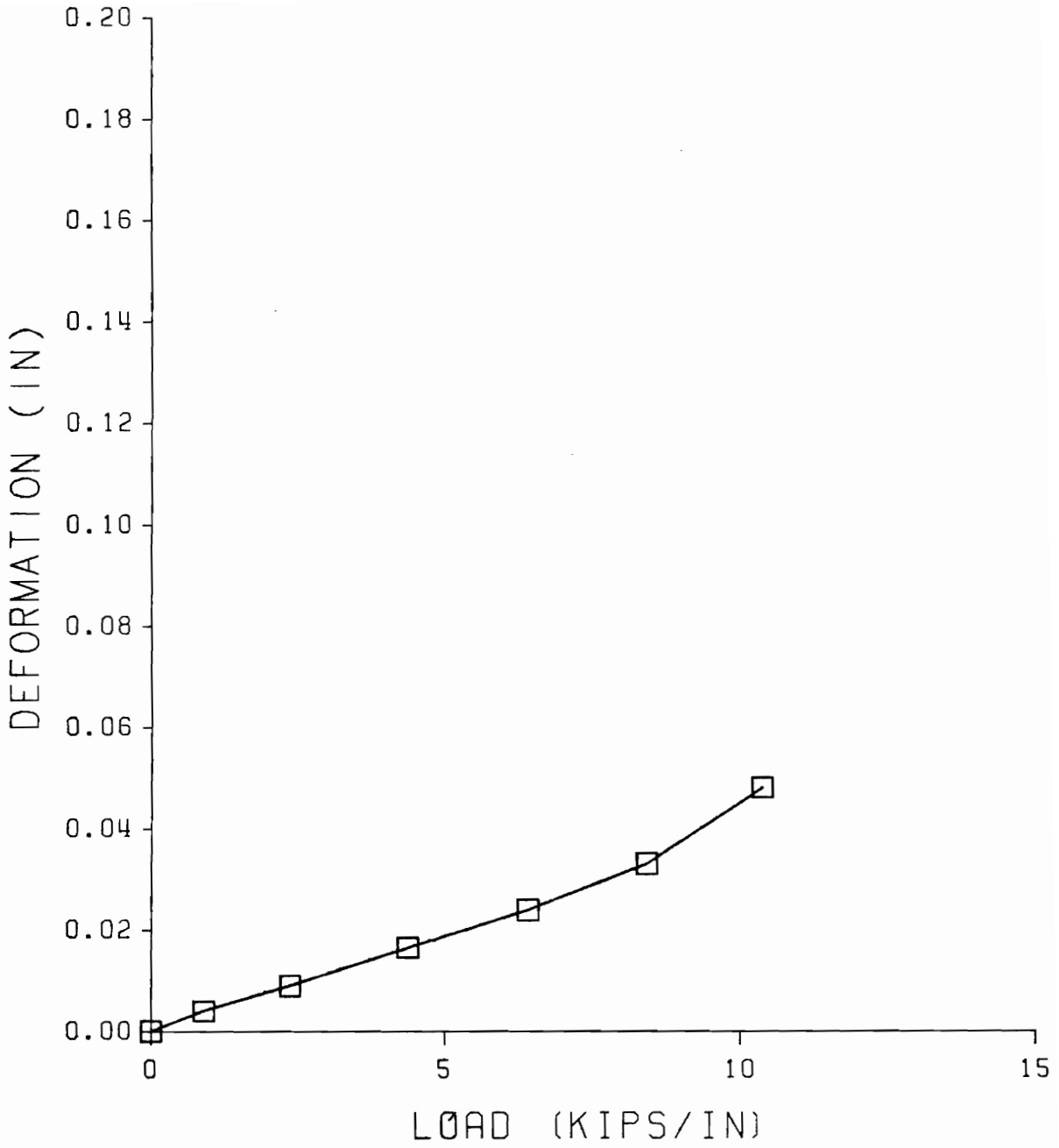

Figure 3.26 Load-Deformation Relationship by Finite Element Analysis

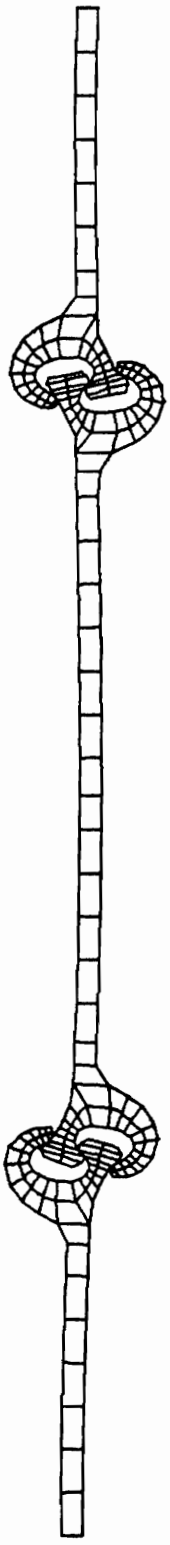

Figure 3.27 Deformed Shape of Sheet Pile at Load Step 1 (0.96 kips/in.)

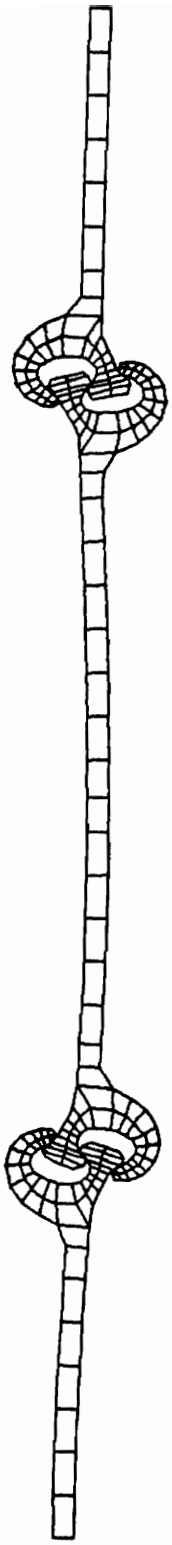

Figure 3.28 Deformed Shape of Sheet Pile at Load Step 2 (2.37 kips/in.)

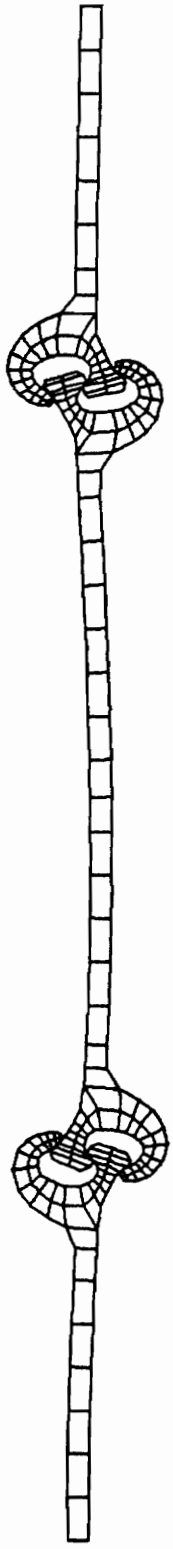

Figure 3.29 Deformed Shape of Sheet Pile at Load Step 3 (4.37 kips/in.)

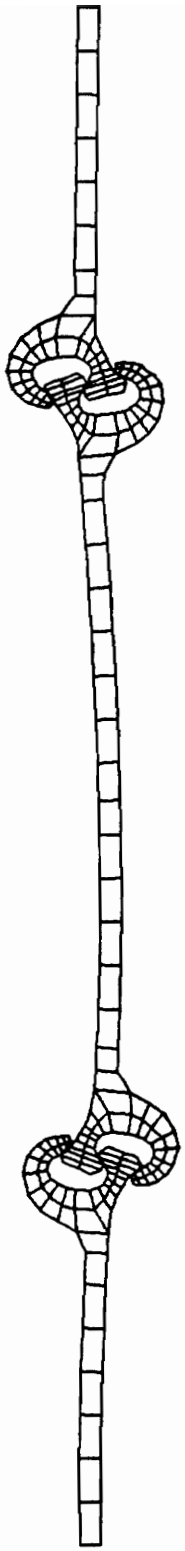

Figure 3.30 Deformed Shape of Sheet Pile at Load Step 4 (6.41 kips/in.)

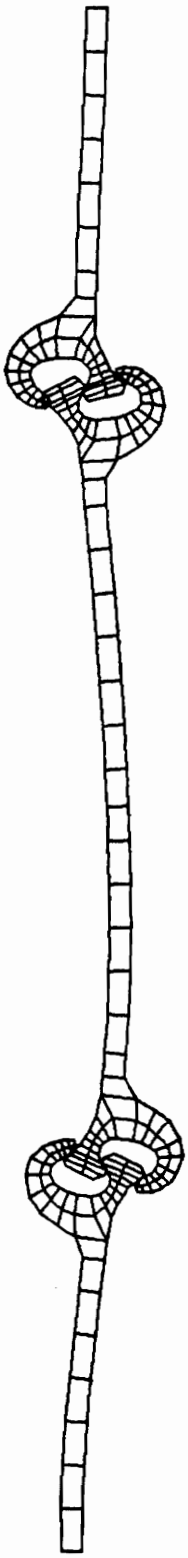

Figure 3.31 Deformed Shape of Sheet Pile at Load Step 5 (8.41 kips/in.)

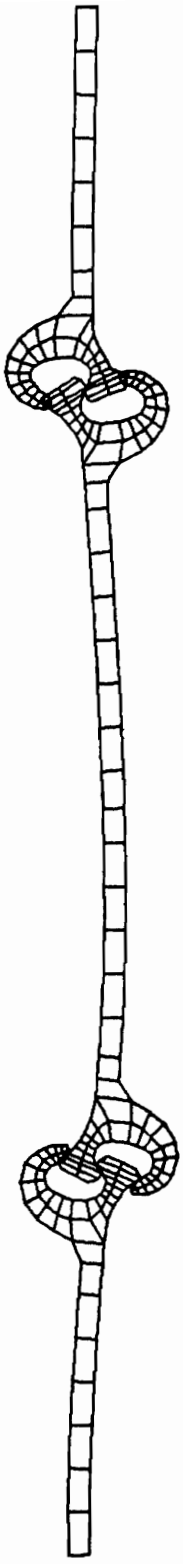

Figure 3.32 Deformed Shape of Sheet Pile at Load Step 6 (10.36 kips/in.)

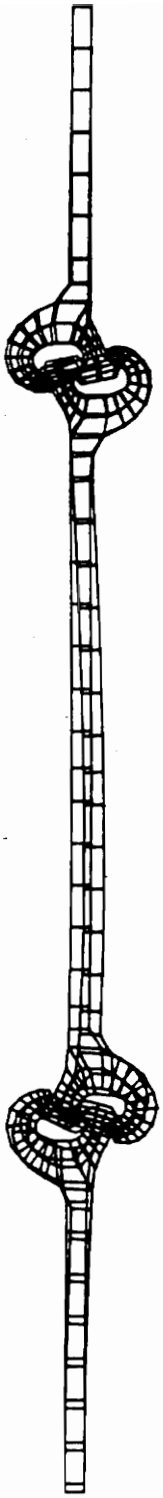

Figure 3.33 Overlay Drawing of Load Step 0 and Load Step 3

Figure 3.34 Overlay Drawing of Load Step 0, 3, 5

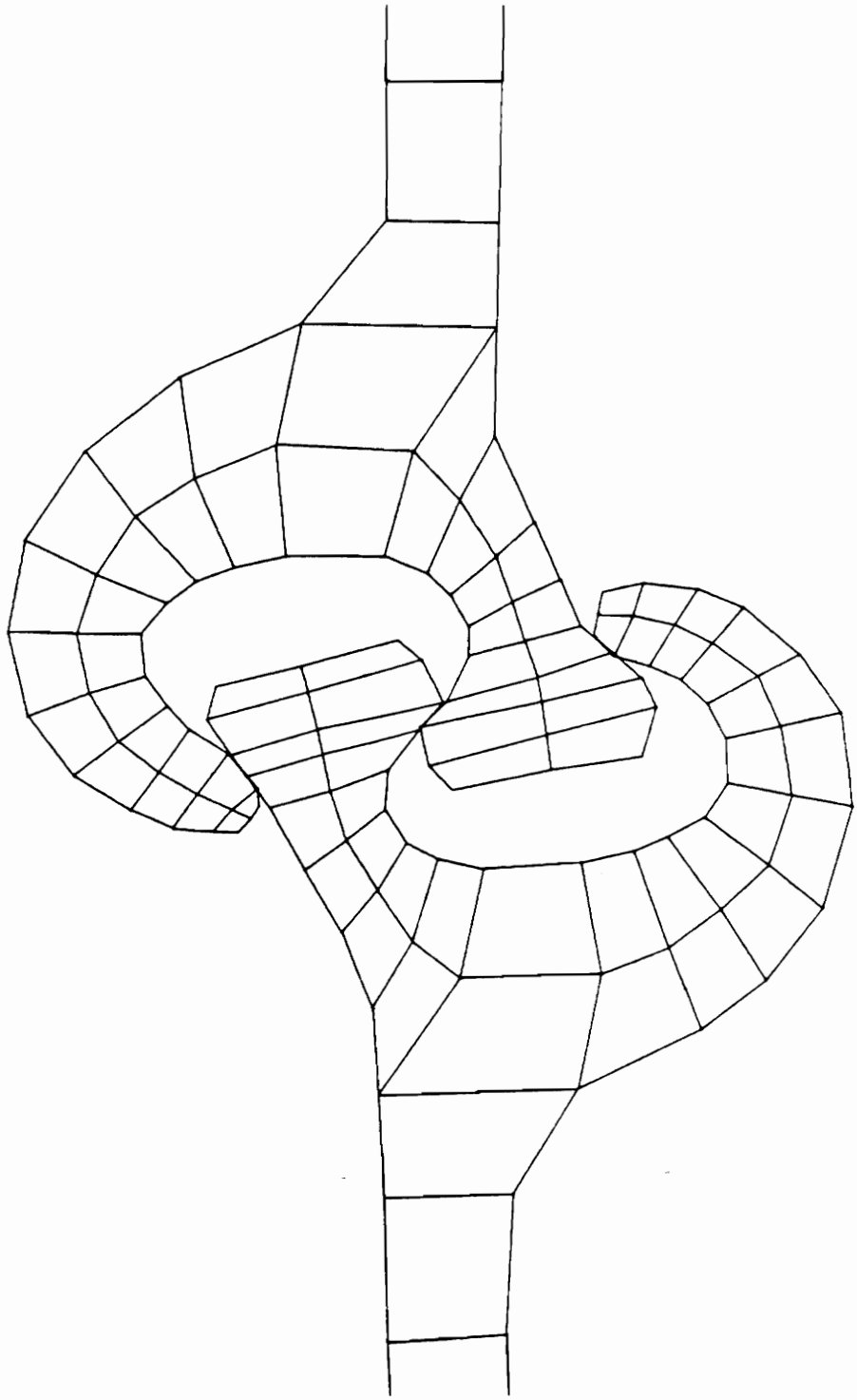

Figure 3.35 Enlarged Drawing of Interlock at Load Step 3

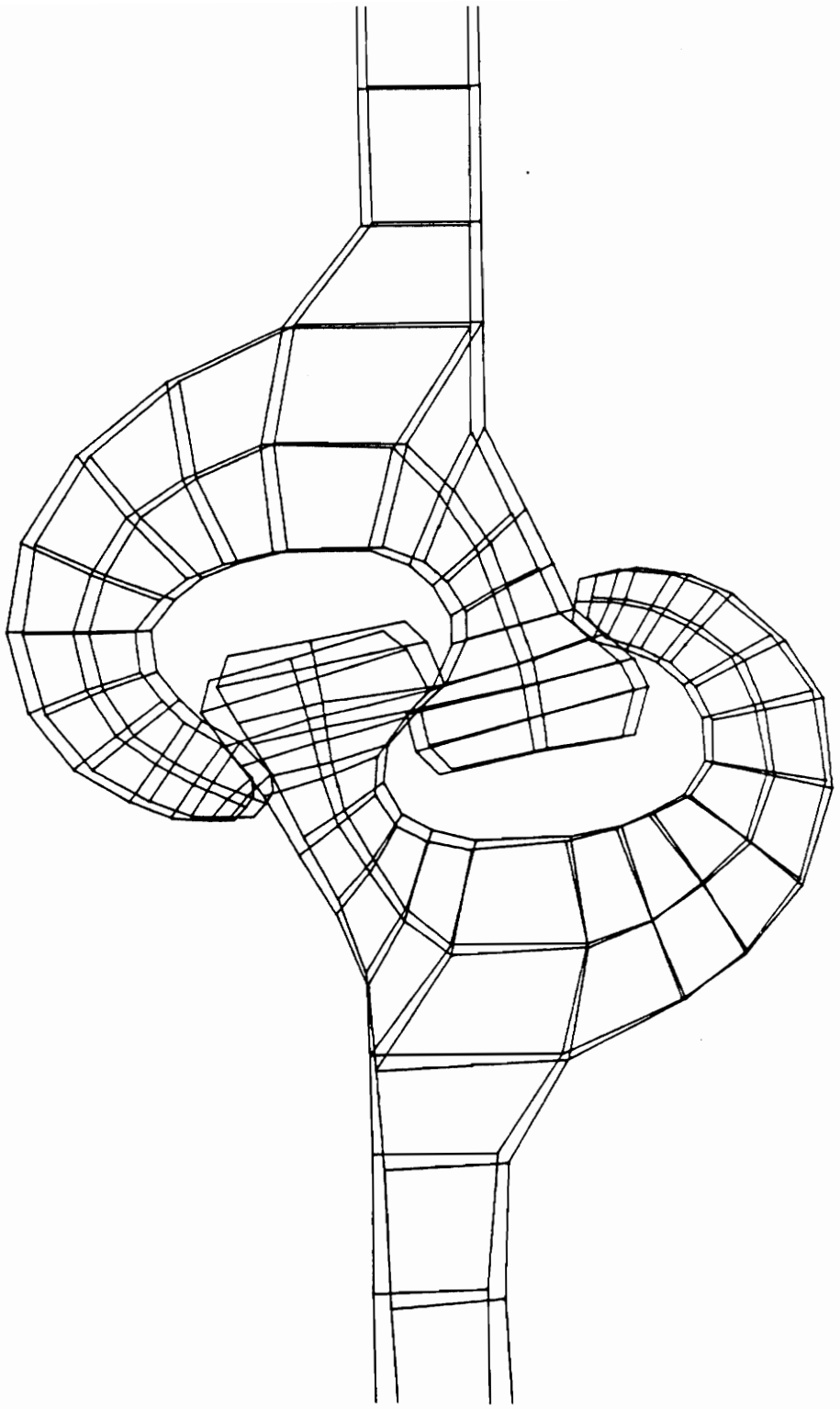

Figure 3.36 Enlarged Overlay Drawing of Interlocks at Load Step 0, 3

Figure 3.37 MENU Developed in This Study

CHAPTER IV

COMPARISON and DISCUSSION

4.1 Regression Analysis

As mentioned in the previous chapter, data obtained from photographic records are not continuous because of the measurement method. Plots of load-deformation relationships are saw-toothed. Sometimes, the saw-toothed curves imply that with increasing load there is a decreasing deformation. It is obvious that deformation can not decrease in a pull-out test like that conducted at WES. To evaluate the nature of the scattered data points, WES suggested that regression analyses should be applied.

For comparing the experimental results of a single PSX31 high-strength steel sheet pile pull-out test (description BETB7) with its corresponding analytical result, the interlock geometry of the sheet pile is used to construct the finite element model. The following

discussion is relevant to the test BETB7 or the whole PSX31 High Strength group (BETB5 to BETB8).

4.1.1 Regression Analyses on Load-Deformation Relationship

The data were first separated into two data groups, namely, failure and non-failure end, instead of top and bottom end. For example, when the top interlock was the failure interlock, deformation of the top gage length was grouped in the failure end data set and deformation of the bottom gage length was designated as the non-failure end data set. The main purpose of the above mentioned grouping was to find out whether or not the two groups behaved differently.

Several types of function were then used to fit the data. It was found that exponential and third order polynomial functions fit the data best because they yielded the highest correlation of coefficients. The equations used to fit the data are listed below:

$$\text{exponential} \qquad Y = Ae^{B(X+X_1)} - Y_1 \tag{4.1}$$

$$\text{polynomial} \qquad Y = A_1 + A_2(X+X_1) + A_3(X+X_1)^2 + A_4(X+X_1)^3 \tag{4.2}$$

where A, B, A_1, A_2 , A_3, A_4, X_1 are the coefficients. Dependent variable Y is the deformation and independent variable X is the load.

WES conducted regression analyses for all four test groups, PS31 Standard Strength, PSX31 High Strength, PS32 Standard Strength, and PSX32 High Strength. Only the corresponding analysis for PSX31 High Strength is discussed herein. The regression curves and the raw data points are shown in Fig. 4.1 to 4.4. Results of the exponential

fit are plotted in Fig. 4.1 and Fig. 4.2., and those of the third order polynomial fit are shown in Fig. 4.3 and Fig. 4.4. Both exponential and third order polynomial yield basically the same coefficients of correlation. However, the polynomial exhibited decreasing deformation with increasing load in the failure end. It is thus decided that exponential curves are more reasonable and will be used in the comparison with the analytical result.

In this study, a regression analysis for the data of test BETB7 was also desired. The computer program Curve Fitter-PC (Interactive Microware Inc., 1984) was used to find the best fit curves. Exponentials and third order polynomials were selected to fit the data because they served well in the regression analyses for PSX31 High Strength group. It was found that both curves did not fit the data of test BETB7 very well because the data points were widely scattered and too few. Though in Fig. 4.5 and Fig. 4.6, polynomial curves along with raw data are plotted, they are only shown to give a general idea of the trend of data. They should not be considered as representing the load-deformation relationship of test BETB7.

4.1.2 Regression Analyses for Stress versus Gross Strain Relationship

WES also applied regression analyses for the plots of stress versus gross strain of the ten tests. Because the gross strain was calculated by dividing the deformations taken from the photo data by the original gage length which was the sum of top and bottom gage lengths, the plots also showed the saw-toothed shapes. The regression analyses were intended to find the modulii of elasticity for the pile assembly. A straight line was used to fit the data and the slope of the line was taken as the modulus of elasticity. Data points near the failure were eliminated from the regression analyses because they were not in the elastic range. The results are shown in Table 4.1.

All the system modulii are less than the standard modulus of 29500 ksi determined from steel coupons. Since the gross strain includes the deformation of interlocks, the modulus of elasticity for a pile assembly is expected to be smaller. From Table 4.1 it can be observed that PSX31 High Strength (BETB5 to BETB8) have generally smaller system modulii of elasticity than PS31 Standard Strength (BET01 to BET04) have. This can be explained because there is greater variability in the geometry of the high strength steel interlocks produced in the rolling mill than in the standard strength section. The greater variability in geometry results in imperfect contact and larger apparent deformation for the assembled system.

4.2 Comparison

To verify the validity of the finite element program which was developed by Chan and Barker (1985) and modified later by Wu and Barker (1986), the analytical results obtained by using this program are compared with the experimental results. Comparisons and discussions of load-deformation relationships and of bending behaviors are presented below.

4.2.1 Comparison of Load-Deformation Relationship

Fig. 4.7 and Fig. 4.8 are plots of curves representing the load-deformation relationship obtained by finite element analysis and data points obtained from laboratory test BETB7. Fig. 4.7 is for top gage length and Fig. 4.8 is for the bottom gage length. The curves used to fit the data points in the two plots are the third order polynomials, details of which have been discussed in previous section. Since the computer program failed to

converge after load step 6 (10.36 kips/in), the curves obtained analytically stop at the that load step.

On the two plots, it can be observed that the analytical results are on the non-conservative side. Deformation obtained from the pull-out test is greater than that predicted by the finite element program. The curves of the finite element analysis are outside the range of the scattered data points of the test. In Fig. 4.7, the curve of the finite element analysis does show a tendency of getting closer to the polynomial curve. In Fig. 4.8, the curve of the finite element analysis shows an approximately straight line. From where the curve stops, it is difficult to tell if the analytical curve will eventually get closer to the polynomial curve which represents deformation measured in test BETB7.

Another attempt was made to compare analytical results with the results of the regression analyses of the PSX31 High Strength group. The results are shown in Fig. 4.9 and Fig. 4.10 for the four tests in the group. Fig. 4.9 is a plot of deformation of the failure end versus load. Fig. 4.10 is for the non-failure end. In test BETB7, the top interlock is the failure interlock (Table 3.1). Hence, the load-deformation curve of the top gage length, predicted by the finite element program, is plotted in Fig. 4.9 and the load-deformation curve of the bottom gage length is plotted in Fig. 4.10. In these cases, the curves obtained from the finite element analysis and from the test results show a better resemblance. Although analytical results are still smaller than the experimental results, the trends of the data are almost the same. The curve of analytical results also falls into the range of the scattered experimental data.

It should be pointed out that a regression curve is not the "real" load-deformation curve. It is the product of a regression analysis for a group of scattered data. A load-

deformation plot will pass through the origin which represents zero deformation with zero load, while a curve obtained from regression analysis may not pass through the origin as observed in Fig. 4.9 and Fig. 4.10. So, the regression curve only represents the nature of the scattered data. It may be similar to the real load-deformation curve. However, a regression curve is not exactly the load-deformation curve. It is considered that the trend of scattered data is well represented by a regression curve.

According to statistics theory, a regression analysis generally yields a better result when more data points are used. The load-deformation data of the single test BETB7 are too few and are widely scattered. Though a curve is presented to fit the data, its accuracy is very doubtful. On the other hand, the regression analysis applied to the whole group of PSX31 High Strength is more reliable because there are more data points.

As stated before, sheet pile interlock geometries vary from one interlock to another. However, the interlock geometries of the PSX31 high strength sheet piles used in test BETB5 to BETB8 are the same. When the piles arrived at WES, the lengths ranged from 1 ft. to over 3 ft. long. They were then cut into 3 in. wide specimens. Thus, the PSX31 high strength sheet pile specimens used in those tests were actually from the same sheet pile and their geometries can fairly be said to be identical. Tests BETB5 to BETB8 were in fact tests performed using the same sheet pile. Data obtained from test BETB7 only represent the behavior of that single test. To study the behavior of PSX31 high strength sheet pile, the whole group, from BETB5 to BETB8, should be used.

4.2.2 Comparison of Bending Behavior

A plot of load versus bending strain of test BETB7 is shown in Fig. 4.11. The picture is used to describe the bending behavior of the pull-out test. Photographic records are available. But it is not easy to study the behavior from the photographs because the deflections are very small. By realizing that positive bending strain represents bending in one direction and negative bending strain represents bending in another direction, one can easily picture the movements of the three pile sections from Fig. 4.11.

Fig. 4.11 shows that the top section experienced larger bending at the early stage of the test, compared to the bending of the two end sections. As the loading increased, the top interlock began to separate and the bending strain in the top section was gradually relieved. As the load exceeded 17 kips/in, the top section stayed in the same state until the top interlock separated. The middle section bent in a direction opposite to the top section when the load was first applied, and then kept the same configuration until the test failed. The bottom section also bent in the opposite direction in the early stage of the test. However, it bent in the other direction once the load reached 11 kips/in..

The bending behavior predicted by the computer program can be observed in Fig. 3.27 to Fig. 3.32. From the plots, the left section, which corresponds to the top section in test BETB7, bends downward while right(bottom) and middle sections bend upward. This agrees with the experimental result. But, the left section in the plots does not have larger bending as suggested in Fig. 4.11. Near the failure location, the computer program predicts quite well. In Fig. 3.32, it is clear that the left interlock is the failure interlock, which is confirmed in test BETB7. On the plot of the deformed shape at load step 6 (Fig. 3.32), it can be observed that the pile system will fail due to the separation

of the thumb of the middle section and the finger of the left section. However, the photographic records of test BETB7 show the pile failed as a result of the separation of the thumb of the top section and the finger of the middle section.

4.3 Discussion

When the finite element model was constructed, its geometry was taken from the specimen of test BETB7. A transparency made from the photographs of the specimen was traced carefully by using an electronic digitizer to obtain the outline of the finite element model geometry. So, the model can be said to fairly represent the shape of PSX31 high strength sheet pile.

However, there are some differences between the analytical results and the test results. The trends of the load-deformation relationship are similar but the deflection depicted by the finite element analysis appears to be too small. The bending behavior has some degree of resemblance but the behavior of the end sections described by the finite element analysis is not the same. All these imply that there are some problems in modeling the interlock connections. Several possible causes are considered and presented.

4.3.1 Initial Slacks in Connection

Test BETB7 was selected because it had a better initial contact condition. Although the contact condition was good, there were still some slacks between interlocks (Fig. 4.12 and Fig. 4.13). Due to the nature of interlock manufacture, slacks in connections are unavoidable. When the new finite element model was first constructed, initial slacks

were included in the model. However, the program does not have a gap element and could not converge with slacks included. It was then decided that a simplified contact condition would be used. After careful studying of the photographic records of test BETB7, contact regions were assumed and slacks were not modeled.

Simplified contact conditions made the finite element analysis possible but it also resulted in a distortion of the results. Deflection was reduced and bending behavior was changed because the initial strains produced by forcing additional contact regions was not considered.

It is obvious that a pile system is more flexible when there are slacks in the connections. Without the constraints of the fingers, slippage between thumb and thumb is easier and the deformation of the pile system is increased. Also, stress in the interlock where slacks exist is higher than the stress in the interlock where all the thumbs and fingers have contact with each other because the cross section for load transfer for the former is smaller. Higher stress creates higher strain and thus increases the deformation of the interlocks.

The initial slacks contribute to the increase of deformation at the early stage of test history. It is suspected that the interceptions of the regression curves with the Y-axis (deformation) in Fig. 4.5 and Fig. 4.6 are the effects of the initial slacks. Since the regression curve describes the trend of the scattered data points, an interception with the Y-axis means that data points with small values of X (load) do not have the tendency to gather around the origin point. Otherwise, those data points would appear close to the origin point. In Fig. 4.5 and Fig. 4.6, it can be observed that most of the data points with small values of X are scattered around the regression curve which is located a distance above the origin point. This implies that the deformation increases very quickly

at the beginning of loading, which is due to the presence of slacks between the interlocks.

While there are slacks in the connections, interlocks are easier to rotate and this changes the bending behavior of the pile assembly. How the bending behavior is changed depends on the locations of the slacks and the width of the gap. When there are fewer constraints in the interlock area, the connection is more flexible and is freer to rotate. The gap between thumb and finger allows the interlock to rotate without causing bending in other pile sections except the one it belongs to. Thus, the bending in the web is less severe if there are slacks in the interlock connections.

In the finite element model, the connections are stiffer because all the thumbs and fingers have contact with each other. The interlocks can not rotate without causing bending of the two adjacent pile sections. Also, the couples which are formed by the eccentricity of the center section force the interlocks to rotate. Hence, bending of the web in the finite element model is higher than that observed in test BETB7. This higher bending not only compromises the deformation in the lateral direction but also causes the separation of the interlocks to happen earlier.

4.3.2 Imperfect Bearing

During the tests, it was found that the bearing of one interlock on another was not always continuous over the entire 3 in. width of the interlock. Two load-unload cycles of 1000 lbs were applied before every test to improve the uniformity of bearing. Although major misalignments were eliminated, the bearing was not as ideal as implied by the finite element model. Since the finite element model is two dimensional, it implies a per-

fect, continuous bearing at the contact region along the width of the interlock, which is unlikely to be encountered in a laboratory test.

Imperfect bearing has the same effects as the initial slack. It increases the deformation in the early stages of loading. However, the bearing uniformity improves as the loading increases.

4.3.3 Modeling

As mentioned before, the geometry of the finite element model was taken from the transparencies provided with the laboratory test report. The transparencies were actually copied from the photographs of undeformed sheet piles. It was later found that there was a flaw in the transparency of the bottom interlock. A shadow in the interlock area was mistakenly taken as part of the interlock geometry and was copied to the transparency. After the mistake was discovered, the finite element model was corrected by tracing the outline of the bottom interlock in a clearer photograph. However, the photograph is not of an undeformed shape and the interlock geometry may have changed.

There is another flaw in the photographic records. The shape of the sheet pile in the photographs was distorted during processing. By carefully comparing the grids scribed on a middle section with the grids scribed on the end sections, distortions can be observed. Grids scribed by laser cutter controlled by computer should be the same on all three sections. It was observed that grids on the end sections are longer than grids on a middle section, which means that the shape of the sheet pile in the photographs is

stretched in the longitudinal direction. The distortion could possibly have resulted from an inclined shooting angle of the camera, too.

It is hard to tell the effects on interlock modeling caused by the flaws in the photographs. However, past experiences with the computer program indicated that the program is very sensitive to the geometry change in the interlock area. The distortion of the pile shape might have affected the results significantly.

Table 4.1 Modulii of Sheet Pile System (adapted from O'Neil and McDonald (1985))

Test Descriptor	Modulus (ksi)
BET01, PS31	5,710
BET02, PS31	7,150
BET03, PS31	6,420
BET04, PS31	8,070
BETB5, PSX31	5,090
BETB6, PSX31	4,370
BETB7, PSX31	4,490
BETB8, PSX31	3,290
USY9 , PSX32	5,000
USR10, PS32	5,390

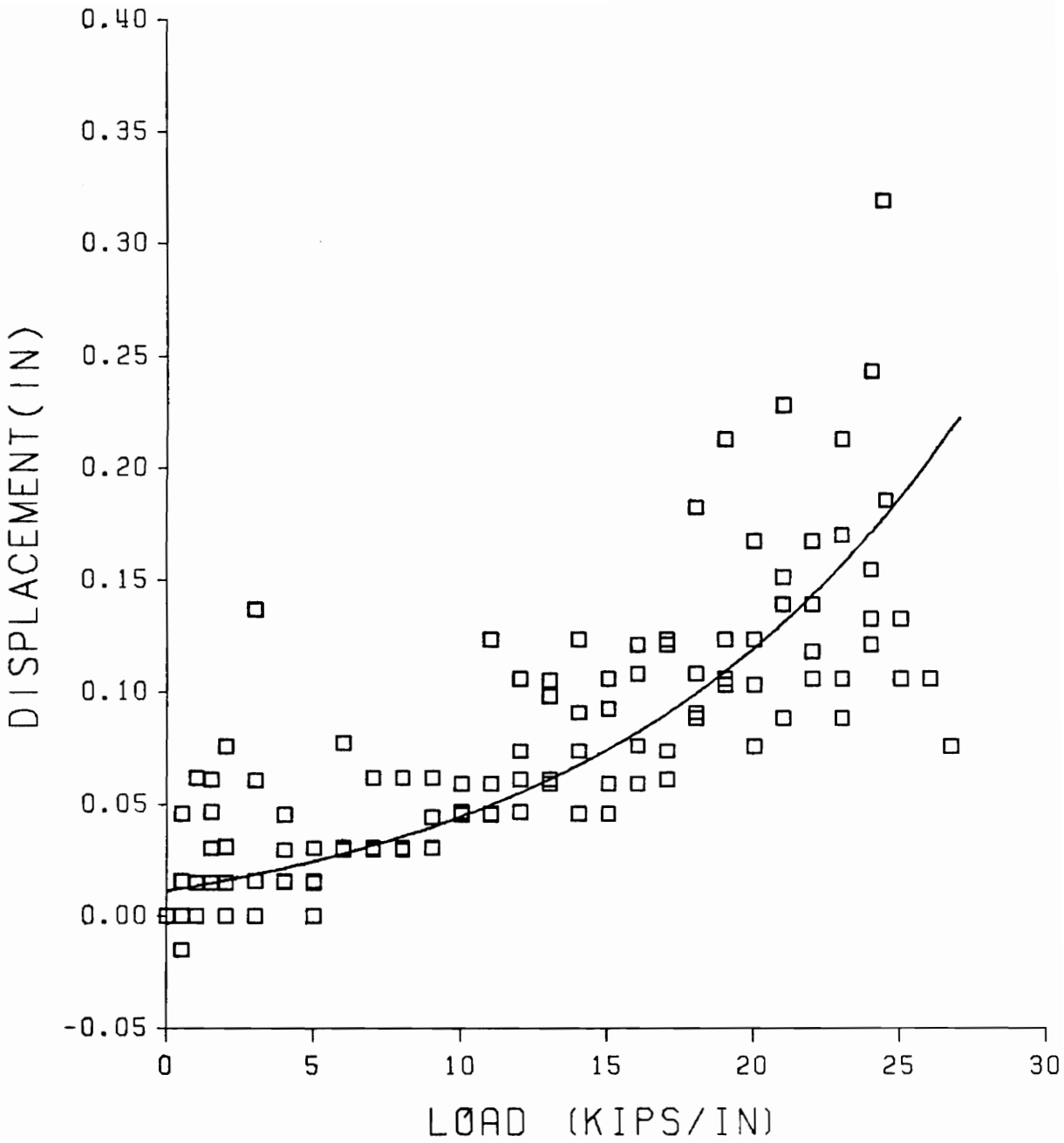

Figure 4.1 Exponential Curve Fit for PSX31 HS Failure End

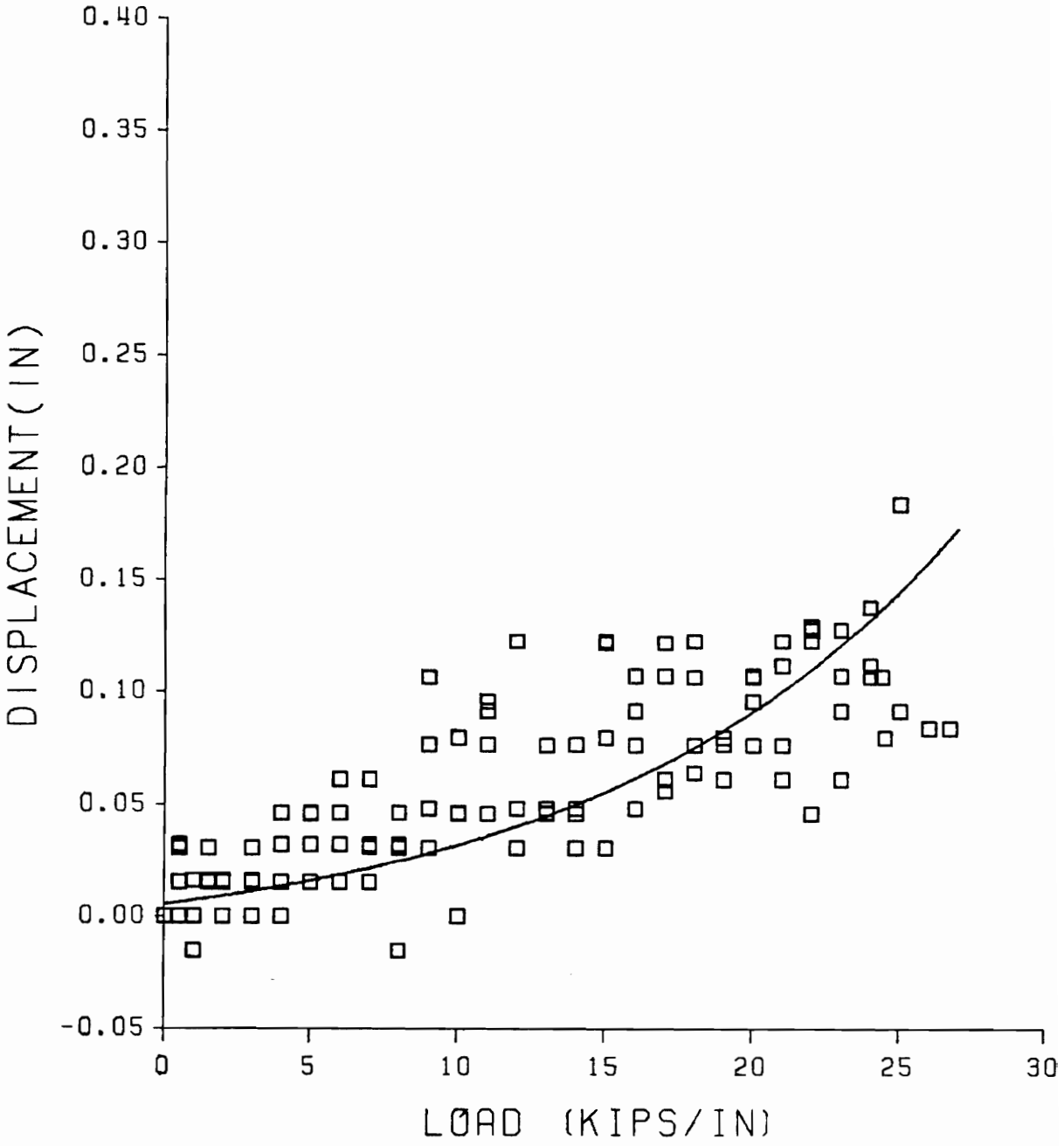

Figure 4.2 Exponential Curve Fit for PSX31 HS Nonfailure End

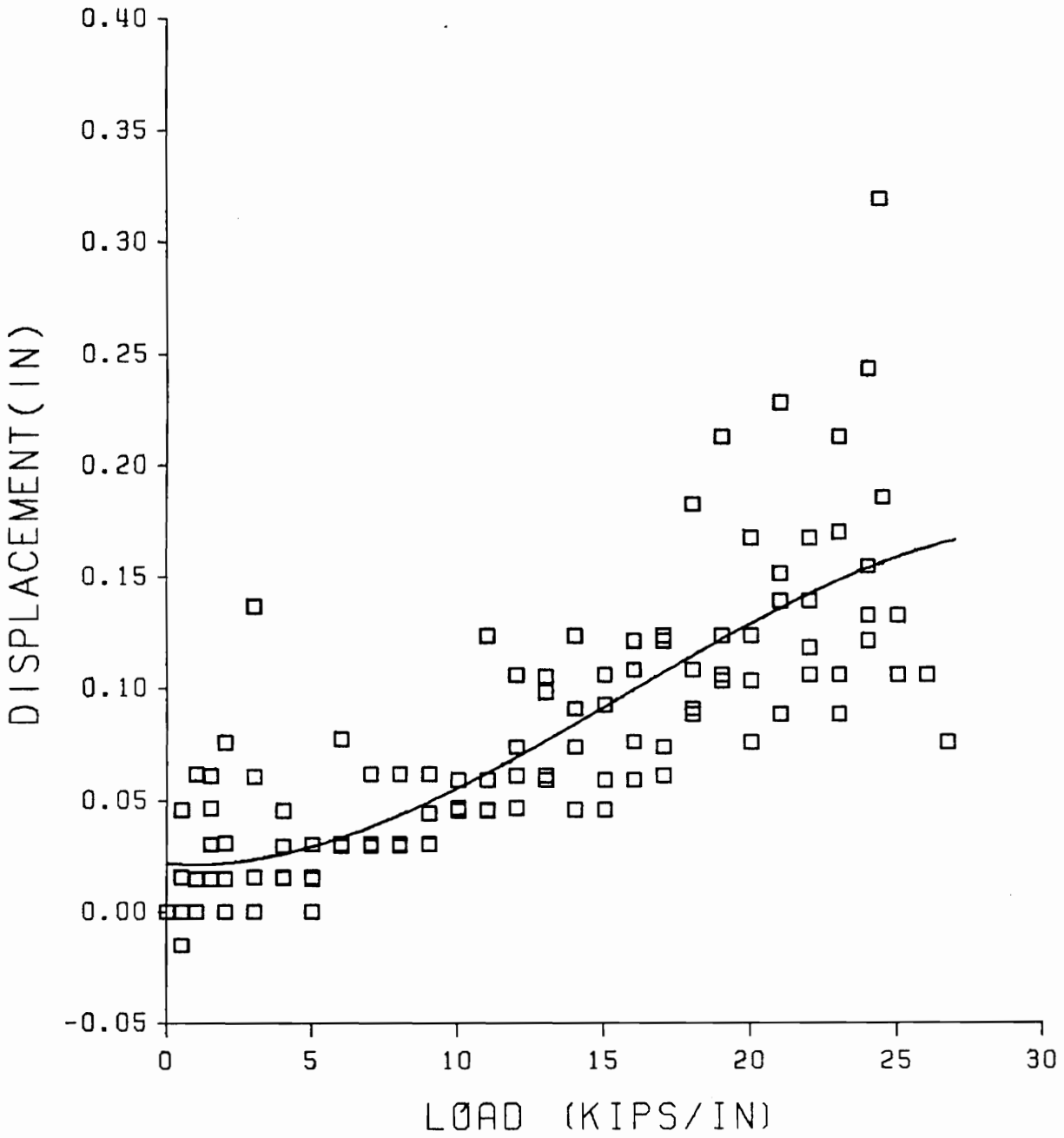

Figure 4.3 Polynomial Curve Fit for PSX31 HS Failure End

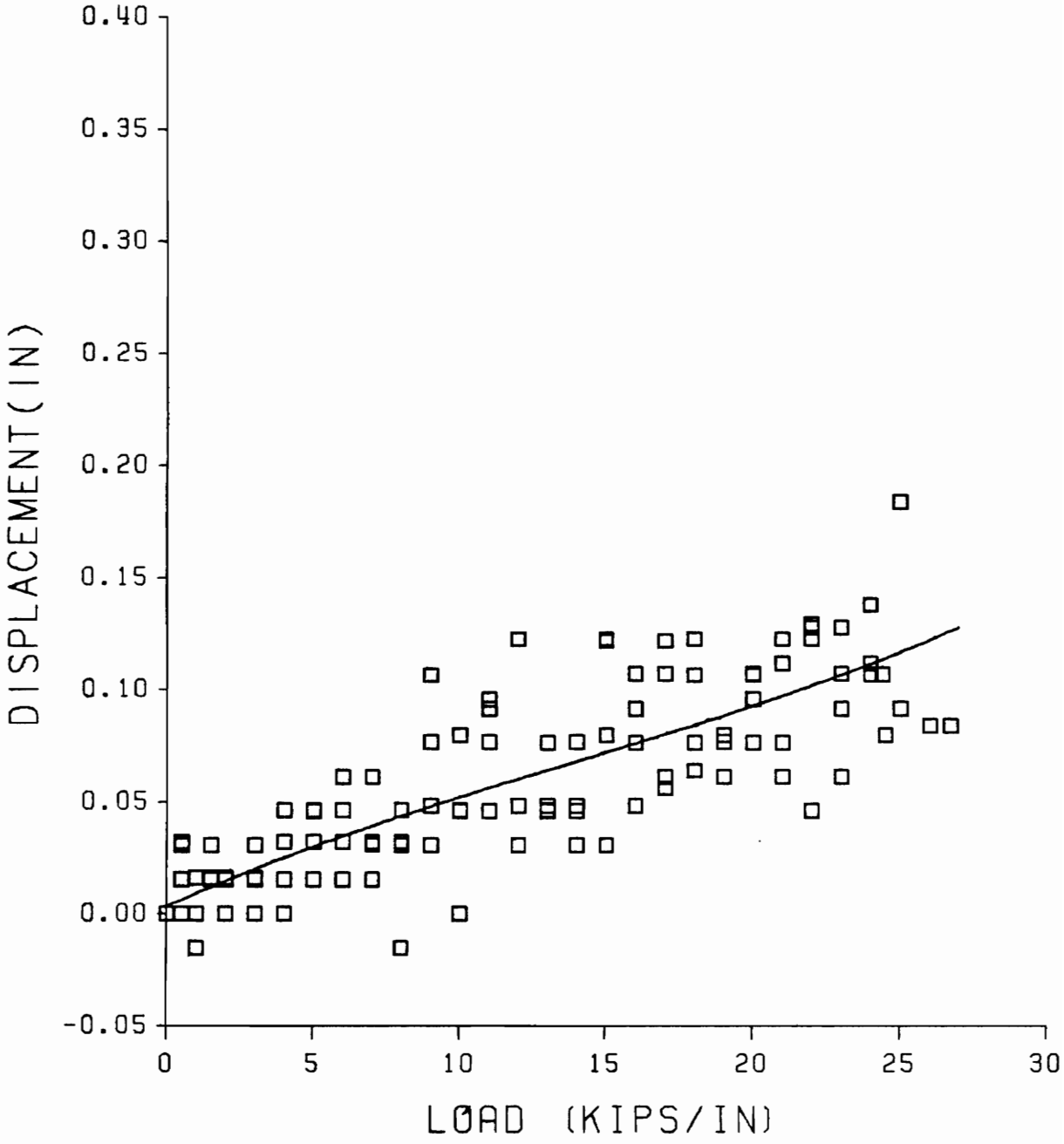

Figure 4.4 Polynomial Curve Fit for PSX31 HS Nonfailure End

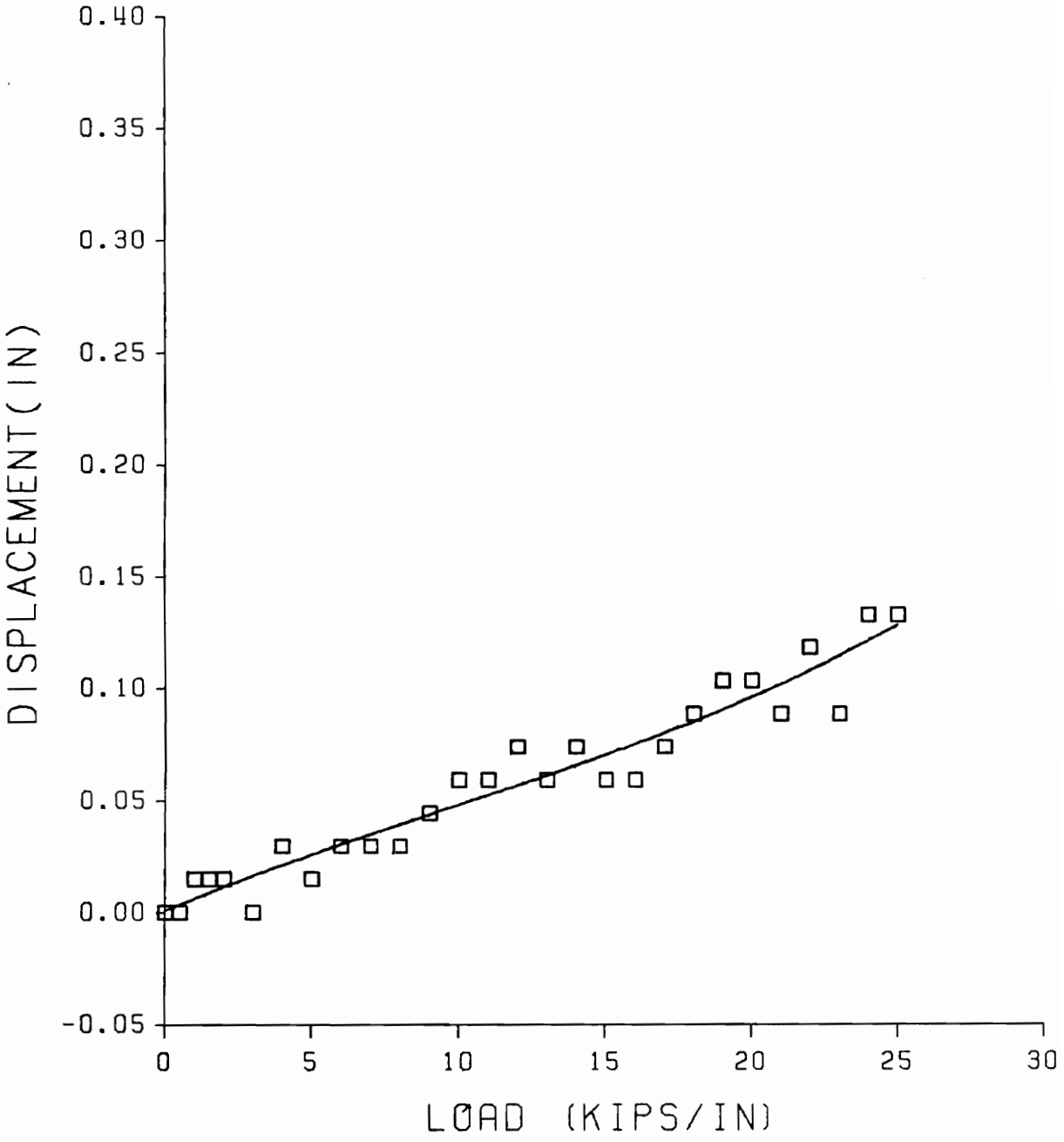

Figure 4.5 Polynomial Curve Fit for BETB7 Top Gage Length

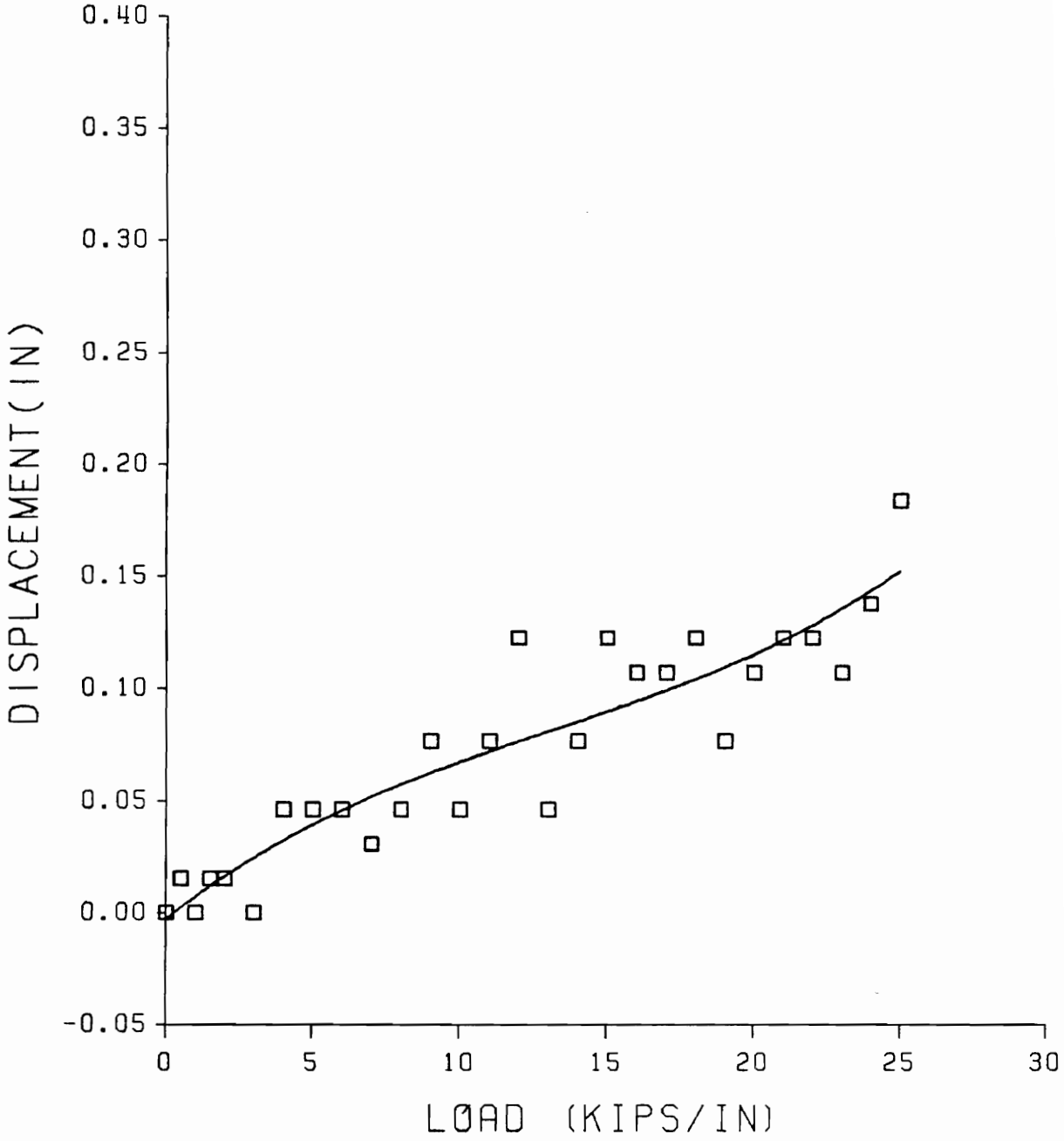

Figure 4.6 Polynomial Curve Fit for BETB7 Bottom Gage Length

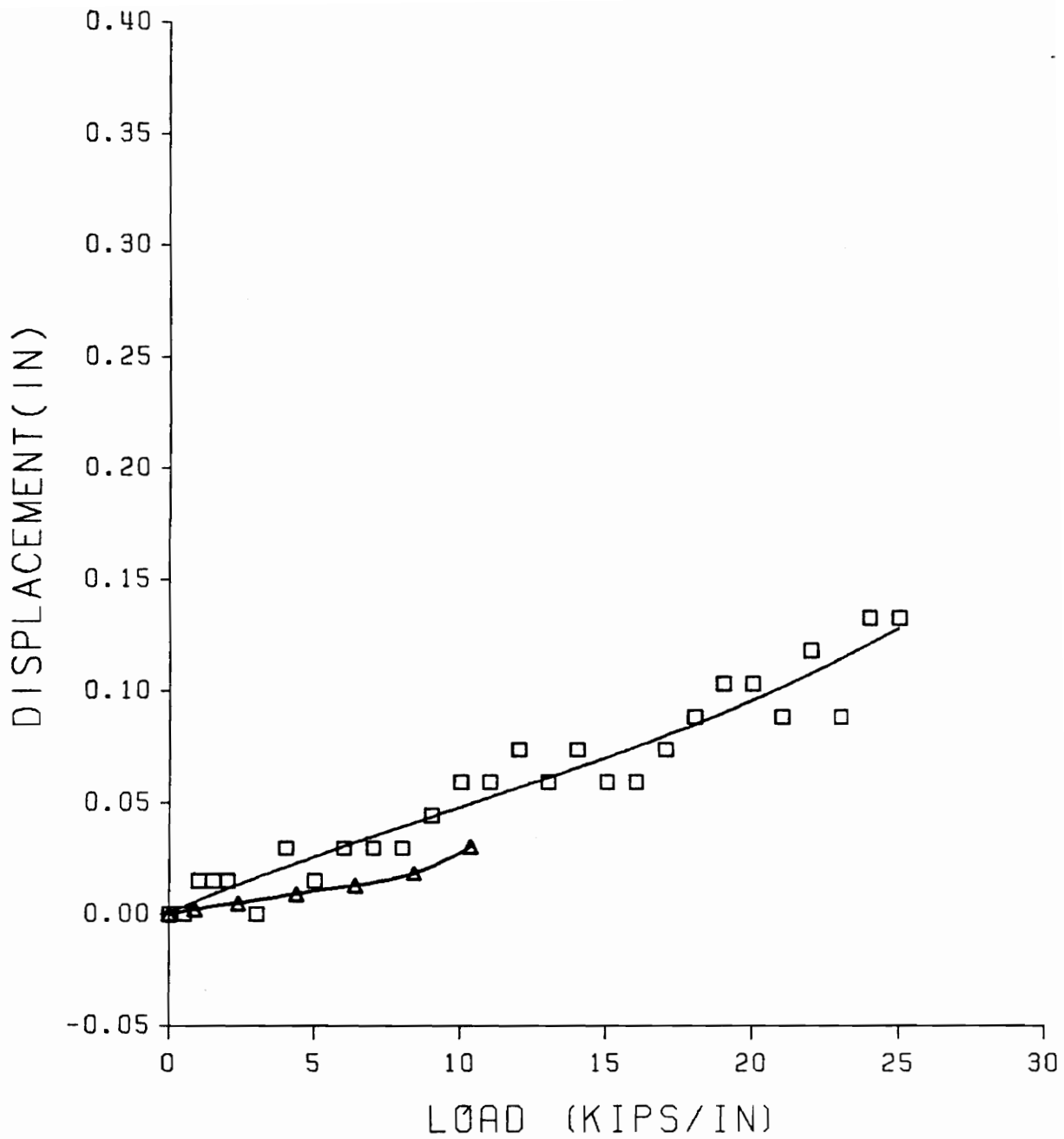

Figure 4.7 Comparison Between Analytical and BETB7 Results, Top End

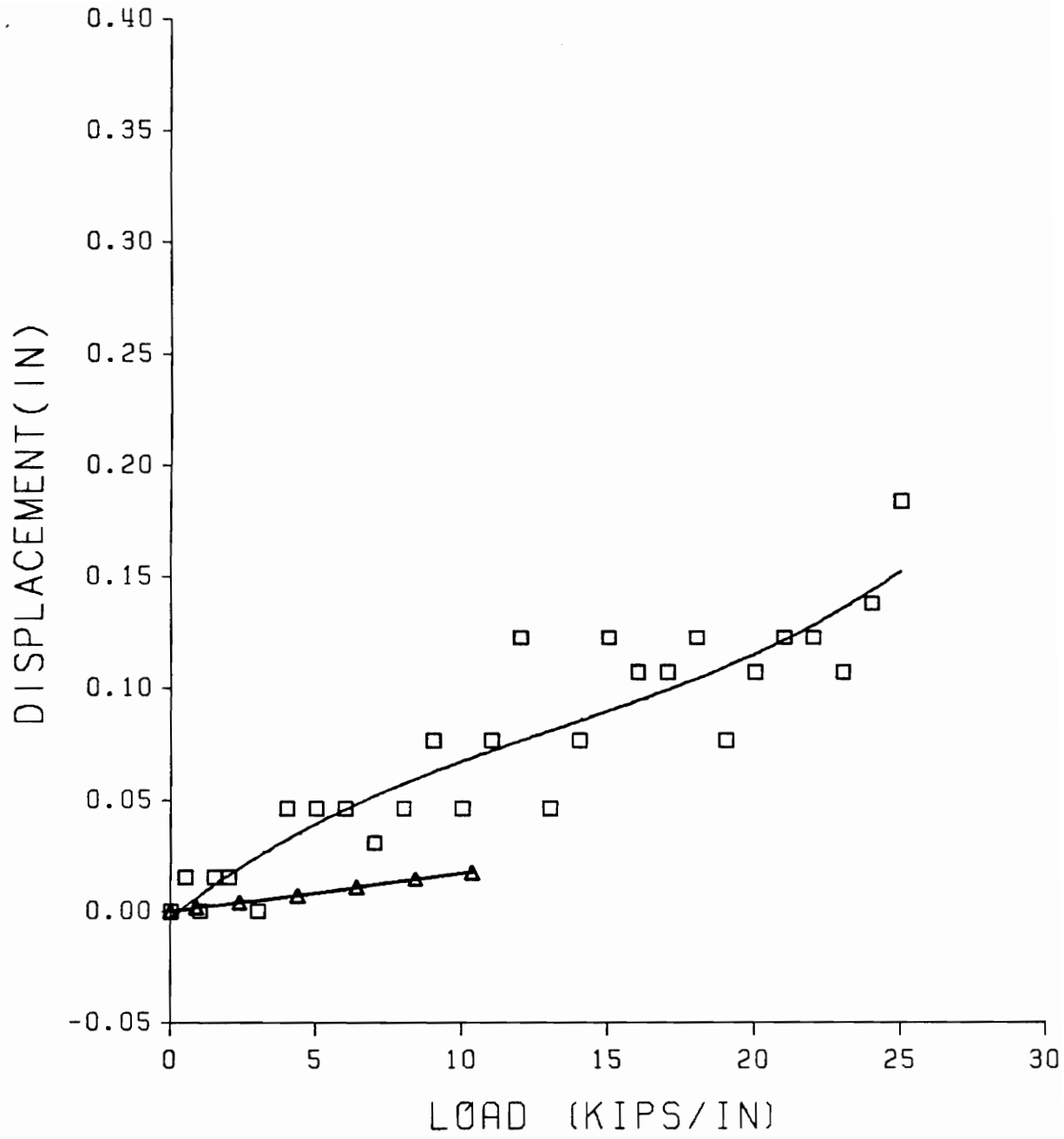

Figure 4.8 Comparison Between Analytical and BETB7 Results, Bottom End

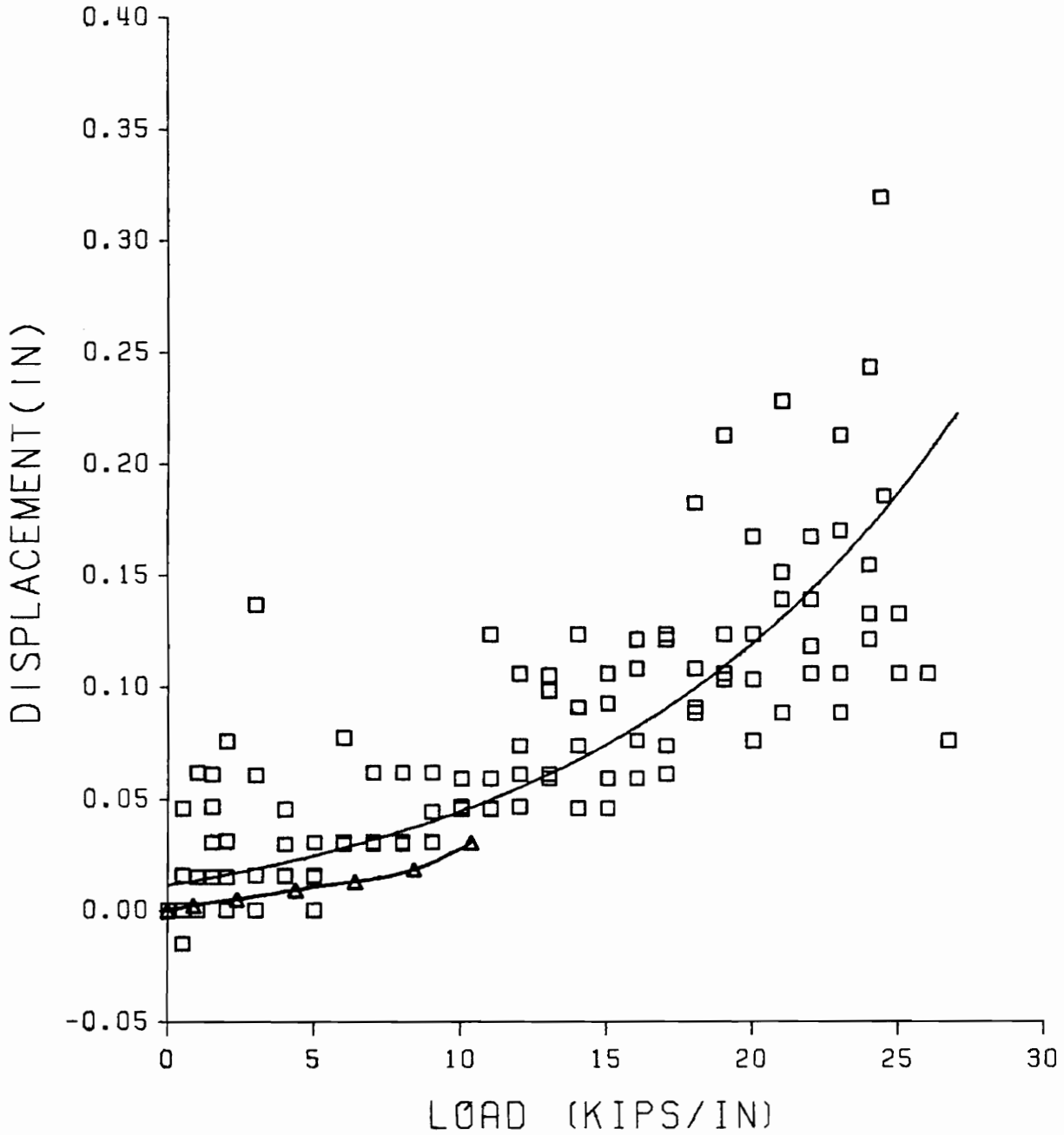

Figure 4.9 Comparison Between Analytical and PSX31 Results, Failure End

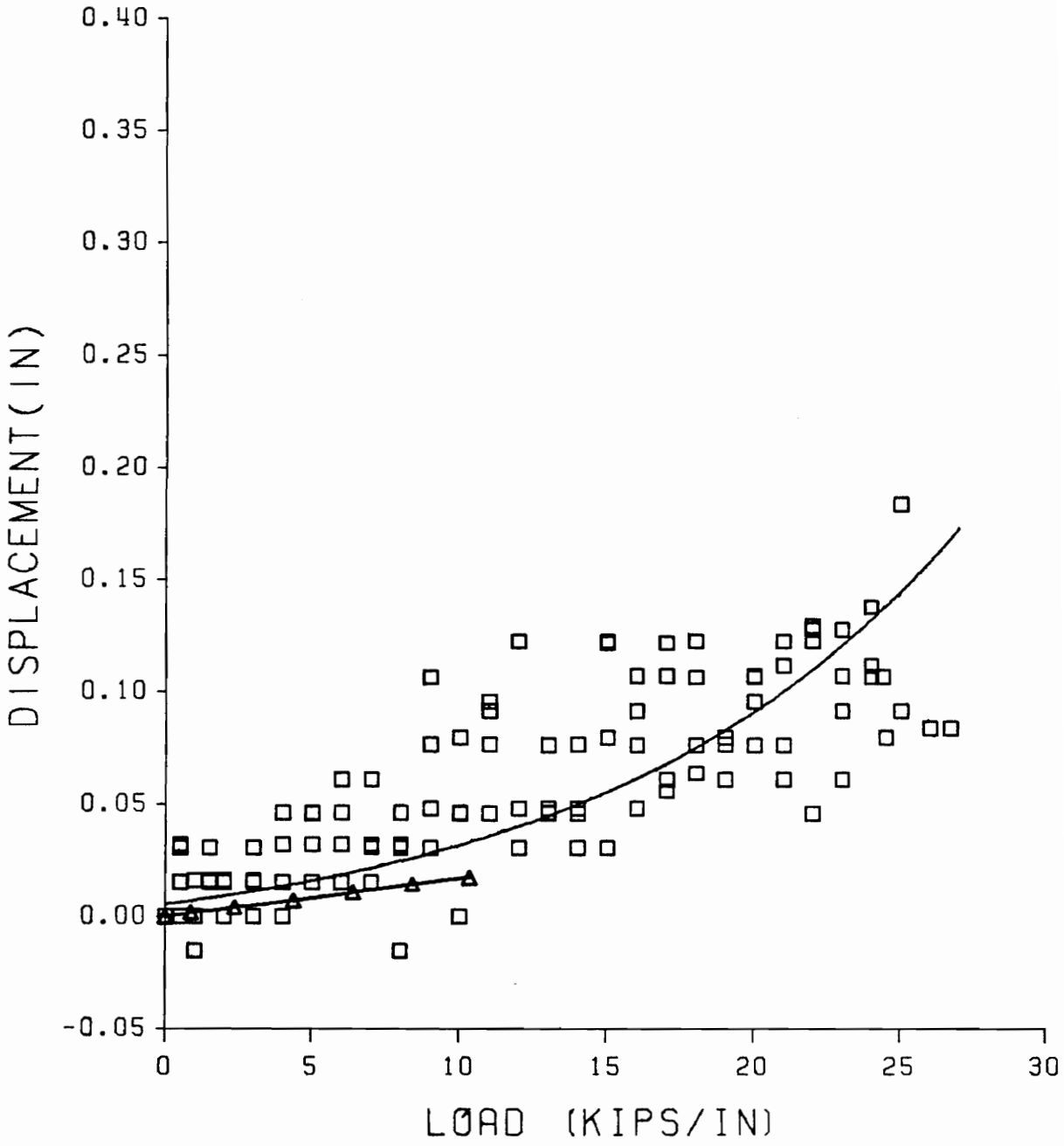

Figure 4.10 Comparison Between Analytical and PSX31 Results, Nonfailure End

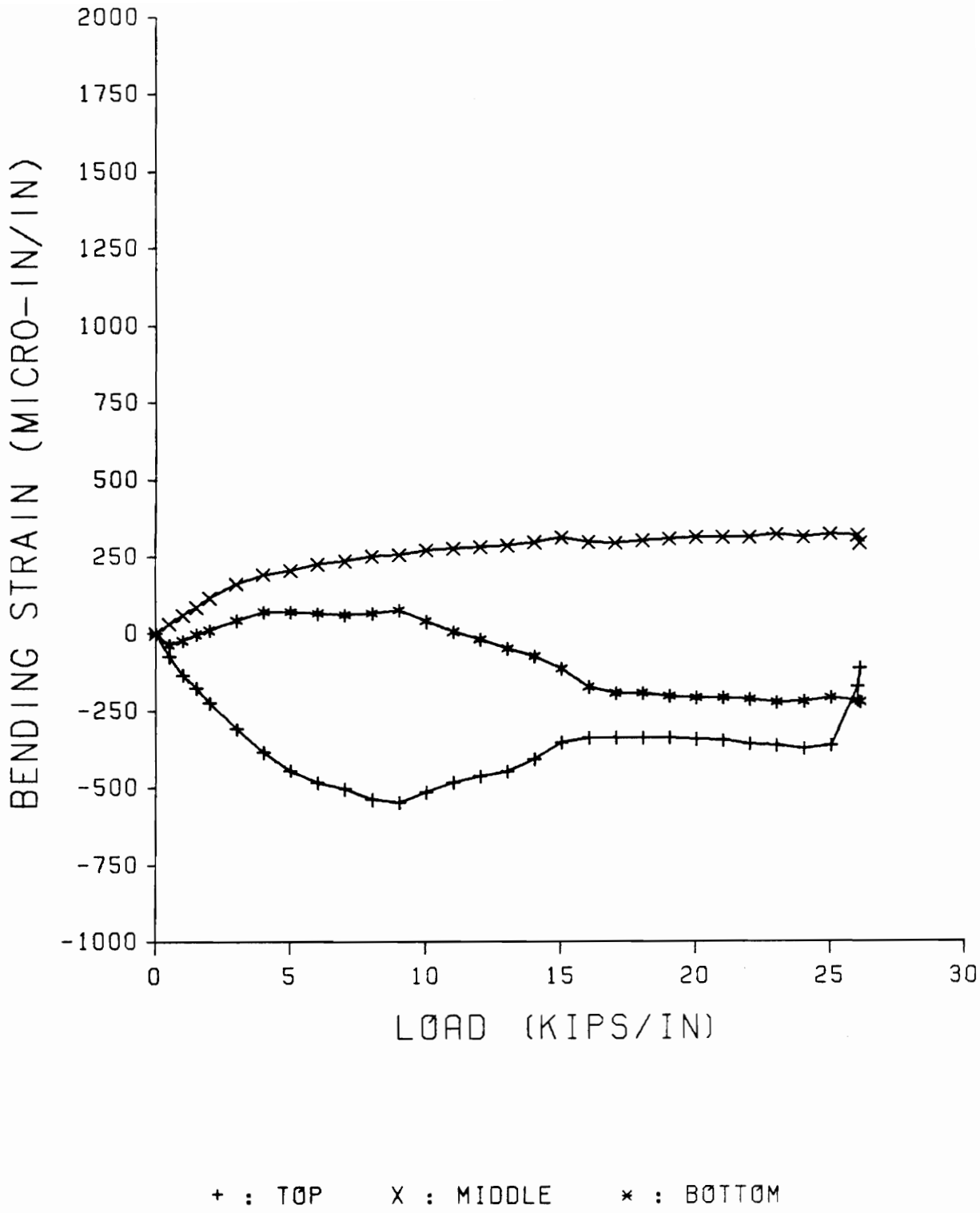

Figure 4.11 Load-Bending Strain Curves of Test BETB7

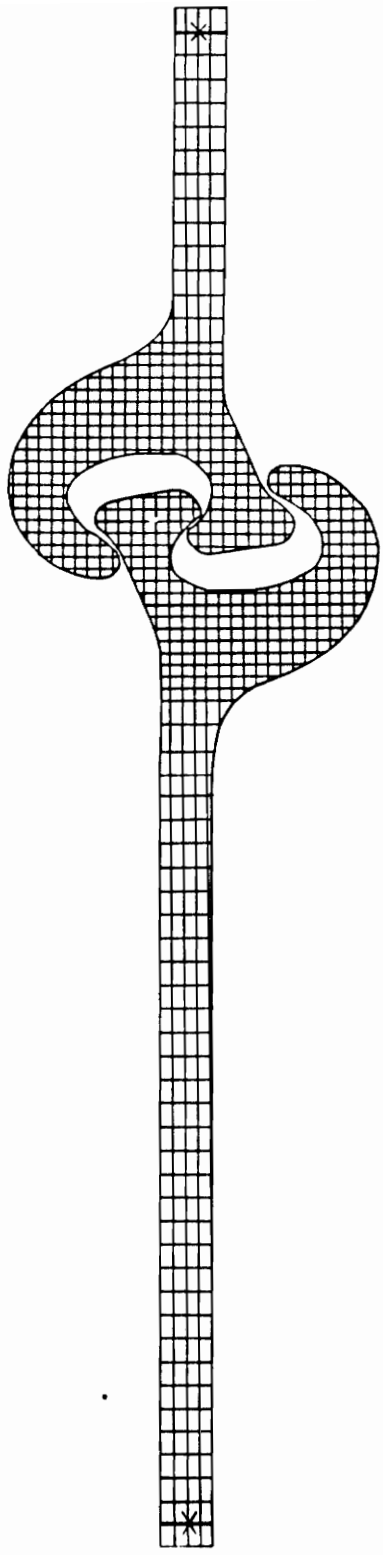

Figure 4.12 Slacks Between the Inerlocks of BETB7, Top End

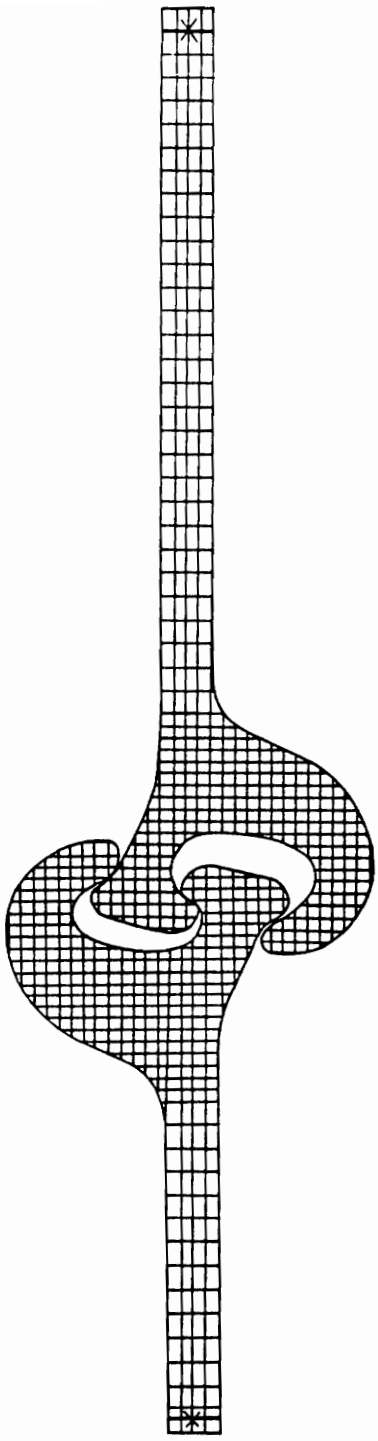

Figure 4.13 Slacks Between the Inerlocks of BETB7, Bottom End

CHAPTER V

CONCLUSIONS and RECOMMENDATIONS

5.1 Conclusions

In this study, interactive computer graphics program AutoCAD was successfully used to interpret the output from a finite element program. Also, a new finite element idealization was constructed to simulate a pull-out test and the results were compared with laboratory tests conducted at WES. The comparison with a single test was not satisfactory. Nonetheless, the program successfully described the response of sheet pile under tensile load. Several observations were made in this study and are discussed below:

1. Computer graphics techniques are very helpful in interpreting the numerical results of a finite element program. In this study, AutoCAD greatly enhanced the study of the

bending behavior of the pile system. By overlapping and zooming, deformed shapes of sheet pile under different loading can be observed thoroughly and easily.

2. Failure of a pull-out test of sheet pile is caused by separation of interlocks. Due to the slope of the contact surfaces between two interlocks, the thumb will try to wedge out of the constraints from opposing thumb and finger when the tensile load is applied. As loading increases, the finger deforms under the pressure exerted from the thumb. When the outward deformation of the finger is large enough for the thumb to slip out of the constraints, the interlock separates and the pile assembly fails.

3. Bending moment is formed when tensile load is applied. The offset of the center section with respect to the two end sections produces couples at the interlock areas. The couples cause the sheet piles to bend and increases the deformation. As the interlocks begin to separate, rotation of the interlock is no longer constrained and bending of the pile sections is relieved by the interlock rotation. This can be observed by overlapping the deformed shapes, plotted by the computer program, at the last two load steps. The web of the middle section at the final load step is flatter than the web of the middle section at the previous load step.

4. The exclusion of initial slacks leads to less satisfactory results of the finite element analysis. Since the locations of the three contact regions in each interlock are assumed to be known, the slacks between interlocks are not modeled and their effects are ignored. A comparison presented in this study shows that ignoring the slacks will change the bending behavior and reduce the elongation of the pile assembly.

5. From the regression analyses applied to the load-deformation data, it was found that equations obtained for failure end group and equations obtained for non-failure end

group are very similar. It indicates that the data points of the two groups, failure end and non-failure end, have the same nature. This implies that both failure and non-failure end deformed in a similar manner until the failure interlock began to separate.

5.2 Recommendations

From this study, several recommendations are made to improve the finite element program and to study the behavior of sheet pile interlocks more deeply.

1. Establish a new moving contact algorithm with a gap element to model the effects of the initial slacks between interlocks. A probabilistic approach could also be used to estimate the magnitude and location of the gaps.

2. Model the load condition for a sheet pile section in a cellular cofferdam. Both lateral pressure and axial tensile load should be considered. Furthermore, the center lines of adjacent pile sections can be set at an angle to reflect the geometry in a cellular cofferdam.

3. Extend the finite element program to include three dimensional elements and study the effects of imperfect bearing in the connection.

4. Perform a sensitivity study of change in interlock geometry for the finite element program and improve the stability.

5. Include an automatic mesh generating technique in the computer program, which will refine the meshes in high-stress areas.

6. Establish a direct communication for data transferring between a finite element program and a computer graphics program so that the progress and results can be monitored and controlled while the program is running.

REFERENCES

1. Argyris, J. H., Doltsinis, J. St., and Kleiber, M., "Incremental Formulation in Nonlinear Mechanics and Large Strain Elasto-Plasticity-Natural Approach", Part II Computer Methods in Applied Mechanics and Engineering ,Vol. 14, 1978, p. 259.

2. Argyris, J. H., and Kleiber, M., "Incremental Formulation in Nonlinear Mechanics and Large Strain Elasto-Plasticity-Natural Approach", Part I Computer Methods in Applied Mechanics and Engineering ,Vol. 11, 1977, p. 215.

3. Barker, R., Lewis, C., Oliver, W., and Mould, K., "Sheet Pile Interlock Connection Testing Program", Report No. VPI/CE-ST-85/01 , Dept. of Civil Engineering, Virginia Tech, Blacksburg, VA, May 1985.

4. Bathe, K.J., Finite Element Procedures In Engineering Analysis , 1st edn, Prentice-Hall, Inc., Englewood Cliffs, New Jersey, 1982.

5. Bathe, K. J., and Chaudhary, A., "A Solution Method for Planar and Axisymmetric Contact Problems", International Journal for Numerical Methods in Engineering , Vol. 21, 1985, pp. 65-88.

6. Bower, J. E., " Predicted Pullout Strength of Sheet-Piling Interlocks", Journal of Soil Mechanics and Foundation Design , ASCE, Vol. 99, Oct. 1973, pp. 765-781

7. Chan, M., and Barker, R., "Finite Element Studies of Sheet Pile Interlock Connection", Report No. VPI/CE-ST-85/02 , Dept. of Civil Engrg. , Virginia Tech, Blacksburg, VA, May, 1985.

8. Chan, M., and Barker, R., "Moving Contact Analysis of Sheet Pile Interlocks", Report No. VPI/CE-ST-85/03 , Dept. of Civil Engrg. , Virginia Tech, Blacksburg, VA, Nov., 1985.

9. Chan, S. K., and Tuba, I. S., "A Finite Element Method for Contact Problems of Solid Bodies", International Journal of Mechanical Science , Vol. 13, 1971, pp. 615-639.

10. Francavilla, A., and Zienkiewicz, O. C., " A Note on Numerical Computation of Elastic Contact Problems", International Journal for Numerical Methods in Engineering , Vol. 9, 1975, pp. 913-924.

11. Fung, Y.C., Foundations of Solid Mechanics , Prentice Hall, Inc., New Jersey, 1965.

12. Gaertner, R., "Investigation of Plane Elastic Contact Allowing for Friction", Computers and Structures , Vol. 7, 1977, pp. 59-63.

13. Hutchinson, J. W., "Finite Strain Analysis of Elastic Plastic Solids and Structures" in Numerical Solution of Nonlinear Structural Problems , (Ed. R. F. Hartung), Vol. 17, ASME, New York, 1973, pp. 17-29.

14. Katona, M. G., "A Simple Contact-Friction Interface Element with Applications to Buried Culverts", International Journal for Numerical and Analytical Methods in Geomechanics ,Vol. 7, 1983, pp. 371-384.

15. Lee, J. K., and Kamemura, K., "Analysis of Elastodynamics with Unilateral Supports", Proceeding Third Engineering Mechanics Division Speciality Conference , ASCE, 1979, pp. 777-780.

16. Lee, K., "Numerical Solution for Elastic Contact Problems", Ph.D. Dissertation, Ohio State University, 1985.

17. Murray, P. W., and Wilson, E. L., "Finite Element Large Deflection Analysis of Plates", Journal of the Engineering Mechanics Division , ASCE, Vol. 94, 1965, pp. 143-165.

18. Oliver, W. B. Jr., "An experimental Investigation of the Static Coefficient of Friction for Sheet Pile Interlocks", M.S. Thesis, Virginia Polytechnic Institute and State University, Blacksburg, Virginia, January, 1985.

19. Osias, J. R., and Swedlow, J. L., "Finite Elasto-plastic Deformation I: Theory and Numerical Examples", International Journal of Solids and Structures , Vol. 10, 1974, pp. 321-339.

20. Tsuta, T., and Yamaji, S., "Finite Element Analysis of Contact Problem", Theory and Practice in Finite Element Structural Analysis , University of Tokyo Press, 1973, pp. 177-194

21. United States Steel, Steel Sheet Piling Handbook , May, 1983.

22. Wu, J. Y. and Barker, R., "Analytical Study of Sheet Pile Interlocks", Report No. VPI/CE-ST-87/01 , Dept. of Civil Engrg. , Virginia Tech, Blacksburg, VA, Jan., 1987.

23. Yaghmai, S. and Popov, E. P., "Incremental Analysis of Large Deflection of Shells of Revolution" International Journal of Solids and Structures , Vol. 7, 1971, pp. 1375-1393.

24. Yamada, Y., "Incremental Formulation for Problems with Geometric and Material Nonlinearities", in Advances in Computational Methods in Structural Mechanics and Design , Second U.S.--Japan Seminar Matrix Methods in Structural Analysis and Design, University of Alabama Press, 1972, pp. 325-335

25. Yamada, Y., Takatsuka, K., and Iwata, K., "Nonlinear Analysis by Finite Element Method and Some Expository Examples", in Theory and Practice in Finite Element Structural Analysis , University of Tokyo Presss, 1973, pp. 125-138.

VITA

The author, Ching-Yang Huang, was born on March 31, 1961 in Taiwan. He received a Bachelor of Science degree in Civil Engineering from the National Chiao-Tung University in Taiwan. After Graduation, he served in the Corps of Engineer for two years. He then came over to the United States to further his studies. In September 1986, he started his pursuit for a Master of Science degree in Civil Engineering in Virginia Tech. He is currently completing the requirement for the degree.